

# Rapidity distribution of pseudoscalar Higgs boson to NNLO<sub>A</sub> + NNLL

V. Ravindran,<sup>1,\*</sup> Aparna Sankar<sup>1,2,3,†</sup> and Surabhi Tiwari<sup>1,4,‡</sup>

<sup>1</sup>*The Institute of Mathematical Sciences, HBNI, Taramani, Chennai 600113, India*

<sup>2</sup>*Physik Department T31, James-Franck-Straße 1, Technische Universität München, D-85748 Garching, Germany*

<sup>3</sup>*Max-Planck-Institut für Physik, Boltzmannstraße 8, 85748 Garching, Germany*

<sup>4</sup>*Institut für Theoretische Teilchenphysik, Karlsruhe Institute of Technology (KIT), Wolfgang-Gaede Straße 1, 76128 Karlsruhe, Germany*



(Received 16 January 2024; accepted 10 June 2024; published 23 July 2024)

We present the differential predictions for the rapidity distribution of pseudoscalar Higgs boson through gluon fusion at the LHC. These results are obtained taking into account the soft-virtual (SV) as well as the next-to-soft virtual (NSV) resummation effects to next-to-next-to-leading-logarithmic (NNLL) accuracy and matching them to the approximate fixed order next-to-next-to-leading-order (NNLO<sub>A</sub>) computation. We perform the resummation in two-dimensional Mellin space by limiting ourselves to the contributions only from gluon-gluon ( $gg$ ) initiated channels. The NNLO<sub>A</sub> rapidity distribution of pseudoscalar Higgs is obtained by applying a ratio method on the NNLO rapidity distribution of the scalar Higgs boson. We also present the first analytical results of N<sup>3</sup>LO rapidity distribution of pseudoscalar Higgs at SV + NSV accuracy. The phenomenological impacts of NNLO<sub>A</sub> + NNLL predictions for 13 TeV LHC are studied. We observe that for  $m_A = 125(700)$  GeV the SV + NSV resummation at the NNLL level brings about 14.76% (11.48%) corrections to the NNLO<sub>A</sub> results at the central scale value of  $\mu_R = \mu_F = m_A$ . Further, we find that the sensitivity to the renormalization scale gets improved substantially by the inclusion of NSV resummed predictions at NNLL accuracy.

DOI: [10.1103/PhysRevD.110.016019](https://doi.org/10.1103/PhysRevD.110.016019)

## I. INTRODUCTION

Measurement of a variety of observables to very high precision is one of the thrust areas in the physics program of the Large Hadron Collider (LHC). Precision studies based on these measurements provide crucial tests of the consistency of the Standard Model (SM), and any significant deviation can also hint toward new physics beyond SM. The discovery of the Higgs boson [1,2], one of the major milestones in particle physics, led to a better understanding of the dynamics behind the electroweak symmetry breaking [3–7] and, in larger picture, opened up a plenty of opportunities to unravel hidden physics behind various phenomena. Despite this success, the SM lacks in fronts in not providing satisfactory explanations for phenomena such as baryon asymmetry in the Universe, the existence

of dark matter, the neutrino mass, etc., and hence falls short of being a complete theory of fundamental interactions. Unravelling these phenomena demands one to go beyond the borderline of the SM. One of the possible extensions of the SM is the supersymmetric theories which provide an elegant solution to the above mentioned problems. Supersymmetric theories generally predict a richer Higgs sector than the Standard Model (SM). In the minimal supersymmetric Standard Model (MSSM), for instance, one introduces two complex Higgs doublets, which originate five physical Higgs bosons: two  $CP$ -even Higgs bosons ( $h, H$ ), two charged Higgs bosons ( $H^\pm$ ), and finally, a  $CP$ -odd (pseudoscalar) Higgs boson ( $A$ ) [8–15].

Ever since the Higgs boson was discovered at the LHC [1,16], there exists curiosity among the high energy physics community to understand whether it is the Higgs boson of the SM or not. This leads to a physics program aiming at probing its interaction with other SM particles with extreme precision that will determine its properties. This can shed light on whether the discovered Higgs boson is the scalar or pseudoscalar Higgs bosons of extended models. Such a study requires precise predictions for their production cross sections and the decay rates. In particular, the production of  $CP$ -odd Higgs boson/pseudoscalar at the LHC has been studied in detail, taking into account the higher order QCD

\*Contact author: [ravindra@imsc.res.in](mailto:ravindra@imsc.res.in)

†Contact author: [aparna@mpp.mpg.de](mailto:aparna@mpp.mpg.de)

‡Contact author: [surabhi.tiwari@kit.edu](mailto:surabhi.tiwari@kit.edu)

Published by the American Physical Society under the terms of the [Creative Commons Attribution 4.0 International license](https://creativecommons.org/licenses/by/4.0/). Further distribution of this work must maintain attribution to the author(s) and the published article's title, journal citation, and DOI. Funded by SCOAP<sup>3</sup>.

radiative corrections, owing to similarities with its  $CP$ -even counter part. Among other channels, it is desirable to look for pseudoscalar Higgs boson in the gluon fusion through heavy fermions due to its appreciable coupling in the small and moderate  $\tan\beta$  in the minimal version of SUSY model, where  $\tan\beta$  is the ratio of vacuum expectation values  $v_i, i = 1, 2$ . Furthermore, the large gluon flux leads to an enhancement in the cross section.

Perturbative QCD (pQCD) provides the most successful framework to compute the observables that can be measured at the LHC. The production of a pseudoscalar Higgs boson through gluon fusion at leading order suffers from large theoretical uncertainties, particularly due to the presence of renormalization scale  $\mu_R$  arising from the strong coupling constant. It also contains mild theoretical uncertainties which result from the factorization scale  $\mu_F$  in the parton distribution functions. In order to deal with these scale uncertainties as well as to uplift the accuracy of theoretical predictions, one has to go beyond the wall of leading-order (LO) computations.

The QCD higher order corrections to the production of  $CP$ -even scalar as well as  $CP$ -odd pseudoscalar bosons through gluon fusion are known for a long time in the literature. For the case of a scalar Higgs boson, results for the inclusive production cross section are available up to next-to-next-to-next-to-leading order ( $N^3LO$ ) QCD [17–20], within the framework of an effective theory that results from the integration of top quark degrees of freedom. This leads to variety of new interactions of the Higgs boson directly with the gluons [21–23]. On the other hand, for the pseudoscalar case, only next-to-next-to-leading-order (NNLO) QCD results [19,24–27] in the effective theory [28] are known. The exact quark mass dependence for scalar and pseudoscalar production is known to next-to-leading-order (NLO) QCD [29,30]. For  $N^3LO$  predictions of a pseudoscalar cross section, both three-loop form factors and real emission contributions are required. The computation of form factors is technically cumbersome [31] as pseudoscalar Higgs boson couples to SM fields through two composite operators that mix under renormalization due to the axial anomaly, and additionally, a finite renormalization constant needs to be introduced in order to restore the chiral Ward identities. Moreover, these operators involve a Levi-Civita tensor and  $\gamma_5$  which are not very straightforward to define in dimensional regularization. The three-loop form factor obtained in [31] was later combined with a suitable soft distribution function [32–34] and mass factorization kernels for the computation of the soft plus virtual (SV) contribution at  $N^3LO$  in [35]. Later, in [36], a new determination of an approximate  $N^3LO$  pseudoscalar boson cross section has been introduced, based on the  $N^3LO$  results of scalar Higgs boson [37].

In addition to the inclusive production cross section, the differential rapidity distribution is among the most important observables, which is expected to be measured in

upcoming days. This demands very precise theoretical predictions of this observable. The computation of the transverse momentum and rapidity distributions for the scalar Higgs boson up to NLO has been done in [38,39] and for the pseudoscalar Higgs boson in [40]. Both inclusive cross section and differential rapidity distribution get large contributions from logarithms arising from certain kinematic regions, thus spoiling the reliability of the fixed order predictions. This usually occurs at the threshold region, namely, when the mass of pseudoscalar Higgs boson becomes equal to the partonic center of mass energy, due to the presence of soft gluons. Hence, the large logarithms resulting from soft gluons in the perturbative series need to be resummed to provide sensible predictions. In the pioneering works of Sterman [41] and of Catani and Trentadue [42], resummation of leading large logarithms for the inclusive rates in the Mellin space and also to differential  $x_F$  distribution [42] using double Mellin moments were achieved. Soft gluon resummation of the gluon fusion cross section has been performed to next-to-next-to-next-to-leading-logarithmic ( $N^3LL$ ) accuracy for the scalar Higgs case [32,33,43–49] and to next-to-next-to-leading-logarithmic (NNLL) accuracy for the pseudoscalar case [50]. In [51], the resummed transverse momentum distribution has been calculated up to  $NNLO_A + NNLL$  for the pseudoscalar Higgs boson.

A generic threshold resummation formula valid to  $N^3LL$  accuracy for color-neutral final states was derived in [49], requiring only the virtual three-loop amplitudes as process-dependent input. Exploiting the factorization properties of differential cross sections as well as the renormalization group (RG) invariance, an all order  $z$ -space formalism was also developed in [52], to study the threshold-enhanced contribution to rapidity distribution of any colorless particle. In [53], the same formalism [52] was used to study the threshold resummation of rapidity distribution of Higgs boson and later to the Drell-Yan (DY) process [54]. For different approaches and their applications, see Refs. [55–63].

The resummed predictions played a crucial role to understand the experimental data in the threshold regions. Besides the threshold enhanced logarithms which are also called as the soft virtual (SV) logarithms, the subleading logarithms, called the next-to-soft-virtual (NSV) logarithms, are also present in the partonic channels beyond leading order in perturbation theory. There have been a surge of interests in the community of theoretical physicists to understand the nature of these subleading logarithms by using various methods [64–76]. Recently, the well-established ideas of collinear factorization and renormalization group invariance have been implemented to understand the perturbative structure of NSV logarithms for inclusive processes in [77,78]. Following the same formalism of [77,78], in a series of articles [79–81], we studied variety of inclusive reactions to understand the impact of NSV

logarithms and found a systematic way to sum them up to all orders in  $z$  as well as in the Mellin  $N$  spaces. We have also studied the perturbative structure of the NSV logarithms in the context of rapidity distributions of DY and Higgs productions in [82]. In addition, for the first time, a procedure to resum them in a systematic manner in the double Mellin space beyond the SV accuracy has also been developed in [82]. Further, we have studied the phenomenological relevance of the NSV resummation in the context of both DY and Higgs rapidity distributions in [83] and [84], respectively. For the pseudoscalar Higgs, the resummed predictions including both SV and NSV are recently available to NNLO +  $\overline{\text{NNLL}}$  accuracy in [85] for the inclusive cross section case. However, similar predictions for the differential case is not available in the literature.

In this article, we explore the role of SV and NSV resummed contributions for the differential rapidity distribution of pseudoscalar Higgs boson in gluon fusion channel by employing the formalism developed in [82]. In particular, we compute the SV and NSV resummed terms to  $\overline{\text{NNLL}}$  accuracy in the double Mellin  $N$ -space. Further, we study the phenomenological impact of adding these resummed predictions to the fixed order results through a matching procedure.

The paper is structured as follows: The first section deals with the theoretical description for the interaction of a pseudoscalar Higgs with the QCD particles. In the next section, we discuss the computation of the rapidity distribution at the fixed order level. We explicitly show the computational steps at NLO and discuss a procedure to obtain an approximate NNLO which is denoted as NNLO<sub>A</sub>. In Sec. IV, we review the framework given in [82] for computing the SV + NSV contributions to the rapidity distribution of a pseudoscalar Higgs in gluon fusion. The following subsections are devoted to the discussions on the ingredients that are required to compute the rapidity distribution at SV + NSV approximation to N<sup>3</sup>LO accuracy. In Sec. V, a relation between inclusive cross section and rapidity distribution has been exploited to determine the unknown coefficients of certain logarithms which contribute to the SV + NSV rapidity distribution. The results of SV + NSV rapidity distribution for pseudoscalar Higgs in gluon fusion at the partonic level are presented up to N<sup>3</sup>LO in Sec. VI. In Sec. VII, we focus on the characteristic structure of the NSV soft-collinear function along with some of its peculiar features. In Sec. VIII, we review the formalism to resum the NSV logarithms to  $\overline{\text{NNLL}}$  accuracy followed by the phenomenological studies of the resummed predictions in Sec. IX. Finally, we conclude our findings in Sec. X.

## II. PSEUDOSCALAR HIGGS EFFECTIVE FIELD THEORY

We begin with setting up the theoretical framework for our analysis. The coupling of a pseudoscalar Higgs boson

with gluons occurs only indirectly through a virtual heavy quark loop which can be integrated out in the infinite quark mass limit. The interaction between pseudoscalar Higgs boson  $\chi^A$  and the QCD particles in the infinitely large top quark mass limit can be described by an effective Lagrangian [28] and it is given by

$$\mathcal{L}_{\text{eff}}^A = \chi^A(x) \left[ -\frac{1}{8} C_G O_G(x) - \frac{1}{2} C_J O_J(x) \right], \quad (1)$$

where the two operators are defined as

$$O_G(x) = G_a^{\mu\nu} \tilde{G}_a^{\rho\sigma} \equiv \epsilon_{\mu\nu\rho\sigma} G_a^{\mu\nu} G_a^{\rho\sigma}, \quad O_J(x) = \partial_\mu (\bar{\psi} \gamma^\mu \gamma_5 \psi).$$

Here,  $G_{\mu\nu}^a = \partial_\mu G_\nu^a - \partial_\nu G_\mu^a + g_s f^{abc} G_\mu^b G_\nu^c$  is the color-field-strength tensor, and  $\tilde{G}^{a\mu\nu} = \epsilon^{\mu\nu\rho\sigma} G_{\rho\sigma}^a$  is its dual with  $\epsilon_{\mu\nu\rho\sigma}$  being the Levi-Civita tensor;  $G_\mu^a$  are the gluon fields,  $g_s = \sqrt{4\pi\alpha_s}$  is the QCD gauge coupling, and  $f^{abc}$  are the structure constants of the SU( $N$ ) algebra. The symbols  $\psi$  and  $\bar{\psi}$  represent fields related to quarks and antiquarks, respectively. The Wilson coefficients  $C_G$  and  $C_J$  of the two operators originate from integrating out the heavy quark loop in effective theory. The coefficient  $C_G$  does not receive any QCD corrections beyond one loop due to Adler-Bardeen theorem [86], whereas  $C_J$  starts only at second order in the strong coupling constant. These Wilson coefficients are given by [28]

$$C_G = -a_s 2^{\frac{5}{2}} G_F^{\frac{1}{2}} \cot \beta, \\ C_J = - \left[ a_s C_F \left( \frac{3}{2} - 3 \ln \frac{\mu_R^2}{m_t^2} \right) + a_s^2 C_J^{(2)} + \dots \right] C_G, \quad (2)$$

where  $a_s = g_s^2/16\pi^2$ . Here,  $G_F$  denotes the Fermi constant,  $\cot \beta$  is the mixing angle in the Two-Higgs-Doublet model and  $C_F$  is the quadratic Casimir in the fundamental representation of QCD. The symbols  $m_A$  and  $m_t$  stand for the masses of the pseudoscalar Higgs boson and top quark (heavy quark), respectively. The bare strong coupling constant in the regularized theory is denoted by  $\hat{a}_s$  which is related to its renormalized counterpart by

$$\hat{a}_s S_\epsilon = \left( \frac{\mu^2}{\mu_R^2} \right)^{\epsilon/2} Z_{a_s} a_s, \quad (3)$$

where  $S_\epsilon = \exp(\frac{\epsilon}{2} [\gamma_E - \ln(4\pi)])$  with  $\gamma_E$  being the Euler-Mascheroni constant. In the above expression,  $\mu_R$  is the mass scale at which the strong coupling constant is renormalized. The scale  $\mu$  is introduced to keep the unrenormalized strong coupling constant dimensionless in  $d = 4 + \epsilon$  space-time dimensions. The renormalization constant  $Z_{a_s}$  up to  $\mathcal{O}(a_s^3)$  is given by

$$Z_{a_s} = 1 + a_s \left[ \frac{2}{\epsilon} \beta_0 \right] + a_s^2 \left[ \frac{4}{\epsilon^2} \beta_0^2 + \frac{1}{\epsilon} \beta_1 \right] + a_s^3 \left[ \frac{8}{\epsilon^3} \beta_0^3 + \frac{14}{3\epsilon^2} \beta_0 \beta_1 + \frac{2}{3\epsilon} \beta_2 \right]. \quad (4)$$

The coefficients of the QCD  $\beta$  function  $\beta_i$  [87] are given in Appendix A.

### III. FIXED ORDER FORMALISM

The rapidity distribution for the production of a pseudoscalar Higgs boson at the hadron colliders can be computed using

$$\frac{d}{dY} \sigma^A(\tau, m_A^2, Y) = \sigma^{A,(0)}(\tau, m_A^2) W(\tau, m_A^2, Y),$$

with

$$W = \sum_{a,b=q,\bar{q},g} \int_0^1 dx_1 \int_0^1 dx_2 \hat{f}_a(x_1) \hat{f}_b(x_2) \int_0^1 dz \delta(\tau - zx_1 x_2) \times \int [dPS_{1+m}] |\bar{\mathcal{M}}_{ab}|^2 \times \delta\left(Y - \frac{1}{2} \ln\left(\frac{P_2 \cdot q}{P_1 \cdot q}\right)\right). \quad (5)$$

Here,  $\sigma^{A,(0)}(\tau, m_A^2)$  is the born cross section corresponding to the leading order (LO) process:  $g(p1) + g(p2) \rightarrow A(q)$  at the parton level. The hadronic scaling variable  $\tau$  is defined by  $\tau \equiv m_A^2/S$  where  $S$  is the square of hadronic center of mass energy, and the dimensionless variable  $z$  is defined as  $z \equiv m_A^2/\hat{s}$ , where  $\hat{s}$  is the square of the partonic center of mass energy.  $\hat{f}_{a(b)}$  are the bare parton distribution functions (PDF) with  $x_{1(2)}$  being the fraction of the initial state hadronic momentum carried by the partons ( $a, b$ ) that take part in the scattering at the partonic level.  $\bar{\mathcal{M}}_{ab}$  denotes the scattering amplitude at the partonic level, and the overline signifies the sum and average over all the quantum numbers for the final and initial state particles, respectively.  $[dPS_{1+m}]$  is the phase space element for the  $A + m$  system where the integer  $m$  depends on the number of radiated partons. The symbol  $Y$  in Eq. (5) stands for the rapidity of the pseudoscalar Higgs boson, and it is defined as

$$Y \equiv \frac{1}{2} \ln\left(\frac{P_2 \cdot q}{P_1 \cdot q}\right), \quad (6)$$

where  $P_l$  ( $l = 1, 2$ ) is the momenta of incoming hadrons, and  $q$  denotes the momentum of pseudoscalar Higgs boson. In order to define the threshold limit at the partonic level and to express the hadronic rapidity distribution in terms of the partonic one through convolution integrals, we choose to work with the symmetric scaling variables  $x_1^0$  and  $x_2^0$ ,

$$Y \equiv \frac{1}{2} \ln\left(\frac{x_1^0}{x_2^0}\right) \quad \text{and} \quad \tau \equiv x_1^0 x_2^0. \quad (7)$$

In terms of these variables, the partonic contributions arising from the subprocesses are found to depend on the ratios

$$z_i \equiv \frac{x_i^0}{x_i}, \quad i = 1, 2, \quad (8)$$

which play the role of scaling variables at the partonic level.

The partonic rapidity distribution can be computed, within the framework of perturbative QCD, order by order in strong coupling constant. The contributions arising from beyond leading order contain the UV, soft, and collinear divergences. Upon performing dimensional regularization, the true nature of the UV divergences arises as poles in  $\epsilon$ , and such divergences go away when the renormalizations of coupling, masses, and fields are performed in modified minimal subtraction ( $\overline{\text{MS}}$ ) scheme. The UV renormalized partonic rapidity distribution denoted by  $\hat{\Delta}_{d,ab}^A$  is identified as

$$\begin{aligned} & \frac{1}{x_1 x_2} \hat{\Delta}_{d,ab}^A(z_1, z_2, \hat{a}_s, \mu^2, m_A^2, \mu_R^2) \\ &= \int [dPS_{1+m}] \int_0^1 dz |\bar{\mathcal{M}}_{ab}|^2 \\ & \times \delta(\tau - zx_1 x_2) \delta\left(Y - \frac{1}{2} \ln\left(\frac{P_2 \cdot q}{P_1 \cdot q}\right)\right). \quad (9) \end{aligned}$$

The soft and collinear divergences are collectively called as infrared (IR) divergences. The soft divergences come from zero momentum gluons in the loops of virtual contributions and real gluons in the gluon emission processes. The massless or light partons are responsible for collinear divergences. Due to the KLN theorem [88,89], soft and collinear divergences resulting from final state partons cancel independently after summing up contributions from all possible degenerate states. However, the collinear singularities arising from the collinear configurations involving initial state particles remain. Those are removed at the hadronic level through the technique, known as mass factorization. The infrared safe partonic rapidity distribution which is also termed as the partonic coefficient function (CF) can be obtained by using the factorization formula given below,

$$\begin{aligned} & \Delta_{d,ac}^A(z_1, z_2, a_s(\mu_R^2), m_A^2, \mu_F^2, \mu_R^2) \\ &= \int_{z_1}^1 \frac{dy_1}{y_1} \int_{z_2}^1 \frac{dy_2}{y_2} \Gamma_{ad'}^{-1}(\hat{a}_s, \mu^2, \mu_F^2, y_1, \epsilon) \\ & \times \hat{\Delta}_{d,d'c'}^A\left(\frac{z_1}{y_1}, \frac{z_2}{y_2}, \hat{a}_s, \mu^2, m_A^2, \mu_R^2, \epsilon\right) \\ & \times \Gamma_{cc'}^{-1}(\hat{a}_s, \mu^2, \mu_F^2, y_2, \epsilon), \quad (10) \end{aligned}$$

where  $\Gamma_{ab}$  are the Altarelli-Parisi (AP) [90] kernels which essentially absorb the initial state collinear singularities. The factored out initial state collinear divergences get

absorbed into the bare PDFs to give a finite renormalized value at the scale  $\mu_F$ . Using Eq. (10) and substituting it in Eq. (5), we obtain the expression for the rapidity distribution in terms of renormalized PDFs and finite CF as given below,

$$\begin{aligned} \frac{d\sigma^A}{dY} &= \sigma^{A,(0)}(\tau, m_A^2) \sum_{a,b=q,\bar{q},g} \int_{x_1^0}^1 \frac{dz_1}{z_1} \int_{x_2^0}^1 \frac{dz_2}{z_2} f_a \\ &\times \left( \frac{x_1^0}{z_1}, \mu_F^2 \right) f_b \left( \frac{x_2^0}{z_2}, \mu_F^2 \right) \times \Delta_{d,ab}^A(z_1, z_2, m_A^2, \mu_F^2, \mu_R^2). \end{aligned} \quad (11)$$

The perturbative expansion of the infrared safe CF in powers of strong coupling constant read as

$$\begin{aligned} \Delta_{d,c}^A(z_1, z_2, m_A^2, \mu_F^2, \mu_R^2) \\ = \sum_{i=0}^{\infty} a_s^i(\mu_R^2) \Delta_{d,c}^{A,(i)}(z_1, z_2, m_A^2, \mu_F^2, \mu_R^2), \quad c = q, \bar{q}, g. \end{aligned} \quad (12)$$

In this article, we have computed  $\frac{d\sigma^A}{dY}$  in Eq. (11) explicitly up to next-to-leading order (NLO) for the production of a pseudoscalar Higgs boson in a gluon fusion channel, which is discussed in the following

subsection. We also discuss how an approximate NNLO which is denoted as NNLO<sub>A</sub> can be obtained by using the NNLO results of a scalar Higgs boson.

### A. Fixed order results at NLO and NNLO<sub>A</sub>

Here, we begin with the computation of the rapidity distribution  $\frac{d\sigma^A}{dY}$  given in Eq. (11) at NLO accuracy. Note that the NLO contribution arises from the one-loop virtual corrections to born process  $g + g \rightarrow A$  and from the real emission processes, namely,  $g + g \rightarrow A + g$ ,  $q + g \rightarrow A + q$ , and  $q + \bar{q} \rightarrow A + g$ . In order to obtain  $\frac{d\sigma^A}{dY}$  at NLO, the first step is to calculate  $\hat{\Delta}_{d,ab}^{A,(i)}$  given in Eq. (9) for  $i = 1$  for the aforementioned processes. One of the ingredients to find  $\hat{\Delta}_{d,ab}^{A,(1)}$  is the phase space element  $dPS_{1+m}$  which is relevant for the processes at NLO. For the virtual contributions to the born process,  $dPS_{1+m} = dPS_1$ , which is given as

$$dPS_1 = \frac{2\pi}{m_A^2} \delta(1 - z_1) \delta(1 - z_2), \quad (13)$$

and for the real emission processes, we have two body phase space element  $dPS_{1+m} = dPS_2$ , which takes the following form:

$$dPS_2 = \frac{1}{8\pi x_1 x_2} \frac{1}{\Gamma(1 + \frac{\epsilon}{2})} \left( \frac{m_A^2}{4\pi} \right)^{\epsilon/2} \frac{2z_1 z_2 (1 + z_1 z_2)}{(z_1 + z_2)^{2-\epsilon}} ((1 - z_1^2)(1 - z_2^2))^{\epsilon/2}. \quad (14)$$

Next, we need to determine the square of the matrix element  $|\bar{\mathcal{M}}_{ab}|^2$  which is averaged over spin, polarization, and color for the NLO processes mentioned above. For the one-loop correction to the LO process, we obtain

$$\begin{aligned} |\bar{\mathcal{M}}_{g+g \rightarrow A}^2|_{\text{one loop}} &= a_s \frac{C_A G_F^2 Q^4}{(N^2 - 1)} \left[ \frac{1}{e^2} \{-2\} + \frac{1}{e} \{-1 - L_{QF}\} + \left\{ \frac{3}{2} + \frac{7}{4} \zeta_2 - \frac{1}{2} L_{QF} - \frac{1}{4} L_{QF}^2 \right\} + e \left\{ -\frac{5}{4} - \frac{7}{12} \zeta_3 \right. \right. \\ &+ \frac{7}{8} \zeta_2 + \frac{3}{4} L_{QF} + \frac{7}{8} L_{QF} \zeta_2 - \frac{1}{8} L_{QF}^2 - \frac{1}{24} L_{QF}^3 \left. \right\} + e^2 \left\{ \frac{7}{8} - \frac{7}{24} \zeta_3 - \frac{21}{16} \zeta_2 - \frac{73}{320} \zeta_2^2 - \frac{5}{8} L_{QF} \right. \\ &- \frac{7}{24} L_{QF} \zeta_3 + \frac{7}{16} L_{QF} \zeta_2 + \frac{3}{16} L_{QF}^2 + \frac{7}{32} L_{QF}^2 \zeta_2 - \frac{1}{48} L_{QF}^3 \left. \right\} + e^3 \left\{ -\frac{9}{16} + \frac{7}{16} \zeta_3 + \frac{35}{32} \zeta_2 + \frac{1}{6} \zeta_2 \zeta_3 \right. \\ &- \frac{73}{640} \zeta_2^2 + \frac{7}{16} L_{QF} - \frac{7}{48} L_{QF} \zeta_3 - \frac{21}{32} L_{QF} \zeta_2 - \frac{73}{640} L_{QF} \zeta_2^2 - \frac{5}{32} L_{QF}^2 - \frac{7}{96} L_{QF}^2 \zeta_3 + \frac{7}{64} L_{QF}^2 \zeta_2 \\ &+ \frac{1}{32} L_{QF}^3 + \frac{7}{192} L_{QF}^3 \zeta_2 \left. \right\} + e^4 \left\{ \frac{5}{16} - \frac{35}{96} \zeta_3 + \frac{37}{144} \zeta_3^2 - \frac{49}{64} \zeta_2 + \frac{1}{12} \zeta_2 \zeta_3 + \frac{219}{1280} \zeta_2^2 - \frac{39}{640} \zeta_2^3 \right. \\ &- \frac{9}{32} L_{QF} + \frac{7}{32} L_{QF} \zeta_3 + \frac{35}{64} L_{QF} \zeta_2 + \frac{1}{12} L_{QF} \zeta_2 \zeta_3 - \frac{73}{1280} L_{QF} \zeta_2^2 + \frac{7}{64} L_{QF}^2 - \frac{7}{192} L_{QF}^2 \zeta_3 \\ &\left. \left. - \frac{21}{128} L_{QF}^2 \zeta_2 - \frac{73}{2560} L_{QF}^2 \zeta_2^2 - \frac{5}{192} L_{QF}^3 - \frac{7}{576} L_{QF}^3 \zeta_3 + \frac{7}{384} L_{QF}^3 \zeta_2 \right\} \right], \end{aligned} \quad (15)$$

where  $L_{QF} = \log\left(\frac{Q^2}{\mu_F^2}\right)$  and  $\zeta_i$  are the Riemann zeta functions. Here,  $Q^2 = m_A^2$ . For the real emission process  $g + g \rightarrow A + g$ , we find

$$\begin{aligned}
|\bar{\mathcal{M}}|_{g+g \rightarrow A+g}^2 = & \frac{a_s}{(\mu_R)^{\epsilon/2}} \frac{\pi^2 C_A G_F^2}{(N^2 - 1)} \left[ \frac{1}{D_1 D_2} (8s^3) + Q^2(32) + \frac{Q^2}{D_2} (16s) + \frac{Q^2}{D_1} (16s) + Q^4 \left( -\frac{16}{s} \right) + \frac{Q^4}{D_2} (-8) \right. \\
& + \frac{Q^4}{D_1} (-8) + \frac{Q^6}{D_2} \left( \frac{8}{s} \right) + \frac{Q^6}{D_1} \left( \frac{8}{s} \right) + D_1(-8) + D_1 Q^2 \left( \frac{8}{s} \right) + D_1^2 \left( -\frac{8}{s} \right) - 16s + \epsilon \left\{ \frac{1}{D_1 D_2} (4s^3) \right. \\
& + Q^2(8) + \frac{Q^2}{D_2} (8s) + \frac{Q^2}{D_1} (8s) + Q^4 \left( -\frac{8}{s} \right) + \frac{Q^4}{D_2} (-4) + \frac{Q^4}{D_1} (-4) + \frac{Q^6}{D_2} \left( \frac{4}{s} \right) + \frac{Q^6}{D_1} \left( \frac{4}{s} \right) \\
& + D_1(-4) + D_1 Q^2 \left( \frac{4}{s} \right) + D_1^2 \left( -\frac{4}{s} \right) - 8s \left. \right\} + \epsilon^2 \left\{ \frac{1}{D_1 D_2} (-2s^3) + Q^2(-4) + \frac{Q^2}{D_2} (-4s) + \frac{Q^2}{D_1} (-4s) \right. \\
& + Q^4 \left( \frac{4}{s} \right) + \frac{Q^4}{D_2} (2) + \frac{Q^4}{D_1} (2) + \frac{Q^6}{D_2} \left( -\frac{2}{s} \right) + \frac{Q^6}{D_1} \left( -\frac{2}{s} \right) + D_1(2) + D_1 Q^2 \left( -\frac{2}{s} \right) + D_1^2 \left( \frac{2}{s} \right) + 4s \left. \right\} \\
& + \epsilon^3 \left\{ \frac{1}{D_1 D_2} (s^3) + Q^2(6) + \frac{Q^2}{D_2} (2s) + \frac{Q^2}{D_1} (2s) + Q^4 \left( -\frac{2}{s} \right) - \frac{Q^4}{D_2} - \frac{Q^4}{D_1} + \frac{Q^6}{D_2} \left( \frac{1}{s} \right) + \frac{Q^6}{D_1} \left( \frac{1}{s} \right) \right. \\
& - D_1 + D_1 Q^2 \left( \frac{1}{s} \right) + D_1^2 \left( -\frac{1}{s} \right) - 2s \left. \right\} + \epsilon^4 \left\{ \frac{1}{D_1 D_2} \left( -\frac{1}{2} s^3 \right) + Q^2(-5) + \frac{Q^2}{D_2} (-s) + \frac{Q^2}{D_1} (-s) \right. \\
& + Q^4 \left( \frac{1}{s} \right) + \frac{Q^4}{D_2} \left( \frac{1}{2} \right) + \frac{Q^4}{D_1} \left( \frac{1}{2} \right) + \frac{Q^6}{D_2} \left( -\frac{1}{2s} \right) + \frac{Q^6}{D_1} \left( -\frac{1}{2s} \right) + D_1 \left( \frac{1}{2} \right) \\
& \left. + D_1 Q^2 \left( -\frac{1}{2s} \right) + D_1^2 \left( \frac{1}{2s} \right) + s \right. \left. \right\}, \tag{16}
\end{aligned}$$

with  $D_1 = \frac{-Q^2}{z}(1-z)(1-y)$  and  $D_2 = \frac{-Q^2}{z}(1-z)y$ , where

$$z = \frac{x_1^0 x_2^0}{x_1 x_2}, \quad y = \frac{x_2 x_2^0 (x_1 + x_1^0) (x_1 - x_1^0)}{(x_1 x_2^0 + x_2 x_1^0) (x_1 x_2 - x_1^0 x_2^0)}. \tag{17}$$

For the real emission process  $q + g \rightarrow A + q$ , we obtain

$$\begin{aligned}
|\bar{\mathcal{M}}|_{q+g \rightarrow A+q}^2 = & \frac{a_s}{(\mu_R)^{\epsilon/2}} \frac{\pi^2 C_F G_F^2}{(N^2 - 1)} \left[ (-4s) + \frac{1}{D_1} (-8s^2) + Q^2(4) + Q^2 \frac{1}{D_1} (8s) + Q^4 \frac{1}{D_1} (-4) + D_2(4) + \epsilon \left\{ \frac{1}{D_1} (-4s^2) \right. \right. \\
& + Q^2(4) + Q^2 \frac{1}{D_1} (4s) + Q^4 \frac{1}{D_1} (-4) + D_2(4) \left. \right\} + \epsilon^2 \left\{ (2s) + \frac{1}{D_1} (2s^2) + Q^2 \frac{1}{D_1} (-2s) \right\} \\
& + \epsilon^3 \left\{ (-s) + \frac{1}{D_1} (-s^2) + Q^2 \frac{1}{D_1} (s) \right\} + \epsilon^4 \left\{ \left( \frac{1}{2} s \right) + \frac{1}{D_1} \left( \frac{1}{2} s^2 \right) + Q^2 \frac{1}{D_1} \left( -\frac{1}{2} s \right) \right. \left. \right\}, \tag{18}
\end{aligned}$$

and for  $g + q \rightarrow A + q$ , we have

$$|\bar{\mathcal{M}}|_{g+q \rightarrow A+q}^2 = |\bar{\mathcal{M}}|_{q+g \rightarrow A+q}^2 |_{D_1 \leftrightarrow D_2}. \tag{19}$$

Finally, for the real emission process  $q + \bar{q} \rightarrow A + g$ , we find

$$\begin{aligned}
|\bar{\mathcal{M}}|_{q+\bar{q} \rightarrow A+g}^2 = & \frac{a_s}{(\mu_R)^{\epsilon/2}} \frac{\pi^2 C_F G_F^2}{N} \left[ (4s) + Q^2(-8) + Q^4 \left( \frac{4}{s} \right) + D_1(8) + D_1 Q^2 \left( -\frac{8}{s} \right) + D_1^2 \left( \frac{8}{s} \right) + \epsilon \left\{ (6s) + Q^2(-12) \right. \right. \\
& + Q^4 \left( \frac{6}{s} \right) + D_1(8) + D_1 Q^2 \left( -\frac{8}{s} \right) + D_1^2 \left( \frac{8}{s} \right) \left. \right\} + \epsilon^2 \left\{ (2s) + Q^2(-4) + Q^4 \left( \frac{2}{s} \right) \right. \left. \right\}. \tag{20}
\end{aligned}$$

Now, we can compute the NLO hadronic rapidity distribution  $\frac{d\sigma^A}{dY}$  in Eq. (11) by performing the convolution of  $\Delta_{d,ab}^A$  for all the contributing processes at NLO discussed above with the corresponding PDFs. Note that  $\Delta_{d,ab}^A$  can be obtained by substituting for  $\hat{\Delta}_{d,d'b'}^A$  in the factorization formula (10) which requires the phase space element as well as the matrix element square computed above according to Eq. (9). We express the NLO rapidity distribution at the hadronic level as

$$\frac{d\sigma^{A,\text{NLO}}}{dY} = \sigma^{A,(0)}(\tau, m_A^2) \left\{ \frac{d\sigma_{gg}^{A,(0)}}{dY} + a_s \frac{d\sigma_{gg}^{A,(1)}}{dY} + a_s \frac{d\sigma_{qg}^{A,(1)}}{dY} + a_s \frac{d\sigma_{gq}^{A,(1)}}{dY} + a_s \frac{d\sigma_{q\bar{q}}^{A,(1)}}{dY} \right\}, \quad (21)$$

where

$$\frac{d\sigma_{gg}^{A,(0)}}{dY} = H_{gg}(x_1^0, x_2^0, \mu_F^2) = f_g(x_1^0, \mu_F^2) f_g(x_2^0, \mu_F^2). \quad (22)$$

The full result of  $\frac{d\sigma^{A,\text{NLO}}}{dY}$  is provided in Appendix B. Here, we mention one interesting observation of the NLO result of pseudoscalar Higgs rapidity distribution. As already noted in [91], the NLO result of the rapidity distribution of the pseudoscalar is related to that of scalar Higgs at a partonic level as follows:

$$\begin{aligned} \Delta_{d,gg}^{A,(1)} &= \Delta_{d,gg}^{H,(1)} + a_s 8C_A \delta(1-z_1) \delta(1-z_2), \\ \Delta_{d,qg}^{A,(1)} &= \Delta_{d,qg}^{H,(1)}, \quad \Delta_{d,q\bar{q}}^{A,(1)} = \Delta_{d,q\bar{q}}^{H,(1)}, \end{aligned} \quad (23)$$

where  $H$  stands for the scalar Higgs boson. From a detailed analysis of the above results, it has been found that the

difference in the rapidity distribution of scalar and pseudoscalar Higgs at NLO for a  $gg$  channel arises only from the one-loop virtual contribution to the respective born processes which is also termed as one-loop form factor (FF). Note that the FFs of both scalar and pseudoscalar Higgs bosons are different due to the presence of different Wilson coefficients corresponding to  $ggA$  (pseudoscalar) and  $ggH$  (scalar) vertices in the Higgs effective field theory [28]. However, we note that the full hadronic NLO rapidity distribution of pseudoscalar Higgs can be correctly obtained from that of scalar Higgs by using the formula given below,

$$\frac{d\sigma^{A,\text{NLO}}}{dY} = \mathcal{R}_{\mathcal{A}\mathcal{H}} \times \left( \frac{\sigma^{A,(0)}}{\sigma^{H,(0)}} \right) \times \frac{1}{C_H^2} \frac{d\sigma^{H,\text{NLO}}}{dY}, \quad (24)$$

with  $\sigma^{H,(0)}$  being the born cross section for scalar Higgs and  $C_H$  is the Wilson coefficient for  $ggH$  effective vertex [92]. In the above formula,  $\mathcal{R}_{\mathcal{A}\mathcal{H}}$  is the ratio of the modulus square of the finite form factors (FF) corresponding to pseudoscalar and scalar Higgs [31,93], that means  $\mathcal{R}_{\mathcal{A}\mathcal{H}} = \frac{|FF_A|^2}{|FF_H|^2}$ . We provide the expression of the ratio factor  $\mathcal{R}_{\mathcal{A}\mathcal{H}}$  up to  $a_s^3$  below,

$$\begin{aligned} \mathcal{R}_{\mathcal{A}\mathcal{H}} &= \left[ 1 + a_s \{8C_A\} + a_s^2 \left\{ n_f C_F (-31 + 12L_{rmt} - 4L_{qr}) + C_A n_f \left( -\frac{2}{3} - \frac{4}{3} L_{qr} \right) + C_A^2 \left( \frac{215}{3} - \frac{20}{3} L_{qr} \right) \right\} \right. \\ &+ a_s^3 \left\{ n_f (-4C_J^{(2)}) + n_f C_F^2 \left( \frac{763}{9} + 4L_{qr} + \frac{32}{3} \zeta_3 \right) + n_f^2 C_F \left( \frac{4520}{81} - \frac{328}{9} L_{qr} + 16L_{qr} L_{rmt} - \frac{8}{3} L_{qr}^2 + 16\zeta_2 \right) \right. \\ &+ C_A n_f C_F \left( -\frac{67094}{81} + 96L_{rmt} + \frac{1492}{9} L_{qr} - 88L_{qr} L_{rmt} + \frac{44}{3} L_{qr}^2 + \frac{224}{3} \zeta_3 - 88\zeta_2 \right) \\ &+ C_A n_f^2 \left( -\frac{631}{81} + \frac{134}{27} L_{qr} - \frac{8}{9} L_{qr}^2 + \frac{16}{3} \zeta_2 \right) + C_A^2 n_f \left( \frac{1973}{81} - \frac{838}{27} L_{qr} + \frac{4}{9} L_{qr}^2 - 16\zeta_3 - \frac{8}{3} \zeta_2 \right) \\ &\left. \left. + C_A^3 \left( \frac{68309}{81} - \frac{6028}{27} L_{qr} + \frac{220}{9} L_{qr}^2 - \frac{208}{3} \zeta_3 - \frac{440}{3} \zeta_2 \right) \right\} \right], \end{aligned} \quad (25)$$

where  $L_{qr} = \ln\left(\frac{q^2}{\mu_R^2}\right)$  and  $L_{rmt} = \ln\left(\frac{\mu_R^2}{m_i^2}\right)$ .

Now we ask the following question: can this ratio factor  $\mathcal{R}_{\mathcal{A}\mathcal{H}}$  be used for computing the rapidity distribution of pseudoscalar from that of scalar Higgs beyond NLO accuracy? In [36], one of the authors had studied the applicability of this ratio method in obtaining the inclusive cross section of pseudoscalar from that of scalar Higgs beyond NLO. In [36], it has been established that an approximate NNLO result can be obtained for the inclusive cross section of pseudoscalar from that of scalar Higgs by using this ratio method. In that case, the difference between the exact and approximate results are found to be in terms of next-to-next-to-soft

contributions which are suppressed by  $(1-z)^2$  with respect to the leading soft terms that means they vanish in the threshold limit  $z \rightarrow 1$ . In addition, there are no  $\log(1-z)$  terms present in the difference of exact and approximate NNLO results. This suggests that one can compute the inclusive cross section of pseudoscalar Higgs from that of scalar Higgs by employing the ratio method up to next-to-soft terms or NSV terms correctly. In addition, in [36], it has been shown that the approximate NNLO results provide an excellent approximation to the exact one where the discrepancy is at most 2% for high mass region, whereas it is around 1% for the low mass case.

Drawing inspiration from the above observation for the inclusive case at NNLO, in this article, we attempt to go beyond NLO for uplifting the theoretical accuracy of the predictions for pseudoscalar Higgs rapidity distribution. We begin with computing the approximate NNLO rapidity distribution of the pseudoscalar from the exact NNLO result of scalar Higgs available in [94] by using a formula which is equivalent to Eq. (24) for the NNLO case. We denote this approximate NNLO result by  $\text{NNLO}_A$ . The analytic expression of this result is too big to be presented in this article; nevertheless, we reserve a section for the detailed numerical analysis of the results we computed. Further, in principle, one can extend the same ratio method discussed here to obtain the approximate results at  $\text{N}^3\text{LO}$  for the rapidity distribution of the pseudoscalar Higgs. However, since the complete  $\text{N}^3\text{LO}$  results for the Higgs rapidity distribution [95] are not yet available publicly, it is not possible to compute approximate  $\text{N}^3\text{LO}$  results for the rapidity distribution of the pseudoscalar Higgs using the ratio method mentioned above. Needless to say, computing the corrections beyond NNLO is not easy, and the

complexity level of the computation increases significantly which often prevents us from achieving it. Hence, we resort to an alternate method based on soft-virtual and next-to-soft-virtual approximations [82] which essentially capture the dominant contribution at the threshold to go beyond the NNLO accuracy, which is the topic of the next section.

#### IV. SV + NSV FORMALISM

The goal of this section is to study the rapidity distribution of pseudoscalar Higgs in gluon fusion at the soft-virtual (SV) + next-to-soft-virtual (NSV) approximations. To be more precise, we consider the contributions to the partonic CF corresponding to the rapidity distribution of a pseudoscalar Higgs boson in gluon fusion in the limit  $z_l \rightarrow 1$  by keeping only SV and NSV terms; hence, we denote them by  $\Delta_{d,g}^{A,\text{SV}+\text{NSV}}$ . Since we restrict ourselves to SV terms, namely, distributions of the kind  $\delta(1 - z_i)$  and  $\mathcal{D}_k(z_i)$  and NSV terms  $\log^k(1 - z_i)$  for the CF with gluon-gluon initiated channel, the expansion coefficients in Eq. (12) can be expressed as follows:

$$\begin{aligned} \Delta_{d,g}^{A,(i)} &= \Delta_{d,g,\delta\delta}^{A,(i)} \delta(\bar{z}_1) \delta(\bar{z}_2) + \sum \Delta_{d,g,\delta\mathcal{D}_j}^{A,(i)} \delta(\bar{z}_1) \mathcal{D}_j(z_2) + \sum \Delta_{d,g,\delta L_j}^{A,(i)} \delta(\bar{z}_1) L_j(z_2) + \sum \Delta_{d,g,\mathcal{D}_j\mathcal{D}_k}^{A,(i)} \mathcal{D}_j(z_1) \mathcal{D}_k(z_2) \\ &\quad + \sum \Delta_{d,g,\mathcal{D}_j L_k}^{A,(i)} \mathcal{D}_j(z_1) L_k(z_2) + (z_1 \leftrightarrow z_2), \end{aligned}$$

with  $\mathcal{D}_j(z_l) = \left[ \frac{\ln^j(1 - z_l)}{(1 - z_l)} \right]_+$ ,  $\delta(\bar{z}_l) = \delta(1 - z_l)$  and  $L_j(z_l) = \log^j(1 - z_l)$  for  $l = 1, 2$ . (26)

In [82], it has been already shown that the SV + NSV contributions to the differential distributions arising from diagonal partonic channels, which is the gluon-gluon channel in our case, can be factorized in terms of the overall operator UV renormalization constant  $Z_g^A$ , the bare form factor  $\hat{F}_g^A$  (FF), a function  $\mathcal{S}_{d,g}^A$  that is sensitive to real emission contributions, and the collinear singular AP kernels  $\Gamma_{gg}$ . This is always possible as  $(Z_g^A)^2$  and  $|\hat{F}_g^A|^2$  are simply proportional to  $\delta(\bar{z}_1)\delta(\bar{z}_2)$  and can be factored out from these partonic channels. Hence, near threshold, we obtain, for  $\Delta_{d,g}^{A,\text{SV}+\text{NSV}}$ ,

$$\begin{aligned} \Delta_{d,g}^{A,\text{SV}+\text{NSV}}(z_1, z_2, m_A^2, \mu_F^2, \mu_R^2, \epsilon) &= \sigma^{A,(0)}(\mu_R^2) (Z_g^A(\hat{a}_s, \mu_R^2, \mu^2, \epsilon))^2 |\hat{F}_g^A(\hat{a}_s, \mu^2, m_A^2, \epsilon)|^2 \\ &\quad \times \delta(\bar{z}_2) \delta(\bar{z}_1) \otimes \mathcal{S}_{d,g}^A(\hat{a}_s, \mu^2, m_A^2, z_1, z_2, \epsilon) \\ &\quad \otimes \Gamma_{gg}^{-1}(\hat{a}_s, \mu^2, \mu_F^2, z_1, \epsilon) \delta(\bar{z}_2) \otimes \Gamma_{gg}^{-1}(\hat{a}_s, \mu^2, \mu_F^2, z_2, \epsilon) \delta(\bar{z}_1). \end{aligned} \quad (27)$$

The symbol  $\otimes$  refers to convolution, which is defined for functions,  $f_i(x_i)$ ,  $i = 1, 2, \dots, n$ , as

$$(f_1 \otimes f_2 \otimes \dots \otimes f_n)(z) = \prod_{i=1}^n \left( \int dx_i f_i(x_i) \right) \delta(z - x_1 x_2 \dots x_n). \quad (28)$$

As long as we are interested in computing the SV + NSV parts of the rapidity distribution, that is those resulting from the phase space region where  $z_{1(2)} \rightarrow 1$ , we keep only those terms that are proportional to distributions  $\delta(\bar{z}_l)$ ,  $\mathcal{D}_i(z_l)$ , and NSV terms  $\log^i(1 - z_l)$  with  $l = 1, 2$  and  $i = 0, 1, \dots$  and drop the rest of the terms resulting from the convolutions. Hence, we have kept only diagonal part of

AP kernel  $\Gamma_{ab}$  in Eq. (27) and dropped the nondiagonal AP kernels. In addition, the diagonal kernels get contributions only from the diagonal splitting functions. The reason for the above simplification is due to the fact that the distributions and NSV logarithms can come only from convolutions of two or more distributions or a distribution with NSV logarithms. In summary, since our main focus

here is on SV and NSV terms resulting from gluon initiated pseudoscalar Higgs production, we have dropped contributions from nondiagonal partonic channels in the mass factorized result of  $\Delta_{d,g}^A$ . All the ingredients in Eq. (27) that are required to get a finite CF, namely,  $Z_g^A$ ,  $\hat{F}_g^A$ ,  $\mathcal{S}_{d,g}^A$ , and  $\Gamma_{gg}$  are known to satisfy certain differential equations with respect to some mass scales [32,78,79,82]. The form of solutions to the respective differential equations which are discussed in the subsequent sections along with the well-

established ideas of collinear factorization lead to an all order formula for computing  $\Delta_{d,g}^{A,SV+NSV}$  in  $z$  space,

$$\Delta_{d,g}^{A,SV+NSV}(q^2, \mu_R^2, \mu_F^2, z_1, z_2) = \mathcal{C} \exp(\Psi_{d,g}^A(q^2, \mu_R^2, \mu_F^2, z_1, z_2, \epsilon))|_{\epsilon=0}, \quad (29)$$

where the function  $\Psi_{d,g}^A$  is given by

$$\begin{aligned} \Psi_{d,g}^A(q^2, \mu_R^2, \mu_F^2, z_1, z_2, \epsilon) &= (\ln(Z_g^A(\hat{a}_s, \mu^2, \mu_R^2, \epsilon)))^2 + \ln|\hat{F}_g^A(\hat{a}_s, \mu^2, Q^2, \epsilon)|^2 \delta(\bar{z}_1) \delta(\bar{z}_2) \\ &+ \mathcal{C} \ln \mathcal{S}_{d,g}^A(\hat{a}_s, \mu^2, q^2, z_1, z_2, \epsilon) - \mathcal{C} \ln \Gamma_{gg}(\hat{a}_s, \mu^2, \mu_F^2, z_1, \epsilon) \delta(\bar{z}_2) \\ &- \mathcal{C} \ln \Gamma_{gg}(\hat{a}_s, \mu^2, \mu_F^2, z_2, \epsilon) \delta(\bar{z}_1). \end{aligned} \quad (30)$$

The symbol “ $\mathcal{C}$ ” stands for the convolution whose actions on a distribution  $g(z_1, z_2)$  is defined as

$$\begin{aligned} \mathcal{C}e^{g(z_1, z_2)} &= \delta(1-z_1)\delta(1-z_2) + \frac{1}{1!}g(z_1, z_2) \\ &+ \frac{1}{2!}(g \otimes g)(z_1, z_2) + \dots, \end{aligned} \quad (31)$$

where  $\otimes$  denotes the Mellin convolution. Though the constituents of  $\Psi_{d,g}^A$  contain UV and IR divergent terms, the sum of all these terms is finite and is regular in the variable  $\epsilon$ . It contains the distributions such as  $\delta(1-z_l)$ ,  $\mathcal{D}_i(z_l)$  and the logarithms of the form  $\log^i(1-z_l)$ ,  $l=1, 2$ ,  $i=0, 1, \dots$

### A. Operator renormalization constant

Besides coupling constant renormalization, the form factor also requires the renormalization of the effective operators in the effective Lagrangian, Eq. (1). This additional renormalization is called the overall operator renormalization which is performed through the constant  $Z_g^A$ . In Eq. (27), the overall operator renormalization  $Z_g^A$  is determined by solving the underlying renormalization group (RG) equation,

$$\mu_R^2 \frac{d}{d\mu_R^2} \ln Z_g^A(\hat{a}_s, \mu_R^2, \mu^2, \epsilon) = \sum_{i=1}^{\infty} a_s^i \gamma_{g,i}^A. \quad (32)$$

Using the results of  $\gamma_{g,i}^A$  given in Appendix A and solving the above RG equation, we obtain the overall renormalization constant up to three-loop level as

$$\begin{aligned} Z_g^A &= 1 + a_s \left[ \frac{22}{3\epsilon} C_A - \frac{4}{3\epsilon} n_f \right] + a_s^2 \left[ \frac{1}{\epsilon^2} \left\{ \frac{484}{9} C_A^2 - \frac{176}{9} C_A n_f + \frac{16}{9} n_f^2 \right\} + \frac{1}{\epsilon} \left\{ \frac{34}{3} C_A^2 - \frac{10}{3} C_A n_f - 2 C_F n_f \right\} \right] \\ &+ a_s^3 \left[ \frac{1}{\epsilon^3} \left\{ \frac{10648}{27} C_A^3 - \frac{1936}{9} C_A^2 n_f + \frac{352}{9} C_A n_f^2 - \frac{64}{27} n_f^3 \right\} \right. \\ &+ \frac{1}{\epsilon^2} \left\{ \frac{5236}{27} C_A^3 - \frac{2492}{27} C_A^2 n_f - \frac{308}{9} C_A C_F n_f + \frac{280}{27} C_A n_f^2 + \frac{56}{9} C_F n_f^2 \right\} \\ &\left. + \frac{1}{\epsilon} \left\{ \frac{2857}{81} C_A^3 - \frac{1415}{81} C_A^2 n_f - \frac{205}{27} C_A C_F n_f + \frac{2}{3} C_F^2 n_f + \frac{79}{81} C_A n_f^2 + \frac{22}{27} C_F n_f^2 \right\} \right], \end{aligned} \quad (33)$$

with the  $SU(N)$  QCD color factors,

$$C_A = N, \quad C_F = \frac{N^2 - 1}{2N}. \quad (34)$$

Here,  $n_f$  is the number of active light quark flavors. It is to be noted that  $Z_g^A = Z_{GG}$  which is given in Eq. (3.49) of [31] has been discussed extensively in [31].

### B. Form factor

The unrenormalized form factor  $F_g^A(\hat{a}_s, Q^2, \mu^2, \epsilon)$  satisfies the so-called K + G differential equation [96–99] which is dictated by the factorization property, gauge, and renormalization group (RG) invariances,

$$Q^2 \frac{d}{dQ^2} \ln \hat{F}_g^A(\hat{a}_s, Q^2, \mu^2, \epsilon) = \frac{1}{2} \left[ K_g^A \left( \hat{a}_s, \frac{\mu_R^2}{\mu^2}, \epsilon \right) + G_g^A \left( \hat{a}_s, \frac{Q^2}{\mu^2}, \frac{\mu_R^2}{\mu^2}, \epsilon \right) \right], \quad (35)$$

where all poles in the dimensional regulator  $\epsilon$  are contained in the  $Q^2$  independent function  $K_g^A$ , and the finite terms in  $\epsilon \rightarrow 0$  are encapsulated in  $G_g^A$ . RG invariance of the form factor implies

$$\begin{aligned} \mu_R^2 \frac{d}{d\mu_R^2} K_g^A \left( \hat{a}_s, \frac{\mu_R^2}{\mu^2}, \epsilon \right) &= -\mu_R^2 \frac{d}{d\mu_R^2} G_g^A \left( \hat{a}_s, \frac{Q^2}{\mu_R^2}, \frac{\mu_R^2}{\mu^2}, \epsilon \right) \\ &= -\sum_{i=1}^{\infty} a_s^i(\mu_R^2) A_{g,i}^A. \end{aligned} \quad (36)$$

The cusp anomalous dimensions  $A_{g,i}^A$  [42,100–103] are given in Appendix A. Solving the above renormalization group equation (RGE) satisfied by  $K_g^A$ , we get

$$K_g^A(\hat{a}_s, \mu^2, \mu_R^2, \epsilon) = \sum_{i=1}^{\infty} \hat{a}_s^i \left( \frac{\mu_R^2}{\mu^2} \right)^{i\frac{\epsilon}{2}} S_\epsilon^i K_g^{A,(i)}(\epsilon), \quad (37)$$

with

$$\begin{aligned} K_g^{A,(1)}(\epsilon) &= \frac{1}{\epsilon} \{-2A_{g,1}^A\}, \\ K_g^{A,(2)}(\epsilon) &= \frac{1}{\epsilon^2} \{2\beta_0 A_{g,1}^A\} + \frac{1}{\epsilon} \{-A_{g,2}^A\}, \\ K_g^{A,(3)}(\epsilon) &= \frac{1}{\epsilon^3} \left\{ -\frac{8}{3} \beta_0^2 A_{g,1}^A \right\} + \frac{1}{\epsilon^2} \left\{ \frac{2}{3} \beta_1 A_{g,1}^A + \frac{8}{3} \beta_0 A_{g,2}^A \right\} \\ &\quad + \frac{1}{\epsilon} \left\{ -\frac{2}{3} A_{g,3}^A \right\}. \end{aligned} \quad (38)$$

Similarly, upon solving the RGE in (36) for  $G_g^A$ , we obtain

$$\begin{aligned} G_g^A \left( \hat{a}_s, \frac{Q^2}{\mu_R^2}, \frac{\mu_R^2}{\mu^2}, \epsilon \right) &= G_g^A \left( a_s(\mu_R^2), \frac{Q^2}{\mu_R^2}, \epsilon \right) = G_g^A(a_s(Q^2), 1, \epsilon) + \int_{Q^2/\mu_R^2}^1 \frac{d\lambda^2}{\lambda^2} A_g^A(a_s(\lambda^2 \mu_R^2)) = G_g^A(a_s(Q^2), 1, \epsilon) \\ &\quad + \sum_{i=1}^{\infty} S_\epsilon^i \hat{a}_s^i \left( \frac{\mu_R^2}{\mu^2} \right)^{i\frac{\epsilon}{2}} \left[ \left( \frac{Q^2}{\mu_R^2} \right)^{i\frac{\epsilon}{2}} - 1 \right] K_g^{A,(i)}(\epsilon). \end{aligned} \quad (39)$$

We expand the finite function  $G_g^A(a_s(Q^2), 1, \epsilon)$  in powers of  $a_s(Q^2)$  as

$$G_g^A(a_s(Q^2), 1, \epsilon) = \sum_{i=1}^{\infty} a_s^i(Q^2) G_{g,i}^A(\epsilon). \quad (40)$$

After substituting these solutions in (35) and performing the final integration, we obtain the following solution for the form factor:

$$\ln \hat{F}_g^A(\hat{a}_s, Q^2, \mu^2, \epsilon) = \sum_{i=1}^{\infty} \hat{a}_s^i \left( \frac{Q^2}{\mu^2} \right)^{i\frac{\epsilon}{2}} S_\epsilon^i \hat{\mathcal{L}}_{g,F}^{A,(i)}(\epsilon), \quad (41)$$

where

$$\begin{aligned} \hat{\mathcal{L}}_{g,F}^{A,(1)} &= \frac{1}{\epsilon^2} (-2A_{g,1}^A) + \frac{1}{\epsilon} (G_{g,1}^A(\epsilon)) \\ \hat{\mathcal{L}}_{g,F}^{A,(2)} &= \frac{1}{\epsilon^3} (\beta_0 A_{g,1}^A) + \frac{1}{\epsilon^2} \left( -\frac{1}{2} A_{g,2}^A - \beta_0 G_{g,1}^A(\epsilon) \right) + \frac{1}{2\epsilon} G_{g,2}^A(\epsilon) \\ \hat{\mathcal{L}}_{g,F}^{A,(3)} &= \frac{1}{\epsilon^4} \left( -\frac{8}{9} \beta_0^2 A_{g,1}^A \right) + \frac{1}{\epsilon^3} \left( \frac{2}{9} \beta_1 A_{g,1}^A + \frac{8}{9} \beta_0 A_{g,2}^A + \frac{4}{3} \beta_0^2 G_{g,1}^A(\epsilon) \right) + \frac{1}{\epsilon^2} \left( -\frac{2}{9} A_{g,3}^A - \frac{1}{3} \beta_1 G_{g,1}^A(\epsilon) \right. \\ &\quad \left. - \frac{4}{3} \beta_0 G_{g,2}^A(\epsilon) \right) + \frac{1}{\epsilon} \left( \frac{1}{3} G_{g,3}^A(\epsilon) \right). \end{aligned} \quad (42)$$

One finds that  $G_{g,i}^A$  can be expressed in terms of collinear  $B_i^q$  and soft  $f_i^q$  anomalous dimensions through the relation [38,104,105],

$$G_{g,i}^A(\epsilon) = 2(B_{g,i}^A - \gamma_{g,i}^A) + f_{g,i}^A + \sum_{k=0}^{\infty} \epsilon^k g_{g,i}^{A,k}. \quad (43)$$

Note that the single pole term of the form factor depends on three different anomalous dimensions, namely, the collinear anomalous dimension  $B_{g,i}^A$ , anomalous dimension of the coupling constant  $\gamma_{g,i}^A$ , and the soft anomalous dimension  $f_{g,i}^A$ .  $B_{g,i}^A$  can be obtained from the  $\delta(1-z)$  parts of the

diagonal splitting function known up to the three-loop level [100,101] which are given in Appendix A. The  $f_{g,i}^A$  for  $i=1,2$  can be found in [38] and in [100] for  $i=3$ . We list them in Appendix A. The constants  $g_{g,i}^{A,0}$  are controlled by the beta function of the strong coupling constant through renormalization group invariance of the bare form factor as

$$\begin{aligned} g_{g,1}^{A,0} &= 0, & g_{g,2}^{A,0} &= -2\beta_0 g_{g,1}^{A,1}, \\ g_{g,3}^{A,0} &= -2\beta_1 g_{g,1}^{A,1} - 2\beta_0 (g_{g,2}^{A,1} + 2\beta_0 g_{g,1}^{A,2}). \end{aligned} \quad (44)$$

Below, we give the expressions of  $g_{g,j}^{A,i}$  which are required to calculate the form factor up to  $a_s^3$ ,

$$\begin{aligned} g_{g,1}^{A,1} &= C_A \{4 + \zeta_2\}, \\ g_{g,1}^{A,2} &= C_A \left\{ -6 - \frac{7}{3} \zeta_3 \right\}, \\ g_{g,1}^{A,3} &= C_A \left\{ 7 - \frac{1}{2} \zeta_2 + \frac{47}{80} \zeta_2^2 \right\}, \\ g_{g,2}^{A,1} &= C_A^2 \left\{ \frac{11882}{81} + \frac{67}{3} \zeta_2 - \frac{44}{3} \zeta_3 \right\} + C_A n_f \left\{ -\frac{2534}{81} - \frac{10}{3} \zeta_2 - \frac{40}{3} \zeta_3 \right\} + C_F n_f \left\{ -\frac{160}{3} + 12 \ln \left( \frac{\mu_R^2}{m_t^2} \right) + 16 \zeta_3 \right\}, \\ g_{g,2}^{A,2} &= C_F n_f \left\{ \frac{2827}{18} - 18 \ln \left( \frac{\mu_R^2}{m_t^2} \right) - \frac{19}{3} \zeta_2 - \frac{16}{3} \zeta_2^2 - \frac{128}{3} \zeta_3 \right\} + C_A n_f \left\{ \frac{21839}{243} - \frac{17}{9} \zeta_2 + \frac{259}{60} \zeta_2^2 + \frac{766}{27} \zeta_3 \right\} \\ &\quad + C_A^2 \left\{ -\frac{223861}{486} + \frac{80}{9} \zeta_2 + \frac{671}{120} \zeta_2^2 + \frac{2111}{27} \zeta_3 + \frac{5}{3} \zeta_2 \zeta_3 - 39 \zeta_5 \right\}, \\ g_{g,3}^{A,1} &= n_f C_J^{(2)} \{-6\} + C_F n_f^2 \left\{ \frac{12395}{27} - \frac{136}{9} \zeta_2 - \frac{368}{45} \zeta_2^2 - \frac{1520}{9} \zeta_3 - 24 \ln \left( \frac{\mu_R^2}{m_t^2} \right) \right\} + C_F^2 n_f \left\{ \frac{457}{2} + 312 \zeta_3 - 480 \zeta_5 \right\} \\ &\quad + C_A^2 n_f \left\{ -\frac{12480497}{4374} - \frac{2075}{243} \zeta_2 - \frac{128}{45} \zeta_2^2 - \frac{12992}{81} \zeta_3 - \frac{88}{9} \zeta_2 \zeta_3 + \frac{272}{3} \zeta_5 \right\} \\ &\quad + C_A^3 \left\{ \frac{62867783}{8748} + \frac{146677}{486} \zeta_2 - \frac{5744}{45} \zeta_2^2 - \frac{12352}{315} \zeta_3 - \frac{67766}{27} \zeta_3 - \frac{1496}{9} \zeta_2 \zeta_3 - \frac{104}{3} \zeta_3^2 + \frac{3080}{3} \zeta_5 \right\} \\ &\quad + C_A n_f^2 \left\{ \frac{514997}{2187} - \frac{8}{27} \zeta_2 + \frac{232}{45} \zeta_2^2 + \frac{7640}{81} \zeta_3 \right\} \\ &\quad + C_A C_F n_f \left\{ -\frac{1004195}{324} + \frac{1031}{18} \zeta_2 + \frac{1568}{45} \zeta_2^2 + \frac{25784}{27} \zeta_3 + 40 \zeta_2 \zeta_3 + \frac{608}{3} \zeta_5 + 132 \ln \left( \frac{\mu_R^2}{m_t^2} \right) \right\}. \end{aligned} \quad (45)$$

After substituting the above expressions in (35) and performing the final integration, we obtain the UV renormalized form factor up to  $\mathcal{O}(a_s^3)$  as

$$\begin{aligned} \ln |\hat{F}_g^A|(-q^2, \epsilon) &= a_s(q^2) \left\{ -\frac{1}{\epsilon^2} 16 C_A + C_A (8 + 14 \zeta_2) \right\} + a_s(q^2)^2 \left\{ \frac{1}{\epsilon^3} [16 C_A n_f - 88 C_A^2] + \frac{1}{\epsilon^2} \left[ C_A n_f \left( \frac{40}{9} \right) \right. \right. \\ &\quad \left. \left. + C_A^2 \left( -\frac{268}{9} + 8 \zeta_2 \right) \right] + \frac{1}{\epsilon} \left[ C_A n_f \left( -\frac{76}{27} + \frac{4}{3} \zeta_2 \right) + C_A^2 \left( \frac{772}{27} - 4 \zeta_3 - \frac{22}{3} \zeta_2 \right) \right] + C_F n_f \left( -\frac{160}{3} \right) \right. \\ &\quad \left. + 12 \ln \left( \frac{\mu_R^2}{m_t^2} \right) + 16 \zeta_3 \right\} + C_A n_f \left( -\frac{1886}{81} - \frac{92}{9} \zeta_3 - \frac{50}{3} \zeta_2 \right) + C_A^2 \left( \frac{8318}{81} - \frac{286}{9} \zeta_3 + \frac{335}{3} \zeta_2 - 24 \zeta_2^2 \right) \\ &\quad + a_s(q^2)^3 \left\{ \frac{1}{\epsilon^4} \left[ C_A n_f^2 \left( -\frac{1408}{81} \right) + C_A^2 n_f \left( \frac{15488}{81} \right) + C_A^3 \left( -\frac{42592}{81} \right) \right] + \frac{1}{\epsilon^3} \left[ C_A n_f^2 \left( -\frac{1600}{243} \right) \right. \right. \end{aligned}$$

$$\begin{aligned}
& + C_A C_F n_f \left( \frac{256}{9} \right) + C_A^2 n_f \left( \frac{31040}{243} - \frac{320}{27} \zeta_2 \right) + C_A^3 \left( -\frac{98128}{243} + \frac{1760}{27} \zeta_2 \right) \Big] + \frac{1}{\epsilon^2} \left[ C_A n_f^2 \left( \frac{224}{81} - \frac{32}{27} \zeta_2 \right) \right. \\
& + C_A C_F n_f \left( \frac{440}{27} - \frac{128}{9} \zeta_3 \right) - C_A^2 n_f \left( \frac{6176}{243} - \frac{544}{27} \zeta_3 - \frac{416}{81} \zeta_2 \right) + C_A^3 \left( \frac{16328}{243} - \frac{880}{27} \zeta_3 + \frac{1384}{81} \zeta_2 \right. \\
& \left. - \frac{704}{45} \zeta_2^2 \right) \Big] + \frac{1}{\epsilon} \left[ C_A n_f^2 \left( -\frac{3728}{2187} + \frac{224}{81} \zeta_3 - \frac{80}{81} \zeta_2 \right) - C_A C_F n_f \left( \frac{3638}{81} - \frac{608}{27} \zeta_3 - \frac{8}{3} \zeta_2 - \frac{64}{15} \zeta_2^2 \right) \right. \\
& + C_A^2 n_f \left( \frac{14980}{2187} - \frac{1424}{81} \zeta_3 + \frac{4792}{243} \zeta_2 - \frac{656}{45} \zeta_2^2 \right) + C_A^3 \left( \frac{234466}{2187} + \frac{64}{3} \zeta_5 - \frac{488}{9} \zeta_3 - \frac{24436}{243} \zeta_2 + \frac{160}{9} \zeta_2 \zeta_3 \right. \\
& \left. + \frac{2552}{45} \zeta_2^2 \right) \Big] - n_f C_J^{(2)} + C_F n_f^2 \left( \frac{1498}{9} - \frac{224}{3} \zeta_3 - \frac{40}{9} \zeta_2 - \frac{32}{45} \zeta_2^2 \right) + C_F^2 n_f \left( \frac{457}{3} - 320 \zeta_5 + 208 \zeta_3 \right) \\
& + C_A n_f^2 \left( \frac{560290}{6561} + \frac{9152}{243} \zeta_3 - \frac{296}{27} \zeta_2 - \frac{424}{27} \zeta_2^2 \right) + C_A C_F n_f \left( -\frac{623255}{486} + \frac{1216}{9} \zeta_5 + \frac{35176}{81} \zeta_3 - \frac{925}{9} \zeta_2 \right. \\
& \left. + \frac{368}{3} \zeta_2 \zeta_3 - \frac{128}{45} \zeta_2^2 \right) + C_A^2 n_f \left( -\frac{7335209}{6561} + \frac{856}{9} \zeta_5 - \frac{2216}{81} \zeta_3 - \frac{37054}{729} \zeta_2 - 104 \zeta_2 \zeta_3 + \frac{10616}{45} \zeta_2^2 \right) \\
& \left. + C_A^3 \left( \frac{35421539}{13122} + \frac{4444}{9} \zeta_5 - \frac{322280}{243} \zeta_3 - \frac{208}{9} \zeta_2^2 + \frac{510619}{729} \zeta_2 - \frac{308}{3} \zeta_2 \zeta_3 - \frac{118534}{135} \zeta_2^2 + \frac{75088}{945} \zeta_2^3 \right) \right\}. \quad (46)
\end{aligned}$$

### C. Mass factorization kernel

The mass factorization kernels are the solutions to the AP evolution equation which is controlled by the AP splitting functions  $P_{aa'}(z_l, \mu_F^2)$  as given below,

$$\begin{aligned}
\mu_F^2 \frac{d}{d\mu_F^2} \Gamma_{ab}(z_l, \mu_F^2, \epsilon) &= \frac{1}{2} \sum_{a'=q, \bar{q}, g} P_{aa'}(z_l, \mu_F^2) \otimes \Gamma_{a'b}(z_l, \mu_F^2, \epsilon), \\
a, b &= q, \bar{q}, g, \quad (47)
\end{aligned}$$

where the perturbative expansion of the AP splitting functions reads as

$$P(z_l, \mu_F^2) = \sum_{i=1}^{\infty} a_s^i(\mu_F^2) P^{(i-1)}(z_l). \quad (48)$$

As discussed in the previous section, only the diagonal parts of splitting functions  $P_{ab}(z, \mu_F^2)$  in  $\Gamma_{ab}(z, \mu_F^2, \epsilon)$  need to be kept since the convolutions of two or more non-diagonal splitting functions give rise to terms which are of beyond NSV type. The diagonal  $P_{gg}(z_l, \mu_F^2)$  are expanded around  $z_l = 1$ , and all those terms which do not contribute to SV + NSV are eliminated. The diagonal AP splitting functions near  $z_l = 1$  take the following form:

$$\begin{aligned}
P_{gg}(z_l, a_s(\mu_F^2)) &= 2[B_g^A(a_s(\mu_F^2))\delta(1-z_l) \\
& + A_g^A(a_s(\mu_F^2))\mathcal{D}_0(z_l) \\
& + C_g^A(a_s(\mu_F^2))\log(1-z_l) \\
& + D_g^A(a_s(\mu_F^2))] + \mathcal{O}((1-z_l)), \quad (49)
\end{aligned}$$

where

$$\begin{aligned}
C_g^A(a_s(\mu_F^2)) &= \sum_{i=1}^{\infty} a_s^i(\mu_F^2) C_{g,i}^A, \\
D_g^A(a_s(\mu_F^2)) &= \sum_{i=1}^{\infty} a_s^i(\mu_F^2) D_{g,i}^A. \quad (50)
\end{aligned}$$

The constants  $C_{g,i}^A$  and  $D_{g,i}^A$  can be obtained from the splitting functions  $P_{gg}$  which are known to three loops in QCD [100,101] (see Refs. [71,100,101,106–112] for the lower order ones). We list  $C_{g,i}^A$  and  $D_{g,i}^A$  below,

$$\begin{aligned}
C_{g,1}^A &= 0, \\
C_{g,2}^A &= 16C_A^2, \\
C_{g,3}^A &= C_A^2 n_f \left\{ -\frac{320}{9} \right\} + C_A^3 \left\{ \frac{2144}{9} - 64\zeta_2 \right\}, \\
D_{g,1}^A &= -4C_A, \\
D_{g,2}^A &= C_A n_f \left\{ \frac{40}{9} \right\} + C_A^2 \left\{ -\frac{268}{9} + 8\zeta_2 \right\}, \\
D_{g,3}^A &= C_A n_f^2 \left\{ \frac{16}{27} \right\} + C_A C_F n_f \left\{ \frac{110}{3} - 32\zeta_3 \right\} \\
& + C_A^2 n_f \left\{ \frac{908}{27} + \frac{112}{3} \zeta_3 - \frac{160}{9} \zeta_2 \right\} \\
& + C_A^3 \left\{ -166 + \frac{56}{3} \zeta_3 + \frac{1072}{9} \zeta_2 - \frac{176}{5} \zeta_2^2 \right\}. \quad (51)
\end{aligned}$$

The RG equation in (47) can be solved by employing the perturbative expansion of the AP kernels,

$$\Gamma_{gg}(z_l, \mu_F^2, \epsilon) = \delta(1 - z_l) + \sum_{i=1}^{\infty} \hat{a}_s^i \left( \frac{\mu_F^2}{\mu^2} \right)^{i\frac{\epsilon}{2}} S_\epsilon^i \Gamma_{gg}^{(i)}(z_l, \epsilon). \quad (52)$$

The solutions of  $\Gamma_{gg}^{(i)}$  in the  $\overline{\text{MS}}$  scheme are given by

$$\begin{aligned} \Gamma_{gg}^{(1)}(z_l, \epsilon) &= \frac{1}{\epsilon} P_{gg}^{(0)}(z_l), \\ \Gamma_{gg}^{(2)}(z_l, \epsilon) &= \frac{1}{\epsilon^2} \left( \frac{1}{2} P_{gg}^{(0)}(z_l) \otimes P_{gg}^{(0)}(z_l) - \beta_0 P_{gg}^{(0)}(z_l) \right) + \frac{1}{\epsilon} \left( \frac{1}{2} P_{gg}^{(1)}(z_l) \right), \\ \Gamma_{gg}^{(3)}(z_l, \epsilon) &= \frac{1}{\epsilon^3} \left( \frac{4}{3} \beta_0^2 P_{gg}^{(0)}(z_l) - \beta_0 P_{gg}^{(0)}(z_l) \otimes P_{gg}^{(0)}(z_l) + \frac{1}{6} P_{gg}^{(0)}(z_l) \otimes P_{gg}^{(0)}(z_l) \otimes P_{gg}^{(0)}(z_l) \right) \\ &\quad + \frac{1}{\epsilon^2} \left( \frac{1}{2} P_{gg}^{(0)}(z_l) \otimes P_{gg}^{(1)}(z_l) - \frac{1}{3} \beta_1 P_{gg}^{(0)}(z_l) - \frac{4}{3} \beta_0 P_{gg}^{(1)}(z_l) \right) + \frac{1}{\epsilon} \left( \frac{1}{3} P_{gg}^{(2)}(z_l) \right). \end{aligned} \quad (53)$$

The most remarkable fact is that these quantities are universal, independent of the insertion of operators. Hence, for the process under consideration, we make use of the existing process independent results of the AP kernels and splitting functions.

#### D. Soft-collinear function

Exploiting the fact that the CF  $\Delta_{d,g}^{A,\text{SV}+\text{NSV}}$  is finite, the infrared structure of  $\mathcal{S}_{d,g}^A$  can be studied using the AP evolution equations of  $\Gamma_{gg}$  and the K + G differential equation of  $\hat{F}_g^P$  provided with the renormalization group equation of  $Z_g^A$ . This is possible as we find that  $\mathcal{S}_{d,g}^A$  also satisfies a K + G type differential equation,

$$\begin{aligned} q^2 \frac{d}{dq^2} \mathcal{S}_{d,g}^A &= \frac{1}{2} \left[ \bar{K}_{d,g}^A \left( \hat{a}_s, \frac{\mu_R^2}{\mu^2}, \epsilon, z_1, z_2 \right) \right. \\ &\quad \left. + \bar{G}_{d,g}^A \left( \hat{a}_s, \frac{q^2}{\mu_R^2}, \frac{\mu_R^2}{\mu^2}, \epsilon, z_1, z_2 \right) \right] \otimes \mathcal{S}_{d,g}^A, \end{aligned} \quad (54)$$

where the infrared singular part is contained in  $\bar{K}_{d,g}^A$  in terms of universal anomalous dimensions while the finite  $\bar{G}_{d,g}^A$  is controlled by certain process independent but initial state dependent functions and also certain process dependent pieces. Since the K + G equation (54) corresponding to  $\mathcal{S}_{d,g}^A$  admits a solution of convoluted exponential form, we write

$$\mathcal{S}_{d,g}^A = \mathcal{C} \exp(2\Phi_{d,g}^A(\hat{a}_s, \mu^2, q^2, z_1, z_2, \epsilon)), \quad (55)$$

where the real emission contributions are encapsulated in the function  $\Phi_{d,g}^A$  which is termed as the soft-collinear function. Furthermore,  $\Phi_{d,g}^A$  being independent of  $\mu_R^2$  satisfies the RG equation,  $\mu_R^2 \frac{d}{d\mu_R^2} \Phi_{d,g}^A = 0$  and consequently

$$\begin{aligned} \mu_R^2 \frac{d}{d\mu_R^2} \bar{K}_{d,g}^A &= -\mu_R^2 \frac{d}{d\mu_R^2} \bar{G}_{d,g}^A \\ &= -\delta(1 - z_1) \delta(1 - z_2) \bar{A}_g^A(a_s(\mu_R^2)). \end{aligned} \quad (56)$$

The right-hand side of the above equation is proportion to  $\delta(1 - z_1) \delta(1 - z_2)$  as the most singular terms resulting from  $\bar{K}_{d,g}^A$  should cancel with those from the form factor contribution which is proportional to only pure delta functions. To make the CF  $\Delta_{d,g}^{A,\text{SV}+\text{NSV}}$  finite, the poles from  $\Phi_{d,g}^A$  have to cancel with those coming from  $\hat{F}_g^A$  and  $\Gamma_{gg}$ . Hence, the constants  $\bar{A}_g^A$  should satisfy  $\bar{A}_g^A = -A_g^A$ . The RGE (56) for  $\bar{G}_{d,g}^A$  can be solved using the above mentioned relation to get

$$\begin{aligned} \bar{G}_{d,g}^A \left( \hat{a}_s, \frac{q^2}{\mu_R^2}, \frac{\mu_R^2}{\mu^2}, z_1, z_2, \epsilon \right) &= \bar{G}_{d,g}^A \left( a_s(\mu_R^2), \frac{q^2}{\mu_R^2}, z_1, z_2, \epsilon \right) \\ &= \bar{G}_{d,g}^A(a_s(q^2), 1, z_1, z_2, \epsilon) \\ &\quad - \delta(1 - z_1) \delta(1 - z_2) \int_{\frac{q^2}{\mu_R^2}}^1 \frac{d\lambda^2}{\lambda^2} A_g^A(a_s(\lambda^2 \mu_R^2)). \end{aligned} \quad (57)$$

With these solutions, it is now straightforward to solve the differential equation (54) for obtaining the form of  $\Phi_{d,g}^A$ . For convenience, we decompose the soft-collinear function as  $\Phi_{d,g}^A = \Phi_{d,g,\text{SV}}^A + \Phi_{d,g,\text{NSV}}^A$  in such a way that  $\Phi_{d,g,\text{SV}}^A$  contains only the SV terms, i.e., all the distributions  $\mathcal{D}_k(z_l)$  and  $\delta(1 - z_l)$ , and  $\Phi_{d,g,\text{NSV}}^A$  contains the NSV terms, namely,  $\log^k(1 - z_l)$ ,  $l = 1, 2$ ,  $k = 0, \dots$  in the limit  $z_{1(2)} \rightarrow 1$ . An all order solution for  $\Phi_{d,g,\text{SV}}^A$  in powers of  $\hat{a}_s$  in dimensional regularization is given in [52], and we reproduce it here for completeness,

$$\Phi_{d,g,\text{SV}}^A = \sum_{i=1}^{\infty} \hat{a}_s^i \left( \frac{q^2 \bar{z}_1 \bar{z}_2}{\mu^2} \right)^{i\epsilon} S_\epsilon^i \left[ \frac{(i\epsilon)^2}{4\bar{z}_1 \bar{z}_2} \hat{\phi}_{d,g}^{A,(i)}(\epsilon) \right], \quad (58)$$

with

$$\hat{\phi}_{d,g}^{A,(i)}(\epsilon) = \frac{1}{i\epsilon} [\bar{K}_{d,g}^{A,(i)}(\epsilon) + \bar{G}_{d,g,\text{SV}}^{A,(i)}(\epsilon)]. \quad (59)$$

The constants  $\bar{K}_{d,g}^{A,(i)}(\epsilon)$  are determined by expanding  $\bar{K}_{d,g}^A$  in powers of  $\hat{a}_s$  as follows:

$$\bar{K}_{d,g}^A \left( \hat{a}_s, \frac{\mu_R^2}{\mu^2}, z_1, z_2, \epsilon \right) = \delta(1-z_1)\delta(1-z_2) \sum_{i=1}^{\infty} \hat{a}_s^i \left( \frac{\mu_R^2}{\mu^2} \right)^{i\epsilon} S_\epsilon^i \bar{K}_{d,g}^{A,(i)}(\epsilon), \quad (60)$$

and solving the RGE (56) for  $\bar{K}_{d,g}^A$ . The constants  $\bar{K}_{d,g}^{A,(i)}(\epsilon)$  are related to the constants  $K_{d,g}^{A,(i)}(\epsilon)$  which appear in the form factor by  $\bar{K}_{d,g}^{A,(i)}(\epsilon) = K_{d,g}^{A,(i)}(\epsilon)|_{A_g^+ \rightarrow -A_g^+}$ , due to the IR pole cancellation.  $\bar{G}_{d,g,\text{SV}}^{A,(i)}(\epsilon)$  are related to the finite functions  $\bar{G}_{d,g,\text{SV}}^A(a_s(q^2), 1, z_1, z_2, \epsilon)$ . In terms of renormalized coupling constant, we find

$$\sum_{i=1}^{\infty} \hat{a}_s^i \left( \frac{q^2(1-z_1)(1-z_2)}{\mu^2} \right)^{i\epsilon} S_\epsilon^i \bar{G}_{d,g,\text{SV}}^{A,(i)}(\epsilon) = \sum_{i=1}^{\infty} a_s^i(q^2(1-z_1)(1-z_2)) \bar{G}_{d,g,i}^A(\epsilon). \quad (61)$$

Using  $\bar{K}_{d,g}^{A,(i)}$  from Eq. (60) after putting the explicit values of  $A_g^A$  and  $\bar{G}_{d,g,\text{SV}}^{A,(i)}$  from Eq. (61), we find that  $\hat{\phi}_{d,g}^{A,(i)}(\epsilon)$  in  $\Phi_{d,g,\text{SV}}^A$  up to third order in  $\hat{a}_s$  takes the following form:

$$\begin{aligned} \hat{\phi}_{d,g}^{A,(1)}(\epsilon) &= \frac{1}{\epsilon^2} 8C_A + \frac{1}{\epsilon} \bar{G}_{d,g,1}^A(\epsilon), \\ \hat{\phi}_{d,g}^{A,(2)}(\epsilon) &= \frac{1}{\epsilon^3} \left\{ C_A n_f \left( \frac{8}{3} \right) + C_A^2 \left( -\frac{44}{3} \right) \right\} + \frac{1}{\epsilon^2} \left\{ n_f \left( \frac{2}{3} \bar{G}_{d,g,1}^A(\epsilon) \right) + C_A \left( -\frac{11}{3} \bar{G}_{d,g,1}^A(\epsilon) \right) \right. \\ &\quad \left. + C_A n_f \left( -\frac{20}{9} \right) + C_A^2 \left( \frac{134}{9} - 4\zeta_2 \right) \right\} + \frac{1}{2\epsilon} \bar{G}_{d,g,2}^A(\epsilon), \\ \hat{\phi}_{d,g}^{A,(3)}(\epsilon) &= \frac{1}{\epsilon^4} \left\{ C_A n_f^2 \left( \frac{128}{81} \right) + C_A^2 n_f \left( -\frac{1408}{81} \right) + C_A^3 \left( \frac{3872}{81} \right) \right\} + \frac{1}{\epsilon^3} \left\{ n_f^2 \left( \frac{16}{27} \bar{G}_{d,g,1}^A(\epsilon) \right) \right. \\ &\quad \left. + C_A n_f \left( -\frac{176}{27} \bar{G}_{d,g,1}^A(\epsilon) \right) + C_A n_f^2 \left( -\frac{640}{243} \right) + C_A C_F n_f \left( \frac{16}{9} \right) + C_A^2 \left( \frac{484}{27} \bar{G}_{d,g,1}^A(\epsilon) \right) \right. \\ &\quad \left. + C_A^2 n_f \left( \frac{8528}{243} - \frac{128}{27} \zeta_2 \right) + C_A^3 \left( -\frac{26032}{243} + \frac{704}{27} \zeta_2 \right) \right\} + \frac{1}{\epsilon^2} \left\{ n_f \left( \frac{8}{9} \bar{G}_{d,g,2}^A(\epsilon) \right) \right. \\ &\quad \left. + C_F n_f \left( \frac{2}{3} \bar{G}_{d,g,1}^A(\epsilon) \right) + C_A \left( -\frac{44}{9} \bar{G}_{d,g,2}^A(\epsilon) \right) + C_A n_f \left( \frac{10}{9} \bar{G}_{d,g,1}^A(\epsilon) \right) + C_A n_f^2 \left( -\frac{32}{243} \right) \right. \\ &\quad \left. + C_A C_F n_f \left( -\frac{220}{27} + \frac{64}{9} \zeta_3 \right) + C_A^2 \left( -\frac{34}{9} \bar{G}_{d,g,1}^A(\epsilon) \right) + C_A^2 n_f \left( -\frac{1672}{243} - \frac{224}{27} \zeta_3 \right) \right. \\ &\quad \left. + \frac{320}{81} \zeta_2 \right\} + C_A^3 \left( \frac{980}{27} + \frac{176}{27} \zeta_3 - \frac{2144}{81} \zeta_2 + \frac{352}{45} \zeta_2^2 \right) \left. \right\} + \frac{1}{3\epsilon} \bar{G}_{d,g,3}^A(\epsilon). \quad (62) \end{aligned}$$

In the above equations,  $\bar{G}_{d,g,i}^A(\epsilon)$  are parametrized as follows:

$$\bar{G}_{d,g,i}^A(\epsilon) = -f_{g,i}^A + \sum_{k=0}^{\infty} \epsilon^k \bar{G}_{d,g,i}^{A,(k)}, \quad (63)$$

where

$$\begin{aligned}\bar{\mathcal{G}}_{d,g,1}^{A,(0)} &= 0, & \bar{\mathcal{G}}_{d,g,2}^{A,(0)} &= -2\beta_0\bar{\mathcal{G}}_{d,g,1}^{A,(1)}, \\ \bar{\mathcal{G}}_{d,g,3}^{A,(0)} &= -2\beta_1\bar{\mathcal{G}}_{d,g,1}^{A,(1)} - 2\beta_0(\bar{\mathcal{G}}_{d,g,2}^{A,(1)} + 2\beta_0\bar{\mathcal{G}}_{d,g,1}^{A,(2)}).\end{aligned}\quad (64)$$

The unknown constants  $\bar{\mathcal{G}}_{d,g,i}^{A,(k)}$  are determined in the next section.

Let us now study in detail the structure of  $\Phi_{d,g,NSV}^A$  using the Eq. (54). Subtracting out the K + G equation for the SV part  $\Phi_{d,g,SV}^A$  from Eq. (54), we find that  $\Phi_{d,g,NSV}^A$  satisfies

$$q^2 \frac{d}{dq^2} \Phi_{d,g,NSV}^A(q^2, z_1, z_2, \varepsilon) = \frac{1}{2} \left[ \bar{\mathcal{G}}_{d,g,NSV}^A \left( \hat{a}_s, \frac{q^2}{\mu_R^2}, \frac{\mu_R^2}{\mu^2}, \varepsilon, z_1, z_2 \right) \right], \quad (65)$$

where  $\bar{\mathcal{G}}_{d,g,NSV}^A = \bar{\mathcal{G}}_{d,g}^A - \bar{\mathcal{G}}_{d,g,SV}^A$ . Now, solving the above differential equation, we obtain the following all order structure for  $\Phi_{d,g,NSV}^A$

$$\Phi_{d,g,NSV}^A = \sum_{i=1}^{\infty} \hat{a}_s^i \left( \frac{q^2 \bar{z}_1 \bar{z}_2}{\mu^2} \right)^{i\frac{\varepsilon}{2}} S_\varepsilon^i \left[ \frac{i\varepsilon}{4\bar{z}_1} \varphi_{d,g}^{A,(i)}(\bar{z}_2, \varepsilon) + \frac{i\varepsilon}{4\bar{z}_2} \varphi_{d,g}^{A,(i)}(\bar{z}_1, \varepsilon) \right], \quad (66)$$

with

$$\varphi_{d,g}^{A,(i)}(\bar{z}_j, \varepsilon) = \frac{1}{i\varepsilon} [\bar{\mathcal{G}}_{d,g,NSV}^{A,(i)}(\bar{z}_j, \varepsilon)]. \quad (67)$$

$\bar{\mathcal{G}}_{d,g,NSV}^{A,(i)}(\bar{z}_j, \varepsilon)$  are related to the finite function  $\bar{\mathcal{G}}_{d,g,NSV}^A(a_s(q^2), 1, z_1, z_2, \varepsilon)$  through the NSV logarithms  $\log^k(1 - z_j)$ . Defining  $\bar{\mathcal{G}}_{d,L,i}^{A,g}(\bar{z}_j, \varepsilon)$  through

$$\sum_{i=1}^{\infty} \hat{a}_s^i \left( \frac{q^2 \bar{z}_j}{\mu^2} \right)^{i\frac{\varepsilon}{2}} S_\varepsilon^i \bar{\mathcal{G}}_{d,g,NSV}^{A,(i)}(\bar{z}_j, \varepsilon) = \sum_{i=1}^{\infty} a_s^i(q^2 \bar{z}_j) \bar{\mathcal{G}}_{d,L,i}^{A,g}(\bar{z}_j, \varepsilon). \quad (68)$$

we find

$$\begin{aligned}\bar{\mathcal{G}}_{d,g,NSV}^{A,(1)}(\bar{z}_j, \varepsilon) &= \bar{\mathcal{G}}_{d,L,1}^{A,g}(\bar{z}_j, \varepsilon), \\ \bar{\mathcal{G}}_{d,g,NSV}^{A,(2)}(\bar{z}_j, \varepsilon) &= \frac{1}{\varepsilon} (-2\beta_0 \bar{\mathcal{G}}_{d,L,1}^{A,g}(\bar{z}_j, \varepsilon)) + \bar{\mathcal{G}}_{d,L,2}^{A,g}(\bar{z}_j, \varepsilon), \\ \bar{\mathcal{G}}_{d,g,NSV}^{A,(3)}(\bar{z}_j, \varepsilon) &= \frac{1}{\varepsilon^2} (4\beta_0^2 \bar{\mathcal{G}}_{d,L,1}^{A,g}(\bar{z}_j, \varepsilon)) + \frac{1}{\varepsilon} (-\beta_1 \bar{\mathcal{G}}_{d,L,1}^{A,g}(\bar{z}_j, \varepsilon) - 4\beta_0 \bar{\mathcal{G}}_{d,L,2}^{A,g}(\bar{z}_j, \varepsilon)) \\ &\quad + \bar{\mathcal{G}}_{d,L,3}^{A,g}(\bar{z}_j, \varepsilon).\end{aligned}\quad (69)$$

Using (67) and (69), we obtain

$$\begin{aligned}\varphi_{d,g}^{A,(1)}(\bar{z}_j, \varepsilon) &= \frac{1}{\varepsilon} \bar{\mathcal{G}}_{d,L,1}^{A,g}(\bar{z}_j, \varepsilon) \\ \varphi_{d,g}^{A,(2)}(\bar{z}_j, \varepsilon) &= \frac{1}{\varepsilon^2} \left\{ n_f \left( \frac{2}{3} \bar{\mathcal{G}}_{d,L,1}^{A,g}(\bar{z}_j, \varepsilon) \right) + C_A \left( -\frac{11}{3} \bar{\mathcal{G}}_{d,L,1}^{A,g}(\bar{z}_j, \varepsilon) \right) \right\} + \frac{1}{2\varepsilon} \bar{\mathcal{G}}_{d,L,2}^{A,g}(\bar{z}_j, \varepsilon) \\ \varphi_{d,g}^{A,(3)}(\bar{z}_j, \varepsilon) &= \frac{1}{\varepsilon^3} \left\{ n_f^2 \left( \frac{16}{27} \bar{\mathcal{G}}_{d,L,1}^{A,g}(\bar{z}_j, \varepsilon) \right) + C_A n_f \left( -\frac{176}{27} \bar{\mathcal{G}}_{d,L,1}^{A,g}(\bar{z}_j, \varepsilon) \right) + C_A^2 \left( \frac{484}{27} \bar{\mathcal{G}}_{d,L,1}^{A,g}(\bar{z}_j, \varepsilon) \right) \right\} \\ &\quad + \frac{1}{\varepsilon^2} \left\{ n_f \left( \frac{8}{9} \bar{\mathcal{G}}_{d,L,2}^{A,g}(\bar{z}_j, \varepsilon) \right) + C_F n_f \left( \frac{2}{3} \bar{\mathcal{G}}_{d,L,1}^{A,g}(\bar{z}_j, \varepsilon) \right) + C_A \left( -\frac{44}{9} \bar{\mathcal{G}}_{d,L,2}^{A,g}(\bar{z}_j, \varepsilon) \right) \right\} \\ &\quad + C_A n_f \left( \frac{10}{9} \bar{\mathcal{G}}_{d,L,1}^{A,g}(\bar{z}_j, \varepsilon) \right) + C_A^2 \left( -\frac{34}{9} \bar{\mathcal{G}}_{d,L,1}^{A,g}(\bar{z}_j, \varepsilon) \right) \left\} + \frac{1}{3\varepsilon} \bar{\mathcal{G}}_{d,L,3}^{A,g}(\bar{z}_j, \varepsilon).\end{aligned}\quad (70)$$

Here,  $\bar{\mathcal{G}}_{d,L,i}^{A,g}(\bar{z}, \epsilon)$  are expanded in powers of  $\epsilon$  as

$$\bar{\mathcal{G}}_{d,L,i}^{A,g}(\bar{z}_j, \epsilon) = 2L_{g,i}^A(a_s, \bar{z}_l) + \sum_{k=0}^{\infty} \epsilon^k \bar{\mathcal{G}}_{d,L,i}^{A,g,(k)}(\bar{z}_j), \quad (71)$$

with

$$\begin{aligned} \bar{\mathcal{G}}_{d,L,1}^{A,g,(0)}(\bar{z}_j) &= 0, \quad \bar{\mathcal{G}}_{d,L,2}^{A,g,(0)}(\bar{z}_j) = -2\beta_0 \bar{\mathcal{G}}_{d,L,1}^{A,g,(1)}(\bar{z}_j), \\ \bar{\mathcal{G}}_{d,L,3}^{A,g,(0)}(\bar{z}_j) &= -2\beta_1 \bar{\mathcal{G}}_{d,L,1}^{A,g,(1)}(\bar{z}_j) - 2\beta_0 (\bar{\mathcal{G}}_{d,L,2}^{A,g,(1)}(\bar{z}_j) + 2\beta_0 \bar{\mathcal{G}}_{d,L,1}^{A,g,(2)}(\bar{z}_j)). \end{aligned} \quad (72)$$

The anomalous dimensions  $L_{g,i}^A$  can be determined by demanding finiteness of  $\Delta_{d,g}^A$ , and it turns out that it is half of NSV part of the AP splitting functions (see Ref. [82]), that is,

$$L_{g,i}^A(a_s, \bar{z}_l) = C_{g,i}^A(a_s) \log(1 - z_l) + D_{g,i}^A(a_s). \quad (73)$$

The coefficients  $\bar{\mathcal{G}}_{d,L,i}^{A,g,(j)}(\bar{z}_j)$  in the above equations are parametrised in terms of  $\log^k(1 - z_j)$ ,  $k = 0, 1, \dots$  and all the terms that vanish as  $z_j \rightarrow 1$  are dropped.

$$\bar{\mathcal{G}}_{d,L,i}^{A,g,(j)}(\bar{z}_j) = \sum_{k=0}^{i+j-1} \bar{\mathcal{G}}_{d,L,i}^{A,g,(j,k)} \log^k(1 - z_j). \quad (74)$$

The highest power of the  $\log(1 - z_j)$  at every order depends on the order of the perturbation, namely, the power of  $a_s$  and also the power of  $\epsilon$  at each order in  $a_s$ . Hence, the summation runs from 0 to  $i + j - 1$ .

Next, we obtain an integral representation of  $\Phi_{d,g,\text{SV}}^A$  which is given by

$$\begin{aligned} \Phi_{d,g,\text{SV}}^A &= \frac{1}{2} \delta(\bar{z}_2) \left( \frac{1}{\bar{z}_1} \left\{ \int_{\mu_F^2}^{q^2 \bar{z}_1} \frac{d\lambda^2}{\lambda^2} A_g^A(a_s(\lambda^2)) + \bar{G}_{d,g,\text{SV}}^A(a_s(q_1^2), \epsilon) \right\} \right)_+ \\ &+ q^2 \frac{d}{dq^2} \left[ \left( \frac{1}{4\bar{z}_1 \bar{z}_2} \left\{ \int_{\mu_F^2}^{q^2 \bar{z}_1 \bar{z}_2} \frac{d\lambda^2}{\lambda^2} A_g^A(a_s(\lambda^2)) + \bar{G}_{d,g,\text{SV}}^A(a_s(q_{12}^2), \epsilon) \right\} \right)_+ \right] \\ &+ \frac{1}{2} \delta(\bar{z}_1) \delta(\bar{z}_2) \sum_{i=1}^{\infty} \hat{a}_s^i \left( \frac{q^2}{\mu^2} \right)^{i\frac{5}{2}} S_\epsilon^i \hat{\phi}_{d,g}^{A,(i)}(\epsilon) + \frac{1}{2} \delta(\bar{z}_2) \left( \frac{1}{\bar{z}_1} \right)_+ \sum_{i=1}^{\infty} \hat{a}_s^i \left( \frac{\mu_F^2}{\mu^2} \right)^{i\frac{5}{2}} S_\epsilon^i K_g^{A,(i)}(\epsilon) + (z_1 \leftrightarrow z_2), \end{aligned} \quad (75)$$

where  $q_1^2 = q^2(1 - z_1)$  and  $q_{12}^2 = q^2 \bar{z}_1 \bar{z}_2$ . The subscript  $+$  indicates the standard plus distribution. Similarly, we find an integral representation of the NSV part,  $\Phi_{d,g,\text{NSV}}^A$  which reads as

$$\begin{aligned} \Phi_{d,g,\text{NSV}}^A &= \frac{1}{2} \delta(\bar{z}_2) \left( \left\{ \int_{\mu_F^2}^{q^2 \bar{z}_1} \frac{d\lambda^2}{\lambda^2} L_g^A(a_s(\lambda^2), \bar{z}_1) + \varphi_{d,f,g}^A(a_s(q_2^2), \bar{z}_1, \epsilon) \right\} \right) \\ &+ q^2 \frac{d}{dq^2} \left[ \left( \frac{1}{2(\bar{z}_2)} \left\{ \int_{\mu_F^2}^{q^2 \bar{z}_1 \bar{z}_2} \frac{d\lambda^2}{\lambda^2} L_g^A(a_s(\lambda^2), \bar{z}_1) + \varphi_{d,f,g}^A(a_s(q_{12}^2), \bar{z}_1, \epsilon) \right\} \right)_+ \right] \\ &+ \frac{1}{2} \delta(\bar{z}_2) \varphi_{d,s,g}^A(\bar{z}_1, \epsilon) + (z_1 \leftrightarrow z_2), \end{aligned} \quad (76)$$

where

$$\varphi_{d,a,g}^A(a_s(\lambda^2), \bar{z}_l) = \sum_{i=1}^{\infty} \hat{a}_s^i \left( \frac{\lambda^2}{\mu^2} \right)^{i\frac{5}{2}} S_\epsilon^i \varphi_{d,a,g}^{A,(i)}(z_l, \epsilon) \quad a = f, s. \quad (77)$$

$\varphi_{d,s,g}^A$  is the singular part of the NSV solution. The finite part  $\varphi_{d,f,g}^A$  is parametrized in the following way:

$$\begin{aligned}\varphi_{d,f,g}^A(a_s(\lambda^2), \bar{z}_l) &= \sum_{i=1}^{\infty} \sum_{k=0}^{\infty} \hat{a}_s^i \left( \frac{\lambda^2}{\mu^2} \right)^{i\frac{\epsilon}{2}} S_\epsilon^i \varphi_{d,g}^{A,(i,k)}(\epsilon) \ln^k \bar{z}_l, \\ &= \sum_{i=1}^{\infty} \sum_{k=0}^i a_s^i(\lambda^2) \varphi_{d,g,i}^{A,(k)} \ln^k \bar{z}_l.\end{aligned}\quad (78)$$

The upper limit on the sum over  $k$  is controlled by the dimensionally regularized Feynman integrals that contribute to order  $a_s^i$ .

## V. MATCHING WITH THE INCLUSIVE

The unknown coefficients of both SV and NSV solutions of  $\Phi_{d,g}^A$ , namely,  $\bar{\mathcal{G}}_{d,g,i}^{A,(k)}$  and  $\varphi_{d,g,i}^{A,(k)}$  can be determined using the fixed order predictions of  $\Delta_{d,g}^A$ , at every order in perturbation theory. However, it can also be determined alternatively from the corresponding inclusive cross section using the relation

$$\int_0^1 dx_1^0 \int_0^1 dx_2^0 (x_1^0 x_2^0)^{N-1} \frac{d\sigma^A}{dy} = \int_0^1 d\tau \tau^{N-1} \sigma^A, \quad (79)$$

where  $\sigma^A$  is the inclusive cross section. This relation in the large  $N$  limit gives

$$\begin{aligned}\sum_{i=1}^{\infty} \hat{a}_s^i \left( \frac{q^2}{\mu^2} \right)^{i\frac{\epsilon}{2}} S_\epsilon^i \left[ t_1^i(\epsilon) \hat{\phi}_{d,g}^{A,(i)}(\epsilon) - t_2^i(\epsilon) \hat{\phi}_g^{A,(i)}(\epsilon) \right. \\ \left. + \sum_{k=0}^{\infty} (t_3^{(i,k)}(\epsilon) \varphi_{d,g}^{A,(i,k)}(\epsilon) - t_4^{(i,k)}(\epsilon) \varphi_g^{A,(i,k)}(\epsilon)) \right] = 0,\end{aligned}\quad (80)$$

where

$$\begin{aligned}t_1^i &= \frac{i\epsilon(2-i\epsilon)}{4N^{i\epsilon}} \Gamma^2 \left( 1 + i\frac{\epsilon}{2} \right), \\ t_2^i &= \frac{i\epsilon(1-i\epsilon)}{2N^{i\epsilon}} \Gamma(1+i\epsilon), \\ t_3^{(i,k)} &= \Gamma \left( 1 + i\frac{\epsilon}{2} \right) \frac{\partial^k}{\partial \alpha^k} \left( \frac{\Gamma(1+\alpha)}{N^{\alpha+i\epsilon/2}} \right)_{\alpha=i\frac{\epsilon}{2}}, \\ t_4^{(i,k)} &= \frac{\partial^k}{\partial \hat{\alpha}^k} \left( \frac{\Gamma(1+\hat{\alpha})}{N^{\hat{\alpha}}} \right)_{\hat{\alpha}=i\epsilon}.\end{aligned}\quad (81)$$

Here, we keep  $\ln^k N$  as well as  $\mathcal{O}(1/N)$  terms for the determination of the SV and NSV coefficients. The constants  $\hat{\phi}_g^{A,(i)}$  and  $\varphi_g^{A,(i,k)}$  are the inclusive counterparts to the SV and NSV coefficients  $\hat{\phi}_{d,g}^{A,(i)}$  and  $\varphi_{d,g}^{A,(i,k)}$ , respectively, which are known to third order in QCD for Drell-Yan, for Higgs production in gluon fusion and in bottom quark annihilation (for NSV see Ref. [78]).

Using the above relations in Eq. (80), the SV coefficients  $\bar{\mathcal{G}}_{d,g,i}^{A,(k)}$  up to second order are found to be

$$\begin{aligned}\bar{\mathcal{G}}_{d,g,1}^{A,(1)} &= C_A(-\zeta_2), \\ \bar{\mathcal{G}}_{d,g,1}^{A,(2)} &= C_A \left( \frac{1}{3} \zeta_3 \right), \\ \bar{\mathcal{G}}_{d,g,1}^{A,(3)} &= C_A \left( \frac{1}{80} \zeta_2^2 \right), \\ \bar{\mathcal{G}}_{d,g,2}^{A,(1)} &= C_A^2 \left( \frac{2428}{81} - \frac{67}{3} \zeta_2 - 4\zeta_2^2 - \frac{44}{3} \zeta_3 \right) \\ &\quad + C_A n_f \left( -\frac{328}{81} + \frac{10}{3} \zeta_2 + \frac{8}{3} \zeta_3 \right).\end{aligned}\quad (82)$$

Note that the above SV coefficients are identical to the corresponding SV coefficients of scalar Higgs given in Eq. (35) of [52]. This universality nature of SV coefficients  $\bar{\mathcal{G}}_{d,g,i}^{A,(k)}$  is expected to hold to all orders in perturbation theory because of the fact that it originates entirely from the soft part of the differential cross section. Further, this property has been explicitly verified to third order in QCD perturbation theory [33] for the case of inclusive cross section. The explicit expressions for NSV coefficients  $\varphi_{d,g,i}^{A,(k)}$  for the pseudoscalar production in gluon fusion can be obtained from the corresponding results for inclusive coefficients  $\varphi_{g,i}^{A,(k)}$  given in [85]. The results up to second order are provided below,

$$\begin{aligned}\varphi_{d,g,1}^{A,(0)} &= 2C_A, \\ \varphi_{d,g,1}^{A,(1)} &= 0, \\ \varphi_{d,g,2}^{A,(0)} &= C_A n_f \left( -\frac{136}{27} + \frac{8}{3} \zeta_2 \right) \\ &\quad + C_A^2 \left( \frac{904}{27} - 28\zeta_3 - \frac{104}{3} \zeta_2 \right), \\ \varphi_{d,g,2}^{A,(1)} &= C_A n_f \left( -\frac{2}{3} \right) + C_A^2 \left( \frac{2}{3} \right), \\ \varphi_{d,g,2}^{A,(2)} &= -4C_A^2.\end{aligned}\quad (83)$$

We notice that the NSV coefficients  $\varphi_{d,g,i}^{A,(k)}$  of the pseudoscalar Higgs are also identical to the corresponding NSV coefficients of scalar Higgs up to second order in  $a_s$  [82,84].

## VI. RESULTS OF THE SV AND NSV RAPIDITY DISTRIBUTIONS

In this section, we present the analytic results of the SV and NSV rapidity distributions,  $\Delta_{d,g}^{A,SV}$  and  $\Delta_{d,g}^{A,NSV}$ , respectively, at the partonic level to N<sup>3</sup>LO in QCD. By expanding the formula in Eq. (29) in powers of  $a_s$  and substituting the explicit expressions for all the anomalous dimensions, also the SV and NSV coefficients, we find, at  $a_s$  order,

$$\Delta_{d,g,1}^{A,NSV} = L_{z_1} \{C_A(-4\bar{\delta})\} + \bar{D}_0 \{C_A(-4)\} + C_A \{2\bar{\delta}\} + (z_1 \leftrightarrow z_2), \quad (84)$$

and at  $a_s^2$  order,

$$\begin{aligned} \Delta_{d,g,2}^{A,NSV} = & L_{z_1}^3 \{C_A^2(-8\bar{\delta})\} + L_{z_1}^2 \left\{ C_A^2(-24\bar{D}_0) + \bar{\delta} \left[ C_A n_f \left( -\frac{4}{3} \right) + C_A^2 \left( \frac{94}{3} \right) \right] \right\} + L_{z_1} \left\{ \bar{D}_0 \left[ C_A n_f \left( -\frac{8}{3} \right) \right. \right. \\ & \left. \left. + C_A^2 \left( \frac{164}{3} \right) \right] + C_A^2(-48\bar{D}_1) + \bar{\delta} \left[ C_A n_f \left( \frac{46}{9} \right) + C_A^2 \left( -\frac{616}{9} - 8\zeta_2 \right) \right] \right\} + \bar{D}_0 \left\{ C_A n_f \left( \frac{52}{9} \right) \right. \\ & \left. + C_A^2 \left( -\frac{622}{9} - 8\zeta_2 \right) \right\} + \bar{D}_1 \left\{ C_A n_f \left( -\frac{8}{3} \right) + C_A^2 \left( \frac{116}{3} \right) \right\} + \bar{D}_2 \{-24C_A^2\} \\ & \left. + \bar{\delta} \left\{ C_A n_f \left( -\frac{136}{27} + \frac{8}{3}\zeta_2 \right) + C_A^2 \left( \frac{1336}{27} - 60\zeta_3 - \frac{80}{3}\zeta_2 \right) \right\} + (z_1 \leftrightarrow z_2). \end{aligned} \quad (85)$$

In the above expressions,  $L_{z_1} = \ln(\bar{z}_1)$ ,  $\bar{\delta} = \delta(\bar{z}_2)$ ,  $\bar{D}_j = \frac{\ln^j(\bar{z}_2)}{(\bar{z}_2)_+}$ , and  $\zeta_2 = 1.6449 \dots$  and  $\zeta_3 = 1.20205 \dots$ .

Next at  $a_s^3$ , the CF requires the third order NSV coefficients  $\varphi_{d,g,3}^{A,(k)}$  with  $k = 0, 1, 2, 3$ . Since the full  $N^3$ LO results for both inclusive and rapidity distribution of pseudoscalar Higgs are not available, we could not extract these NSV coefficients either directly from the rapidity results or by matching with the inclusive results. However, we apply the same ratio method discussed in Sec. III A on the SV + NSV results of scalar Higgs rapidity distribution computed in [82] to obtain the third order CF of pseudoscalar Higgs at SV + NSV accuracy. At  $a_s^3$ , we find

$$\begin{aligned} \Delta_{d,g,3}^{A,NSV} = & L_{z_1}^5 \{C_A^3(-8\bar{\delta})\} + L_{z_1}^4 \left\{ C_A^3(-40\bar{D}_0) + \bar{\delta} \left[ C_A^3 \left( \frac{616}{9} \right) + n_f C_A^2 \left( -\frac{40}{9} \right) \right] \right\} + L_{z_1}^3 \left\{ \bar{D}_0 \left[ C_A^3 \left( \frac{2320}{9} \right) \right. \right. \\ & \left. \left. + n_f C_A^2 \left( -\frac{160}{9} \right) \right] - C_A^3(160\bar{D}_1) + \bar{\delta} \left[ C_A^3 \left( -\frac{2560}{9} + 64\zeta_2 \right) + n_f C_A^2 \left( \frac{1036}{27} \right) + n_f^2 C_A \left( -\frac{16}{27} \right) \right] \right\} \\ & + L_{z_1}^2 \left\{ \bar{D}_0 \left[ C_A^3 \left( -\frac{7516}{9} + 192\zeta_2 \right) + n_f C_A^2 \left( \frac{1016}{9} \right) + n_f^2 C_A \left( -\frac{16}{9} \right) \right] + \bar{D}_1 \left[ C_A^3 \left( \frac{2128}{3} \right) + n_f C_A^2 \left( -\frac{160}{3} \right) \right] \right. \\ & \left. - C_A^3(240\bar{D}_2) + \bar{\delta} \left[ C_A^3 \left( \frac{24982}{27} - 488\zeta_3 - 400\zeta_2 \right) + n_f C_A^2 \left( -\frac{3668}{27} + 38\zeta_2 \right) - 4C_A C_F n_f + n_f^2 C_A \left( \frac{88}{27} \right) \right] \right\} \\ & + L_{z_1} \left\{ \bar{D}_0 \left[ C_A^3 \left( \frac{44800}{27} - 976\zeta_3 - \frac{2288}{3}\zeta_2 \right) + n_f C_A^2 \left( -\frac{6860}{27} + \frac{224}{3}\zeta_2 \right) - 8C_A C_F n_f + n_f^2 C_A \left( \frac{184}{27} \right) \right] \right. \\ & \left. + \bar{D}_1 \left[ C_A^3 \left( -\frac{14528}{9} + 384\zeta_2 \right) + n_f C_A^2 \left( \frac{1960}{9} \right) + n_f^2 C_A \left( -\frac{32}{9} \right) \right] + \bar{D}_2 \left[ C_A^3 \left( \frac{1888}{3} \right) + n_f C_A^2 \left( -\frac{160}{3} \right) \right] \right. \\ & \left. + C_A^3(-160\bar{D}_3) + \bar{\delta} \left[ C_A^3 \left( -\frac{145670}{81} + \frac{4936}{3}\zeta_3 + 336\zeta_2 + \frac{64}{5}\zeta_2^2 \right) + n_f C_A^2 \left( \frac{8528}{27} - 40\zeta_3 - \frac{920}{9}\zeta_2 \right) \right. \right. \\ & \left. \left. + C_A C_F n_f \left( 258 - 48 \ln \left( \frac{\mu_R^2}{m_t^2} \right) - 96\zeta_3 - \frac{8}{3}\zeta_2 \right) + n_f^2 C_A \left( -\frac{328}{81} + \frac{32}{9}\zeta_2 \right) \right] \right\} + \bar{D}_0 \left[ C_A^3 \left( -\frac{127114}{81} + 1400\zeta_3 \right. \right. \\ & \left. \left. + \frac{2200}{9}\zeta_2 + \frac{64}{5}\zeta_2^2 \right) + n_f C_A^2 \left( \frac{24488}{81} - 32\zeta_3 - \frac{232}{3}\zeta_2 \right) + C_A C_F n_f \left( 254 - 48 \ln \left( \frac{\mu_R^2}{m_t^2} \right) - 96\zeta_3 \right) \right. \\ & \left. \left. + n_f^2 C_A \left( -\frac{496}{81} + \frac{32}{9}\zeta_2 \right) \right] + \bar{D}_1 \left[ C_A^3 \left( \frac{35044}{27} - 976\zeta_3 - \frac{2384}{3}\zeta_2 \right) + n_f C_A^2 \left( -\frac{6056}{27} + \frac{224}{3}\zeta_2 \right) - 8C_A C_F n_f \right. \right. \end{aligned}$$

$$\begin{aligned}
& + n_f^2 C_A \left( \frac{208}{27} \right) \Big] + \bar{\mathcal{D}}_2 \left[ C_A^3 \left( -\frac{6748}{9} + 192\zeta_2 \right) + n_f C_A^2 \left( \frac{896}{9} \right) + n_f^2 C_A \left( -\frac{16}{9} \right) \right] + \bar{\mathcal{D}}_3 \left[ C_A^3 \left( \frac{1600}{9} \right) \right. \\
& + n_f C_A^2 \left( -\frac{160}{9} \right) + C_A^3 (-40\bar{\mathcal{D}}_4) \Big] + \bar{\delta} \left[ C_A^3 \left( \frac{859052}{729} - 192\zeta_5 - \frac{51068}{27}\zeta_3 - \frac{64400}{81}\zeta_2 + \frac{608}{3}\zeta_2\zeta_3 - 128\zeta_2^2 \right) \right. \\
& + n_f C_A^2 \left( -\frac{150088}{729} + \frac{488}{3}\zeta_3 + \frac{12200}{81}\zeta_2 + \frac{88}{15}\zeta_2^2 \right) + C_A C_F n_f \left( -\frac{5038}{27} + 24 \ln \left( \frac{\mu_R^2}{m_t^2} \right) + \frac{760}{9}\zeta_3 + \frac{16}{3}\zeta_2 + \frac{32}{5}\zeta_2^2 \right) \\
& \left. + n_f^2 C_A \left( -\frac{232}{729} + \frac{32}{27}\zeta_3 - \frac{176}{27}\zeta_2 \right) \right] + (z_1 \leftrightarrow z_2). \tag{86}
\end{aligned}$$

Now, using the above result of  $\Delta_{d,g,3}^{A,\text{NSV}}$  at  $a_s^3$ , we extract the NSV coefficients  $\varphi_{d,g,3}^{A,(k)}$  with  $k = 0, 1, 2, 3$ , and they are given by

$$\begin{aligned}
\varphi_{d,g,3}^{A,(0)} &= C_A n_f^2 \left( -\frac{232}{729} + \frac{32}{27}\zeta_3 - \frac{176}{27}\zeta_2 \right) + C_A^2 n_f \left( -\frac{80860}{729} + \frac{704}{9}\zeta_3 + \frac{11960}{81}\zeta_2 - \frac{24}{5}\zeta_2^2 \right) + C_A^3 \left( \frac{423704}{729} + 192\zeta_5 \right. \\
& \quad \left. - \frac{18188}{27}\zeta_3 - \frac{55448}{81}\zeta_2 + \frac{176}{3}\zeta_2\zeta_3 + \frac{1384}{15}\zeta_2^2 + C_F C_A n_f \left( -\frac{2158}{27} + \frac{472}{9}\zeta_3 + \frac{16}{3}\zeta_2 + \frac{32}{5}\zeta_2^2 \right) \right), \\
\varphi_{d,g,3}^{A,(1)} &= C_A n_f^2 \left( \frac{56}{27} \right) + C_A^2 n_f \left( \frac{1528}{81} - 8\zeta_3 - \frac{152}{9}\zeta_2 \right) + C_A^3 \left( -\frac{18988}{81} + \frac{448}{3}\zeta_3 + \frac{752}{9}\zeta_2 \right) + C_F C_A n_f \left( 4 - \frac{8}{3}\zeta_2 \right), \\
\varphi_{d,g,3}^{A,(2)} &= C_A n_f^2 \left( \frac{8}{27} \right) + C_A^2 n_f \left( \frac{164}{27} + \frac{2}{3}\zeta_2 \right) + C_A^3 \left( -\frac{1432}{27} + \frac{40}{3}\zeta_2 \right), \\
\varphi_{d,g,3}^{A,(3)} &= C_A^2 n_f \left( \frac{32}{27} \right) + C_A^3 \left( -\frac{176}{27} \right). \tag{87}
\end{aligned}$$

Here, we notice that the above NSV coefficients are same for both pseudoscalar and scalar Higgs production via gluon fusion [82]. However, the universality of  $\varphi_{d,g,3}^{A,(k)}$  at third order can be checked only when the explicit N<sup>3</sup>LO results are available for the pseudoscalar Higgs boson production in gluon fusion. The results of SV rapidity distributions to N<sup>3</sup>LO can be found in Appendix D.

## VII. MORE ON THE $\bar{z}$ SPACE SOLUTION $\Phi_{d,g}^A$

In the following, we discuss in detail the characteristic structure of SV and NSV solutions given in (58) and (68), respectively. Both the SV and NSV parts of  $\Phi_{d,g}^A$  satisfy the K + G equation, and they contain singular as well as finite parts at every order. The pole part in the SV solution, namely, the soft and collinear divergences which are proportional to the distributions  $\delta(1 - z_l)$  and  $\mathcal{D}_0(z_l)$ , get canceled against those resulting from the FFs entirely and the AP kernels partially. The  $z$  dependent finite part correctly reproduces all the distributions in the SV part of CFs  $\Delta_{d,g}^A$ . The NSV part,  $\Phi_{d,g,\text{NSV}}^A$ , which comprises terms like  $\mathcal{D}_i(z_l) \ln^k(1 - z_j)$  and  $\delta(1 - z_l) \ln^k(1 - z_j)$  with  $(l, j = 1, 2)$ ,  $(i, k = 0, 1, \dots)$ , removes the remaining collinear divergences of the AP kernels. The finite part of it along with SV counterpart give rises to next to SV terms to

CFs  $\Delta_{d,g}^A$ . Note that the SV part  $\Phi_{d,g}^A$  plays a vital role in producing the next to SV terms for the CFs  $\Delta_{d,g}^A$  at every order, when the exponential is expanded in powers of  $a_s$ . This is due to the fact that the convolutions of two or more distributions contribute to certain next-to-SV logarithms in addition to the distributions.

Let us now focus on a peculiar feature that the NSV solution exhibits. Unlike in the case of SV solution, the NSV solution has the explicit  $z$  dependency due to two pieces. One of them is from the ansatz  $(1 - z_l)^{ie/2} (1 - z_j)^{ie/2} / (1 - z_l)$ , and the other one is from the coefficient  $\varphi_{d,g}^{A,(i)}(z_j, \epsilon)$ . This enables us to construct a class of solutions, a minimal class, to the K + G equation, satisfying the correct divergent structure as well as the dependence on  $\ln^k(1 - z_j)$  with  $(l, j = 1, 2)$ ,  $(i, k = 0, 1, \dots)$  [78] as given below,

$$\begin{aligned}
\Phi_{d,g,\text{NSV}}^{A,j} &= \sum_{i=1}^{\infty} \hat{a}_s^i \frac{(q^2 \bar{z}_1^{\alpha_1} \bar{z}_2^{\alpha_2} i^{\frac{\epsilon}{2}})}{\mu^2} S_\epsilon \left[ \frac{i\epsilon}{4\bar{z}_1} \varphi_{d,g,\alpha_2}^{A,(i)}(\bar{z}_2, \epsilon) \right] \\
& \quad + (\bar{z}_1 \leftrightarrow \bar{z}_2) |_{(\alpha_1 \rightarrow \beta_1, \alpha_2 \rightarrow \beta_2)}, \tag{88}
\end{aligned}$$

with  $j = (\alpha_1, \alpha_2, \beta_1, \beta_2)$  and  $\bar{z}_l = (1 - z_l)$  for  $l = 1, 2$ . It is to be noted that  $\alpha_1 = \beta_1 = 1$  for obtaining a finite  $\Delta_{d,g}^A$ , whereas  $\alpha_2$  and  $\beta_2$  can be arbitrary. The predictions from the

solutions  $\Phi_{d,g,\text{NSV}}^{A,j}$  are found to be independent of the choice of  $\alpha_2$  and  $\beta_2$  owing to the explicit  $z$  dependence of the coefficients  $\varphi_{d,g,j}^{A,(i)}(z_l, \epsilon)$  with  $j = \alpha_2$  for  $l = 2$  and  $j = \beta_2$  for  $l = 1$  at every order in  $\hat{a}_s$  and in  $\epsilon$ . It is straightforward to show that any variation of  $\alpha_2$  and  $\beta_2$  in the factors  $(1 - z_2)^{i\alpha_2\epsilon/2}$  and  $(1 - z_1)^{i\beta_2\epsilon/2}$  can always be compensated by suitably adjusting the  $z$  independent coefficients of  $\ln(1 - z_1)$  and  $\ln(1 - z_2)$  terms in  $\varphi_{d,g,\beta_2}^{A,(i)}(z_1, \epsilon)$  and  $\varphi_{d,g,\alpha_2}^{A,(i)}(z_2, \epsilon)$ , respectively, at every order in  $\hat{a}_s$ . Here, the logarithmic structure of  $\varphi_{d,f,g}^{A,j}$  plays a crucial role. Under this

scale transformation, the expression given in (78) takes the following form:

$$\varphi_{d,f,g}^{A,j}(a_s(q^2 \bar{z}_l^j), \bar{z}_l) = \sum_{i=1}^{\infty} \sum_{k=0}^i a_s^i(q^2 \bar{z}_l^j) \varphi_{d,g,j,i}^{A,(k)} \ln^k \bar{z}_l. \quad (89)$$

The fact that the predictions are insensitive to  $j$  relate the coefficients  $\varphi_{d,g,j,i}^{A,(k)}$  and  $\varphi_{d,g,i}^{A,(k)}$ , the solution corresponding to  $j = 1$ , as given below,

$$\begin{aligned} \varphi_{d,g,j,1}^{A,(0)} &= \varphi_{d,g,1}^{A,(0)}, & \varphi_{d,g,j,1}^{A,(1)} &= -D_1^A \bar{j} + \varphi_{d,g,1}^{A,(1)}, & \varphi_{d,g,j,2}^{A,(0)} &= \varphi_{d,g,2}^{A,(0)}, \\ \varphi_{d,g,j,2}^{A,(1)} &= -\bar{j}(D_2^A - \beta_0 \varphi_{d,g,1}^{A,(0)}) + \varphi_{d,g,2}^{A,(1)}, \\ \varphi_{d,g,j,2}^{A,(2)} &= -\frac{1}{2} \bar{j}^2 \beta_0 D_1^A - \bar{j}(C_2^A - \beta_0 \varphi_{d,g,1}^{A,(1)}) + \varphi_{d,g,2}^{A,(2)}, \\ \varphi_{d,g,j,3}^{A,(0)} &= \varphi_{d,g,3}^{A,(0)}, & \varphi_{d,g,j,3}^{A,(1)} &= -\bar{j}(D_3^A - \beta_1 \varphi_{d,g,1}^{A,(0)} - 2\beta_0 \varphi_{d,g,2}^{A,(0)}) + \varphi_{d,g,3}^{A,(1)}, \\ \varphi_{d,g,j,3}^{A,(2)} &= -\bar{j}^2 \left( \frac{1}{2} \beta_1 D_1^A + \beta_0 D_2^A - \beta_0^2 \varphi_{d,g,1}^{A,(0)} \right) - \bar{j}(C_3^A \bar{j} - \beta_1 \varphi_{d,g,1}^{A,(1)} - 2\beta_0 \varphi_{d,g,2}^{A,(1)}) + \varphi_{d,g,3}^{A,(2)}, \\ \varphi_{d,g,j,3}^{A,(3)} &= \beta_0^2 \left( -\frac{1}{3} D_1^A \bar{j}^3 + \bar{j}^2 \varphi_{d,g,1}^{A,(1)} \right) + \beta_0 \bar{j}(-C_2^A \bar{j} + 2\varphi_{d,g,2}^{A,(2)}) + \varphi_{d,g,3}^{A,(3)}, \\ \varphi_{d,g,j,4}^{A,(0)} &= \varphi_{d,g,4}^{A,(0)}, & \varphi_{d,g,j,4}^{A,(1)} &= -D_4^A \bar{j} + \beta_2 \bar{j} \varphi_{d,g,1}^{A,(0)} + 2\beta_1 \bar{j} \varphi_{d,g,2}^{A,(0)} + 3\beta_0 \bar{j} \varphi_{d,g,3}^{A,(0)} + \varphi_{d,g,4}^{A,(1)}, \\ \varphi_{d,g,j,4}^{A,(2)} &= -C_4^A \bar{j} - \frac{1}{2} \beta_2 D_1^A \bar{j}^2 - \beta_1 D_2^A \bar{j}^2 - \frac{3}{2} \beta_0 D_3^A \bar{j}^2 + \frac{5}{2} \beta_0 \beta_1 \bar{j}^2 \varphi_{d,g,1}^{A,(0)} + \beta_2 \bar{j} \varphi_{d,g,1}^{A,(1)} + 3\beta_0^2 \bar{j}^2 \varphi_{d,g,2}^{A,(0)} \\ &\quad + 2\beta_1 \bar{j} \varphi_{d,g,2}^{A,(1)} + 3\beta_0 \bar{j} \varphi_{d,g,3}^{A,(1)} + \varphi_{d,g,4}^{A,(2)}, \\ \varphi_{d,g,j,4}^{A,(3)} &= \beta_0^3 \bar{j}^3 \varphi_{d,g,1}^{A,(0)} + \beta_0^2 \bar{j}^2 (-D_2^A \bar{j} + 3\varphi_{d,g,2}^{A,(1)}) - \frac{1}{6} \beta_1 \bar{j} (6C_2^A \bar{j} + 5\beta_0 \bar{j} (D_1^A \bar{j} - 3\varphi_{d,g,1}^{A,(1)}) \\ &\quad - 12\varphi_{d,g,2}^{A,(2)}) - \frac{3}{2} \beta_0 \bar{j} (C_3^A \bar{j} - 2\varphi_{d,g,3}^{A,(2)}) + \varphi_{d,g,4}^{A,(3)}, \\ \varphi_{d,g,j,4}^{A,(4)} &= \beta_0^3 \left( -\frac{1}{4} D_1^A \bar{j}^4 + \bar{j}^3 \varphi_{d,g,1}^{A,(1)} \right) + \beta_0^2 \bar{j}^2 (-C_2^A \bar{j} + 3\varphi_{d,g,2}^{A,(2)}) + 3\beta_0 \bar{j} \varphi_{d,g,3}^{A,(3)} + \varphi_{d,g,4}^{A,(4)}, \end{aligned} \quad (90)$$

with  $j$  being  $\alpha_2$  and  $\beta_2$  for the coefficients of  $\ln(1 - z_2)$  and  $\ln(1 - z_1)$ , respectively. In the above equations,  $\bar{j} = (\alpha_2 - 1)$  and  $(\beta_2 - 1)$  for  $j = \alpha_2$  and  $\beta_2$ , respectively. The above relations are the transformations for  $\varphi_{d,g,j,i}^{A,(k)}$  that are required to compensate the contributions resulting from the change in the exponents of  $(1 - z_1)$  and  $(1 - z_2)$  from  $(i\epsilon)/2$  to  $(ij\epsilon)/2$ . The function  $\Phi_{d,g,\text{NSV}}^{A,j}$  being insensitive to the choice of the scales  $\alpha_2$  and  $\beta_2$  indicates its invariance under certain gauge like transformations on both  $(1 - z_1)^{i\epsilon/2}$  and  $\varphi_{d,f,g}^{A,j}(z_l, \epsilon)$ . Due to this invariance, these transformations neither alter the divergent structure nor the finite parts of  $\Phi_{d,g,\text{NSV}}^A$ . However, we choose to work with  $\alpha_2 = \beta_2 = 1$  in the NSV solution to have more resemblance with its SV counterpart. In summary, we find a minimal class of

solutions to the K + G equation without affecting neither the all order structure nor the predictions for  $\Delta_{d,g}^A$ . We show later that this choice will allow us to study resummation in two-dimensional Mellin space for SV as well as NSV parts with single  $\mathcal{O}(1)$  term denoted by  $\omega = a_s \beta_0 \ln(N_1 N_2)$ .

## VIII. RESUMMATION IN THE MELLIN $\bar{N}$ SPACE

This section is devoted to the study of all order perturbative structure of  $\Delta_{d,g}^A$  in the Mellin space. To find the structure of  $\Delta_{d,g}^A$  in the Mellin space, we use the integral representations of both  $\Phi_{d,g,\text{SV}}^A$  and  $\Phi_{d,g,\text{NSV}}^A$  given in (75) and (76), respectively. As a result,  $\Psi_{d,g}^A$  in (29) takes the following form:

$$\begin{aligned}
\Psi_{d,g}^A(q^2, \mu_F^2, z_1, z_2) &= \frac{\delta(\bar{z}_1)}{2} \left( \int_{\mu_F^2}^{q^2 \bar{z}_2} \frac{d\lambda^2}{\lambda^2} \mathcal{P}_{gg}(a_s(\lambda^2), \bar{z}_2) + \mathcal{Q}_{d,g}^A(a_s(q_2^2), \bar{z}_2) \right)_+ \\
&+ \frac{1}{4} \left( \frac{1}{\bar{z}_1} \left\{ \mathcal{P}_{gg}(a_s(q_{12}^2), \bar{z}_2) + 2L_g^A(a_s(q_{12}^2), \bar{z}_2) \right. \right. \\
&+ \left. \left. q^2 \frac{d}{dq^2} (\mathcal{Q}_{d,g}^A(a_s(q_2^2), \bar{z}_2) + 2\varphi_{d,f,g}^A(a_s(q_2^2), \bar{z}_2)) \right\} \right)_+ \\
&+ \frac{1}{2} \delta(\bar{z}_1) \delta(\bar{z}_2) \ln(g_{d,g,0}^A(a_s(\mu_F^2))) + \bar{z}_1 \leftrightarrow \bar{z}_2,
\end{aligned} \tag{91}$$

where  $\mathcal{P}_{gg}(a_s, \bar{z}_l) = P_{gg}(a_s, \bar{z}_l) - 2B_g^A(a_s)\delta(\bar{z}_l)$ ,  $q_l^2 = q^2(1 - z_l)$ , and  $q_{12}^2 = q^2 \bar{z}_1 \bar{z}_2$ . The subscript + indicates standard plus distribution. The function  $\mathcal{Q}_{d,g}^A$  in (91) is given as

$$\mathcal{Q}_{d,g}^A(a_s, \bar{z}_l) = \frac{2}{\bar{z}_l} \mathbf{D}_{d,g}^A(a_s) + 2\varphi_{d,f,g}^A(a_s, \bar{z}_l). \tag{92}$$

The SV coefficients  $\mathbf{D}_{d,g}^A$  are given in Appendix C. The constant  $g_{d,g,0}^A$  in (91) results from finite part of the virtual contributions and pure  $\delta(\bar{z}_l)$  terms of  $\Phi_{d,g}^A$ .

Now, we take the double Mellin transform of  $\Delta_{d,g}^A$  in  $\vec{N}$  space as

$$\begin{aligned}
\Delta_{d,g,\vec{N}}^A(q^2, \mu_R^2, \mu_F^2) &= \int_0^1 dz_1 z_1^{N_1-1} \int_0^1 dz_2 z_2^{N_2-1} \Delta_{d,g}^A(z_1, z_2)(q^2, \mu_R^2, \mu_F^2) \\
&= \tilde{g}_{d,g,0}^A(q^2, \mu_R^2, \mu_F^2) \exp(\Psi_{d,g,\vec{N}}^A(q^2, \mu_F^2)).
\end{aligned} \tag{93}$$

The  $N$ -independent constant  $\tilde{g}_{d,g,0}^A$  is given in Appendix E. The resummed result for  $\Psi_{d,g,\vec{N}}^A$  takes the following form:

$$\begin{aligned}
\Psi_{d,g,\vec{N}}^A &= \left( g_{d,g,1}^A(\omega) + \frac{1}{N_1} \bar{g}_{d,g,1}^A(\omega) \right) \ln N_1 + \sum_{i=0}^{\infty} a_s^i \left( \frac{1}{2} g_{d,g,i+2}^A(\omega) + \frac{1}{N_1} \bar{g}_{d,g,i+2}^A(\omega) \right) \\
&+ \frac{1}{N_1} \left( h_{d,g,0}^A(\omega, N_1) + \sum_{i=1}^{\infty} a_s^i h_{d,g,i}^A(\omega, \omega_1, N_1) \right) + (N_1 \leftrightarrow N_2, \omega_1 \leftrightarrow \omega_2),
\end{aligned} \tag{94}$$

with

$$\begin{aligned}
h_{d,g,0}^A(\omega, N_l) &= h_{d,g,00}^A(\omega) + h_{d,g,01}^A(\omega) \ln N_l, \\
h_{d,g,i}^A(\omega, \omega_l, N_l) &= \sum_{k=0}^{i-1} h_{d,g,ik}^A(\omega) \ln^k N_l + \tilde{h}_{d,g,ii}^A(\omega, \omega_l) \ln^k N_l.
\end{aligned} \tag{95}$$

In the above expressions,  $\omega = a_s \beta_0 \ln N_1 N_2$  and  $\omega_l = a_s \beta_0 \ln N_l$  for  $l = 1, 2$ . Here,  $g_{d,g,i}^A$  are the resummation constants resulting from the SV contributions, and  $\bar{g}_{d,g,i}^A$  result entirely from  $A_g^A, B_g^A$  coefficients of  $P_{gg}$  and from the function  $\mathbf{D}_{d,g}^A$  in (92). The function  $\bar{g}_{d,g,1}^A$  is found to be identically zero, and we find that none of the coefficients  $\bar{g}_{d,g,i}^A$  contains explicit  $\ln N_l$ . The functions  $h_{d,g,i}^A$  comprise of  $C_g^A$  and  $D_g^A$  which are present in  $P_{gg}$  as well as the pure NSV coefficients present in  $\varphi_{d,f,g}^A$ . We find that coefficient of  $h_{d,g,01}^A$  is proportional to  $C_{g,1}^A$  which is identically zero. Hence, at order  $a_s^0$ , there is no  $\frac{\ln N_l}{N_l}$  term. The SV resummation constant  $g_{d,g,i}^A$  has been discussed in great

detail in Refs. [53,113,114], and the NSV resummation coefficients  $\bar{g}_{d,g,i}^A$ ,  $h_{d,g,ij}^A$  and  $\tilde{h}_{d,g,ii}^A$  are provided in Appendixes F and G. Our next aim is to include these resummed contributions consistently in the fixed order predictions to understand the phenomenological relevance of resumming the NSV contributions for the case of pseudoscalar Higgs production in gluon fusion channel.

## IX. NUMERICAL ANALYSIS

In this section, we study the impact of resummed soft-virtual and next-to-soft-virtual (SV + NSV) contributions for the rapidity distribution of the pseudoscalar Higgs

production in gluon fusion channel at the LHC to NNLO<sub>A</sub> + NNLL accuracy. We use the MMHT2014 (68cl) PDF set [115] and the corresponding strong coupling  $a_s$  through the Les Houches Accord PDF (LHAPDF) interface [116] at each order in perturbation theory with  $n_f = 5$  active massless quark flavors throughout. Our predictions are based on Higgs effective field theory where the top quarks are integrated out at higher orders. Nevertheless, we retain the top quark mass dependence at LO. The term  $C_J^{(2)}$  in the Wilson coefficient  $C_J$  in (2) is taken to be zero in our analysis because it is not available in the literature yet. For simplicity, we have set  $\cot\beta = 1$  in our numerical analysis. Results for other values of  $\cot\beta$  can be easily obtained by rescaling the cross sections with  $\cot^2\beta$ . For the fixed order rapidity distribution of the pseudoscalar Higgs, we use the publicly available code FEHiP [94] of the scalar Higgs by taking into account the ratio factor discussed in Sec. III A. The resummed contribution is obtained from  $\Delta_{d,g,\bar{N}}^A$  in (93) after performing Mellin inversion which is done using an in-house FORTRAN based code. The resummed results are matched to the fixed order result in order to avoid any double counting of threshold logarithms as

$$\frac{d\sigma^{A, \text{match}}}{dY} = \left( \frac{d\sigma^{A, (\text{SV}+\text{NSV})}}{dY} \Big|_{\text{resum}} - \frac{d\sigma^{A, (\text{SV}+\text{NSV})}}{dY} \Big|_{\text{FO}} + \frac{d\sigma^{A, \text{FO}}}{dY} \right). \quad (96)$$

We do the analysis for center of mass energy  $\sqrt{S} = 13$  TeV with the pseudoscalar Higgs mass  $m_A = 125$  GeV and  $m_A = 700$  GeV, top quark pole mass  $m_t = 173.3$  GeV, and the Fermi constant  $G_F = 4541.63$  pb. The numerical values for the aforementioned parameters are taken from the Particle Data Group 2020 [117]. To distinguish between the SV and SV + NSV resummed results, the NSV included resummed results have been denoted by  $\overline{\text{N}}^n\text{LL}$  for the  $n$ th level logarithmic accuracy.

### A. K-factor analysis

We begin our analysis by studying the higher order effects which are quantified through the K-factors as

$$K = \frac{\frac{d\sigma}{dY}(\mu_R = \mu_F = m_A)}{\frac{d\sigma^{\text{LO}}}{dY}(\mu_R = \mu_F = m_A)}. \quad (97)$$

We fix the central scale at  $\mu_R = \mu_F = m_A$  throughout our analysis. In Table I, we present the K-factor values of fixed order and resummed predictions at  $m_A = 125$  GeV for benchmark rapidity values. We observe that the NLO result at the central scale is enhanced by 83.9% with respect to the LO one around the central rapidity region. However, the enhancement of the approximate NNLO (NNLO<sub>A</sub>) result at

TABLE I. K-factor values of fixed order and resummed results at the central scale  $\mu_R = \mu_F = m_A$  for  $m_A = 125$  GeV.

$y$	$K_{\text{LO}+\overline{\text{LL}}}$	$K_{\text{NLO}}$	$K_{\text{NLO}+\overline{\text{NLL}}}$	$K_{\text{NNLO}_A}$	$K_{\text{NNLO}_A+\overline{\text{NNLL}}}$
0–0.4	1.602	1.839	2.505	2.352	2.699
0.4–0.8	1.681	1.806	2.469	2.297	2.644
0.8–1.2	1.703	1.792	2.472	2.285	2.643
1.2–1.6	1.713	1.746	2.433	2.248	2.613
1.6–2.0	1.748	1.688	2.397	2.151	2.533

TABLE II. K-factor values of fixed order and resummed results at the central scale  $\mu_R = \mu_F = m_A$  for  $m_A = 700$  GeV.

$y$	$K_{\text{LO}+\overline{\text{LL}}}$	$K_{\text{NLO}}$	$K_{\text{NLO}+\overline{\text{NLL}}}$	$K_{\text{NNLO}_A}$	$K_{\text{NNLO}_A+\overline{\text{NNLL}}}$
0–0.4	1.533	2.200	2.749	2.478	2.763
0.4–0.8	1.547	2.199	2.755	2.414	2.703
0.8–1.2	1.579	2.200	2.769	2.315	2.613
1.2–1.6	1.653	2.212	2.819	2.266	2.592
1.6–2.0	1.797	2.238	2.947	2.370	2.781

the central scale is 27.9% in comparison to the NLO result. For the SV + NSV resummed results, we notice an enhancement of 60% and 36.2% when  $\overline{\text{LL}}$  and  $\overline{\text{NLL}}$  are added to LO and NLO, respectively, at the central rapidity region. The rapidity distribution increases by 14.76% when we include  $\overline{\text{NNLL}}$  to NNLO<sub>A</sub>. Further, at the central scale, the resummed rapidity distribution at NLO +  $\overline{\text{NLL}}$  (25.6 pb) mimics that at NNLO<sub>A</sub> (24 pb) around the central rapidity region. We also study the K-factor values for the high mass region, i.e.,  $m_A = 700$  GeV as given in Table II. For the fixed order results, there is a large increment of 120% when we go from LO to NLO. Interestingly, the higher order effects at NNLO<sub>A</sub> give rise to only 12.6% correction to NLO around the central rapidity region. We find that there is an enhancement of 53.3% and 24.97% by the inclusion of  $\overline{\text{LL}}$  and  $\overline{\text{NLL}}$  resummed results at LO and NLO, respectively, around the central rapidity region. At NNLO<sub>A</sub>, the rapidity distribution increases by 11.48% when we include  $\overline{\text{NNLL}}$ . From Tables I and II, it can be observed that resummed predictions not only bring in considerable enhancement in the fixed order results, but also improve the perturbative convergence to NNLO<sub>A</sub> +  $\overline{\text{NNLL}}$  accuracy.

### B. 7-point scale variation

Next, we study the theoretical uncertainties due to the unphysical renormalization ( $\mu_R$ ) and factorization ( $\mu_F$ ) scales in our results using the standard canonical 7-point variation approach. Here,  $\mu = \{\mu_F, \mu_R\}$  is varied in the range  $\frac{1}{2} \leq \frac{\mu}{m_A} \leq 2$ , keeping the ratio  $\mu_R/\mu_F$  not larger than 2 and smaller than 1/2. In Fig. 1, we depict the bin-integrated

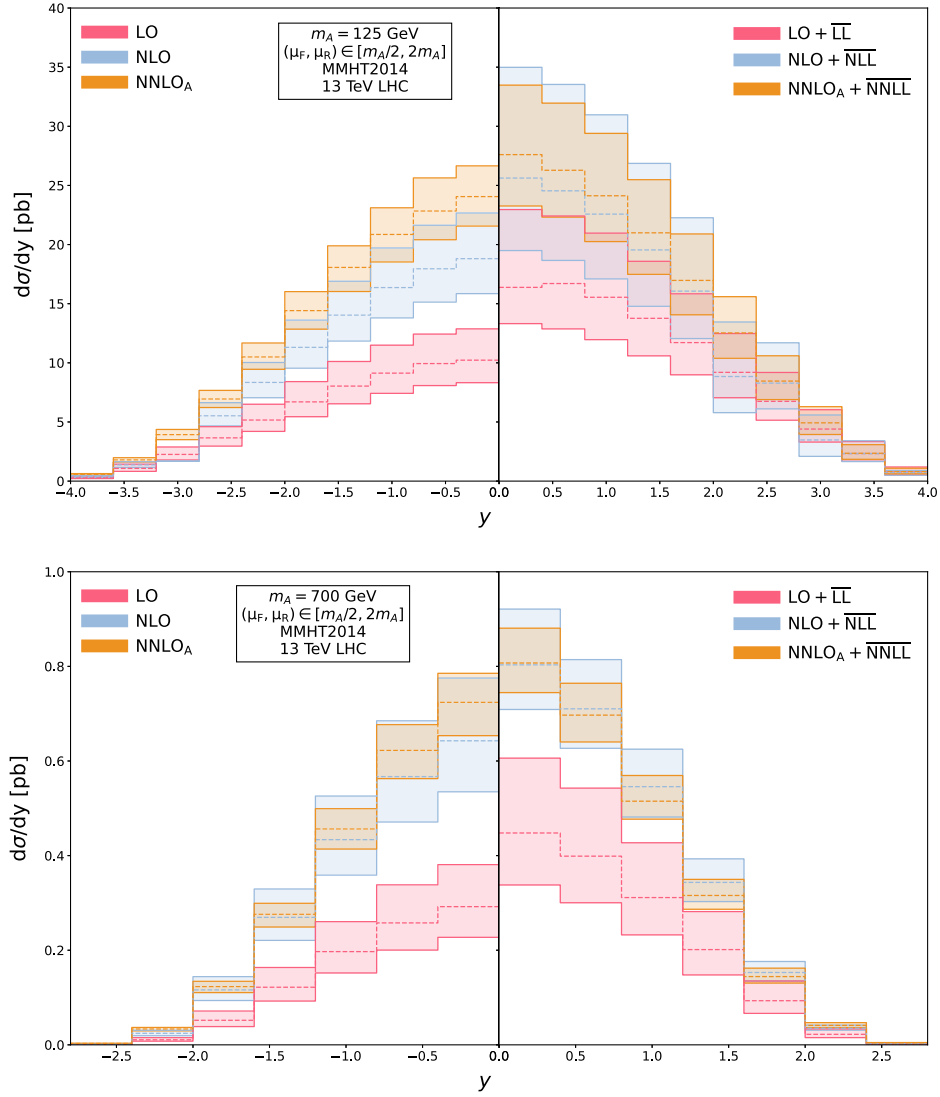


FIG. 1. Comparison of 7-point scale variation between fixed order and SV + NSV resummed results for  $m_A = 125$  (top) and  $m_A = 700$  (bottom) GeV. The dashed lines refer to the corresponding central scale values at each order.

rapidity distribution of the pseudoscalar Higgs boson for the fixed order results in the left panel and the resummed results in the right panel around the central scale  $\mu_R = \mu_F = m_A$  for  $m_A = 125$  GeV (top) and  $m_A = 700$  GeV (bottom). We have provided the fixed order as well as

SV + NSV resummed results for benchmark rapidity values at the central scale  $\mu_R = \mu_F = m_A$  for  $m_A = 125$  GeV and  $m_A = 700$  GeV in Tables III and IV, respectively, at various perturbative orders. These tables also contain the maximum increments and decrements from the

TABLE III. Values of resummed rapidity distribution at various orders in comparison to the fixed order results in pb at the central scale  $\mu_R = \mu_F = m_A = 125$  GeV for 13 TeV LHC.

$y$	LO	LO + $\overline{\text{LL}}$	NLO	NLO + $\overline{\text{NLL}}$	NNLO <sub>A</sub>	NNLO <sub>A</sub> + $\overline{\text{NNLL}}$
0–0.4	10.225 <sup>+2.645</sup> <sub>-1.902</sub>	16.379 <sup>+6.580</sup> <sub>-3.064</sub>	18.805 <sup>+3.862</sup> <sub>-2.953</sub>	25.623 <sup>+9.360</sup> <sub>-6.130</sub>	24.054 <sup>+2.599</sup> <sub>-2.490</sub>	27.605 <sup>+5.873</sup> <sub>-4.340</sub>
0.4–0.8	9.938 <sup>+2.490</sup> <sub>-1.860</sub>	16.704 <sup>+5.7120</sup> <sub>-3.833</sub>	17.951 <sup>+3.682</sup> <sub>-2.815</sub>	24.543 <sup>+8.994</sup> <sub>-5.883</sub>	22.836 <sup>+2.798</sup> <sub>-2.428</sub>	26.281 <sup>+5.675</sup> <sub>-3.959</sub>
0.8–1.2	9.128 <sup>+2.363</sup> <sub>-1.707</sub>	15.54 <sup>+5.424</sup> <sub>-3.581</sub>	16.362 <sup>+3.350</sup> <sub>-2.563</sub>	22.572 <sup>+8.396</sup> <sub>-5.474</sub>	20.856 <sup>+2.251</sup> <sub>-2.327</sub>	24.126 <sup>+5.273</sup> <sub>-3.873</sub>
1.2–1.6	8.033 <sup>+2.080</sup> <sub>-1.495</sub>	13.763 <sup>+4.820</sup> <sub>-3.171</sub>	14.034 <sup>+2.863</sup> <sub>-2.193</sub>	19.546 <sup>+7.315</sup> <sub>-4.765</sub>	18.067 <sup>+1.825</sup> <sub>-2.037</sub>	20.992 <sup>+4.491</sup> <sub>-3.508</sub>
1.6–2.0	6.698 <sup>+1.714</sup> <sub>-1.252</sub>	11.711 <sup>+4.123</sup> <sub>-2.723</sub>	11.311 <sup>+2.299</sup> <sub>-1.762</sub>	16.061 <sup>+6.203</sup> <sub>-4.008</sub>	14.412 <sup>+1.607</sup> <sub>-1.566</sub>	16.968 <sup>+3.926</sup> <sub>-2.906</sub>

TABLE IV. Values of resummed rapidity distribution at various orders in comparison to the fixed order results in pb at the central scale  $\mu_R = \mu_F = m_A = 700$  GeV for 13 TeV LHC.

$y$	LO	LO + $\overline{\text{LL}}$	NLO	NLO + $\overline{\text{NLL}}$	NNLO <sub>A</sub>	NNLO <sub>A</sub> + $\overline{\text{NNLL}}$
0–0.4	0.292 <sup>+0.088</sup> <sub>-0.065</sub>	0.123 <sup>+0.158</sup> <sub>-0.1098</sub>	0.643 <sup>+0.0132</sup> <sub>-0.1078</sub>	0.803 <sup>+0.1178</sup> <sub>-0.0943</sub>	0.724 <sup>+0.0613</sup> <sub>-0.07045</sub>	0.807 <sup>+0.0735</sup> <sub>-0.0625</sub>
0.4–0.8	0.257 <sup>+0.0804</sup> <sub>-0.0574</sub>	0.399 <sup>+0.14379</sup> <sub>-0.09845</sub>	0.567 <sup>+0.1179</sup> <sub>-0.0959</sub>	0.710 <sup>+0.1040</sup> <sub>-0.0834</sub>	0.622 <sup>+0.0543</sup> <sub>-0.0596</sub>	0.697 <sup>+0.06733</sup> <sub>-0.0566</sub>
0.8–1.2	0.197 <sup>+0.0633</sup> <sub>-0.0450</sub>	0.311 <sup>+0.1158</sup> <sub>-0.0788</sub>	0.434 <sup>+0.0922</sup> <sub>-0.0749</sub>	0.546 <sup>+0.07919</sup> <sub>-0.0641</sub>	0.456 <sup>+0.0428</sup> <sub>-0.0424</sub>	0.515 <sup>+0.0543</sup> <sub>-0.0379</sub>
1.2–1.6	0.122 <sup>+0.0417</sup> <sub>-0.0291</sub>	0.201 <sup>+0.0803</sup> <sub>-0.0535</sub>	0.434 <sup>+0.06</sup> <sub>-0.0486</sub>	0.343 <sup>+0.0497</sup> <sub>-0.0405</sub>	0.276 <sup>+0.02322</sup> <sub>-0.02688</sub>	0.316 <sup>+0.03399</sup> <sub>-0.0291</sub>
1.6–2.0	0.052 <sup>+0.0195</sup> <sub>-0.0132</sub>	0.093 <sup>+0.0416</sup> <sub>-0.0267</sub>	0.116 <sup>+0.0279</sup> <sub>-0.0224</sub>	0.153 <sup>+0.0232</sup> <sub>-0.0181</sub>	0.123 <sup>+0.01131</sup> <sub>-0.0125</sub>	0.144 <sup>+0.0177</sup> <sub>-0.01365</sub>

corresponding central scale values obtained by varying  $\{\mu_R, \mu_F\}$  in the range  $\{1/2, 2\}m_A$ .

Let us first look at the plot with  $m_A = 125$  GeV in Fig. 1. This plot shows that the addition of SV + NSV resummed results to the fixed order ones increases the rapidity distribution at each order up to NNLO<sub>A</sub> in perturbation theory. However, the percentage enhancement in the rapidity distribution decreases from 60% at LO to 14.76% at NNLO<sub>A</sub> by the inclusion of  $\overline{\text{LL}}$  and  $\overline{\text{NNLL}}$ , respectively, at the central rapidity region. This indicates better perturbative convergence of the truncated series at higher orders due to the addition of the resummed predictions. We now compare the 7-point uncertainties of fixed order and SV + NSV resummed results due to  $\mu_R$  and  $\mu_F$  scales. We find that the combined uncertainty due to  $\mu_R$  and  $\mu_F$  scales lies in the range (+25.87%, -18.60%) at LO, while at NNLO<sub>A</sub> it gets substantially reduced to (+10.80%, -10.35%) around the central rapidity region. We see that the bands of resummed predictions to NNLO<sub>A</sub> +  $\overline{\text{NNLL}}$  are wider than that of the corresponding fixed order results throughout the rapidity spectrum for  $m_A = 125$  GeV. Numerically, the combined uncertainty due to these unphysical scales lies between (+40.17%, -18.71%) at LO +  $\overline{\text{LL}}$ , (+36.53%, -23.92%) at NLO +  $\overline{\text{NLL}}$ , and (+21.27%, -15.72%) at NNLO<sub>A</sub> +  $\overline{\text{NNLL}}$  order around  $y = 0$ . This shows that there is a systematic decrease in the uncertainty when we go to higher logarithmic accuracy for SV + NSV resummed results. The plot for  $m_A = 700$  GeV in Fig. 1 shows a similar trend of enhancement in the rapidity distribution by the addition of SV + NSV resummed results as was depicted above. The 7-point uncertainty values show that at lower orders the resummed results show significantly more  $\mu_R$  and  $\mu_F$  variation as compared to the fixed order ones similar to the case of  $m_A = 125$  GeV. However, at NNLO<sub>A</sub> +  $\overline{\text{NNLL}}$  accuracy, the combined uncertainty of the resummed result lies in the range (+9.11%, -7.74%) which is comparable to the uncertainty of (+8.47%, -9.73%) for the fixed order prediction at NNLO<sub>A</sub> around the central rapidity region. Thus, the SV + NSV resummed results become more relevant for higher values of pseudoscalar Higgs boson mass. The above analysis suggests the need to understand

the behavior of the resummed results with respect to  $\mu_R$  and  $\mu_F$  scale variations in a better way. Hence, we study the impact of each scale individually by keeping the other fixed.

### C. Uncertainties due to $\mu_R$ and $\mu_F$ scales individually

We now discuss the effect of the factorization scale  $\mu_F$  individually by keeping the renormalization scale  $\mu_R$  fixed. Figure 2 shows the bin-integrated rapidity distributions for the fixed order (left panel) as well as the SV + NSV resummed results (right panel) at various perturbative orders for  $m_A = 125$  GeV (top) and  $m_A = 700$  GeV (bottom) keeping the renormalization scale fixed at  $\mu_R = m_A$ . The factorization scale is varied in the range  $\{1/2, 1\}m_A$  around the central scale  $\mu_F = \mu_R = m_A$  to get the uncertainty bands. The fixed order results show negligible dependence on the  $\mu_F$  scale both at  $m_A = 125$  GeV and  $m_A = 700$  GeV. On the other hand, the resummed predictions show substantial dependence with respect to the  $\mu_F$  scale especially at  $m_A = 125$  GeV. The uncertainty lies in the range (+36.53%, -23.92%) at NLO +  $\overline{\text{NLL}}$  accuracy which comes down to (+21.27%, -15.72%) at NNLO<sub>A</sub> +  $\overline{\text{NNLL}}$  accuracy around central rapidity region for  $m_A = 125$  GeV. When we compare these  $\mu_F$  scale uncertainty values with those at  $m_A = 700$  GeV, we find that it vary in the range (+14.66%, -9.88%) and (+9.11%, -7.75%) at NLO +  $\overline{\text{NLL}}$  and NNLO<sub>A</sub> +  $\overline{\text{NNLL}}$  order, respectively, around  $y = 0$ . Hence, as suggested by the 7-point scale variation analysis, the uncertainty decreases considerably at the higher value of the pseudoscalar Higgs Boson mass. The uncertainty due to the factorization scale decreases at higher orders for both the cases of  $m_A$ . Also, the higher order uncertainty bands lie within the lower order ones. These two observations hint toward improved reliability of the perturbative results and better perturbative convergence at higher orders.

Next, we study the variation in the fixed order and SV + NSV resummed results with respect to the renormalization scale by keeping the factorization scale fixed at  $\mu_F = m_A$ . The uncertainty bands are obtained by varying  $\mu_R$  in the range  $\{1/2, 1\}m_A$  around the central scale  $\mu_F = \mu_R = m_A$ . In Fig. 3, we observe that from the NLO level, the  $\mu_R$  scale

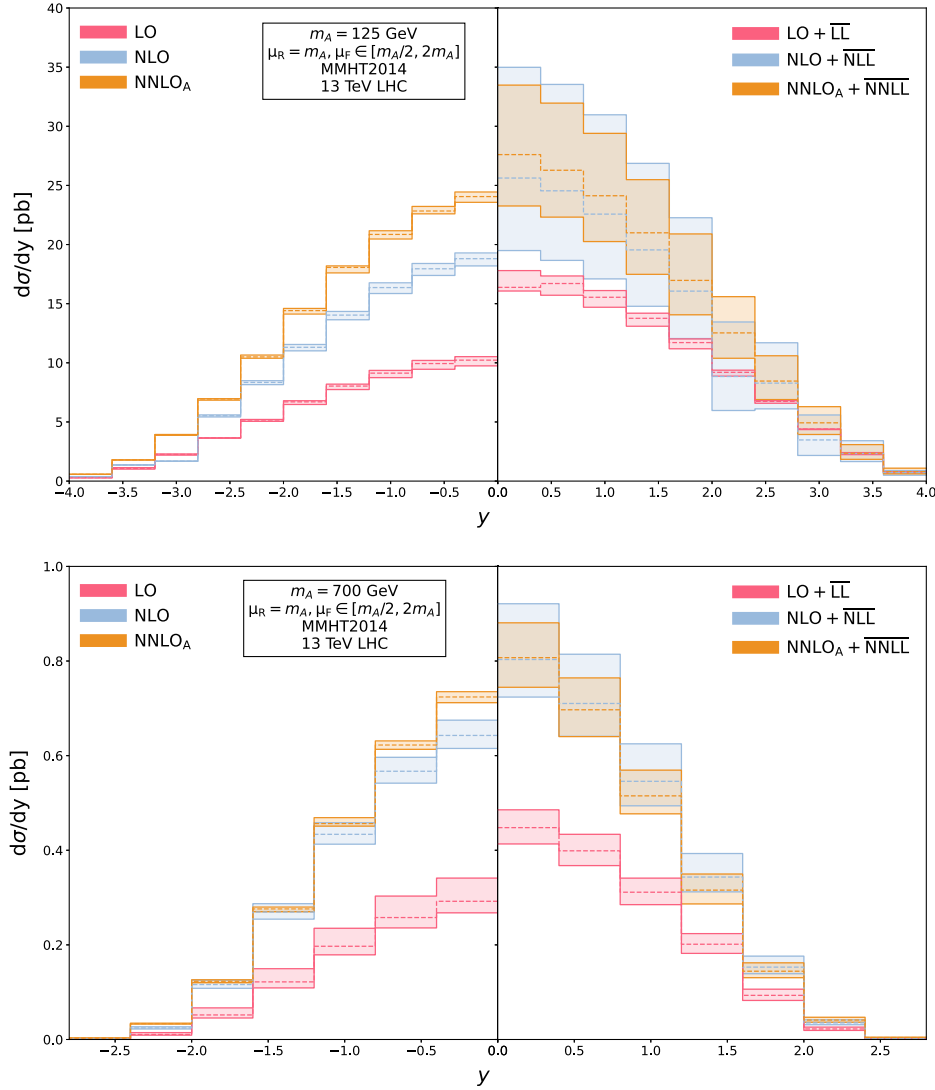


FIG. 2. Comparison of  $\mu_F$  scale variation between fixed order and SV + NSV resummed results for  $m_A = 125$  (top) and  $m_A = 700$  (bottom) GeV. The dashed lines refer to the corresponding central scale values at each order.

uncertainty of the fixed order results decreases by the addition of resummed predictions for  $m_A = 125$  GeV as well as  $m_A = 700$  GeV. The numerical values of the  $\mu_R$  uncertainties lie between (+18.45%, -15.24%) and (+4.16%, -6.69%) at NLO +  $\overline{\text{NLL}}$  and NNLO<sub>A</sub> +  $\overline{\text{NNLL}}$  order, respectively, which is a considerable reduction from (+20.54%, -15.70%) and (+10.80%, -10.35%) at NLO and NNLO<sub>A</sub> accuracy, respectively, around  $y = 0$  for  $m_A = 125$  GeV. Similarly, for the case of  $m_A = 700$  GeV, they lie in the range (+13.33%, -11.74%) and (+2.62%, -5.19%) at NLO +  $\overline{\text{NLL}}$  and NNLO<sub>A</sub> +  $\overline{\text{NNLL}}$ , respectively, whereas they vary between (+15.48%, -12.69%) and (+6.76%, -8.04%) for NLO and NNLO<sub>A</sub> order, respectively, around central rapidity region. From the above percentages, we also find that the uncertainty decreases as we go to higher orders for both cases of pseudoscalar Higgs boson masses. In addition, the uncertainty bands of

resummed results at higher orders are well within the lower orders from NLO level onwards.

Here, we performed a comparative study between the fixed order results and the SV + NSV resummed predictions for the rapidity distribution of pseudoscalar Higgs boson in gluon fusion process. This has been done through the K-factor analysis, 7-point variation approach, and finally by studying the variation of  $\mu_F$  and  $\mu_R$  scales individually. We did the analysis for two different cases of pseudoscalar Higgs boson masses  $m_A = 125, 700$  GeV. The K-factor analysis showed that the inclusion of SV + NSV resummed predictions resulted in the enhancement of the fixed order results at every order in perturbation theory up to NNLO<sub>A</sub> accuracy for both the cases of  $m_A$ . Also, we observed that the percentage enhancement by adding the resummed results decreases as we go from LO to NNLO<sub>A</sub> accuracy. This shows that the resummed results are more

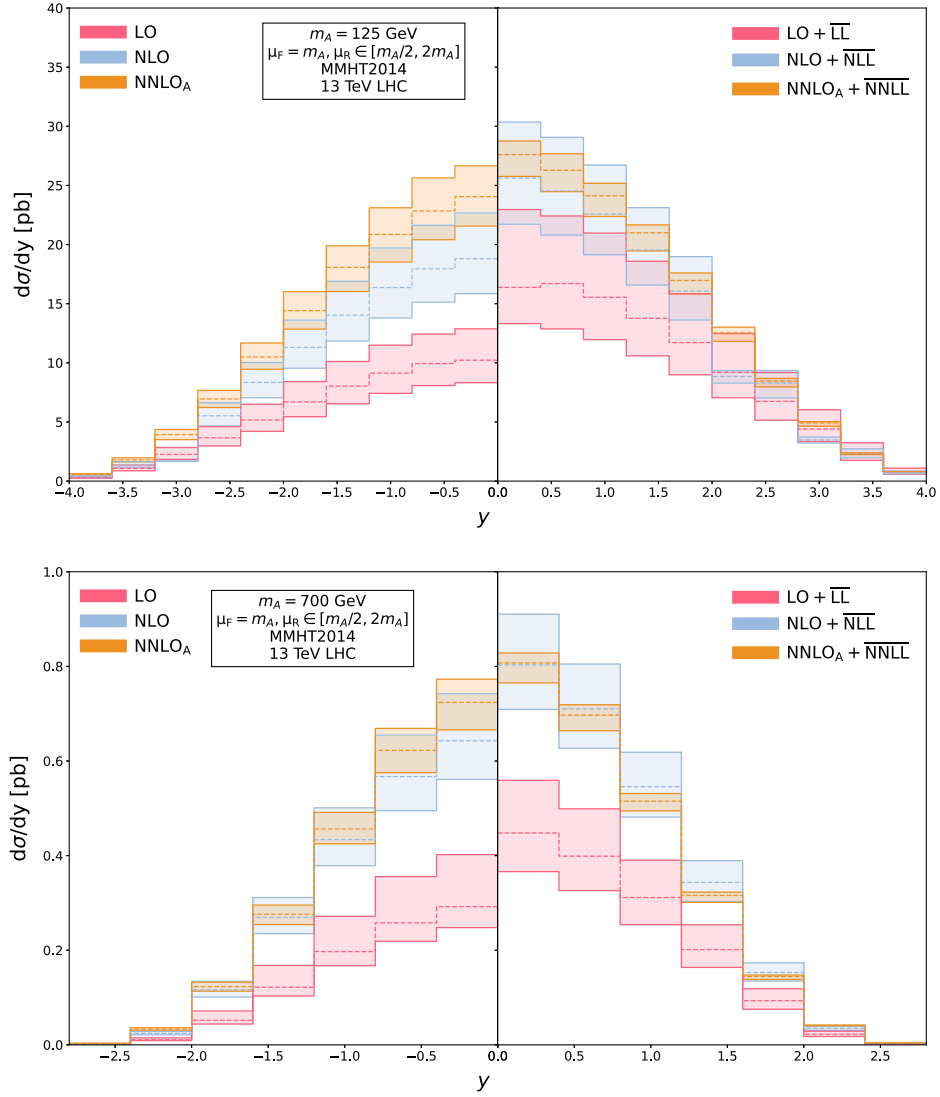


FIG. 3. Comparison of  $\mu_R$  scale variation between fixed order and SV + NSV resummed results for  $m_A = 125$  (top) and  $m_A = 700$  (bottom) GeV. The dashed lines refer to the corresponding central scale values at each order.

reliable and have a better perturbative convergence. The study of factorization scale variation showed that the addition of the resummed results especially at  $m_A = 125$  GeV significantly increased the uncertainty of the fixed order results, which otherwise was almost independent of the  $\mu_F$  scale variation. However, the dependence of the resummed results on the  $\mu_F$  scale decreases considerably for the case of  $m_A = 700$  GeV. The renormalization scale dependence, on the other hand, gets improved by the inclusion of resummed predictions. In order to understand this behavior of SV + NSV resummed results in a better way, we compare them with the well established SV resummed results at various orders in the next section.

#### D. SV + NSV vs SV resummed predictions

In previous sections, we presented the observations on the behavior of SV + NSV resummed corrections by

comparing them with the fixed-order results at various perturbative orders. Here, we try to understand the reasons behind those observations by comparing the full SV + NSV resummed predictions with the well-established SV resummed results which would help us to infer the behavior of resummed NSV logarithms in particular.

We begin our analysis with the K-factor values of SV and SV + NSV resummed results. We provide the K-factor values of SV and SV + NSV resummed results at various perturbative orders for benchmark rapidity values for  $m_A = 125, 700$  GeV in Tables V and VI. Looking at the values in Tables V and VI, we find that the addition of resummed NSV logarithms enhances the SV resummed predictions for the rapidity distribution at each order in perturbation theory for both the values of  $m_A$ . For instance, there is an enhancement of 16.03% and 7.87% by the inclusion of resummed NSV logarithms at NLO + NLL

TABLE V. K-factor values of SV and SV + NSV resummed results at the central scale  $\mu_R = \mu_F = m_A = 125$  GeV.

$y$	$K_{\text{LO+LL}}$	$K_{\text{LO+LL}}$	$K_{\text{NLO+NLL}}$	$K_{\text{NLO+NLL}}$	$K_{\text{NNLO}_A+\text{NNLL}}$	$K_{\text{NNLO}_A+\text{NNLL}}$
0–0.4	1.411	1.602	2.159	2.505	2.502	2.699
0.4–0.8	1.410	1.681	2.126	2.469	2.447	2.644
0.8–1.2	1.428	1.703	2.125	2.472	2.441	2.643
1.2–1.6	1.437	1.713	2.086	2.433	2.409	2.613
1.6–2.0	1.466	1.748	2.047	2.397	2.324	2.533

TABLE VI. K-factor values of SV and SV + NSV resummed results at the central scale  $\mu_R = \mu_F = m_A = 700$  GeV.

$y$	$K_{\text{LO+LL}}$	$K_{\text{LO+LL}}$	$K_{\text{NLO+NLL}}$	$K_{\text{NLO+NLL}}$	$K_{\text{NNLO}_A+\text{NNLL}}$	$K_{\text{NNLO}_A+\text{NNLL}}$
0–0.4	1.375	1.533	2.530	2.749	2.630	2.763
0.4–0.8	1.388	1.547	2.536	2.755	2.571	2.703
0.8–1.2	1.416	1.579	2.550	2.769	2.479	2.613
1.2–1.6	1.480	1.653	2.596	2.819	2.451	2.593
1.6–2.0	1.6035	1.797	2.703	2.947	2.612	2.781

and  $\text{NNLO}_A + \overline{\text{NNLL}}$ , respectively, for  $m_A = 125$  GeV. Similarly, for  $m_A = 700$  GeV, the rapidity distribution increases by 8.66% and 5.06% when we go from  $\text{NLO} + \text{NLL}$  and  $\text{NNLO}_A + \text{NNLL}$  to  $\text{NLO} + \overline{\text{NLL}}$  and  $\text{NNLO}_A + \overline{\text{NNLL}}$ , respectively. We also observe that the percentage enhancement in the rapidity distribution due to the resummed NSV logarithms decreases as we go from  $\text{NLO} + \overline{\text{NLL}}$  to  $\text{NNLO}_A + \overline{\text{NNLL}}$ . This suggests better perturbative convergence of the SV + NSV resummed result which was already noticed while comparing it with the fixed order results.

Next, we study the uncertainties of the resummed NSV logarithms with respect to the  $\mu_R$  and  $\mu_F$  scale variations. We first present the plots for canonical 7-point scale variation of the bin-integrated rapidity distribution in Fig. 4 for the pseudoscalar Higgs boson mass,  $m_A = 125, 700$  GeV in the top and bottom panels, respectively. The scales  $\mu = \{\mu_F, \mu_R\}$  are varied in the range  $\frac{1}{2} \leq \frac{\mu}{m_A} \leq 2$ , keeping the ratio  $\mu_R/\mu_F$  not larger than 2 and smaller than 1/2 around the central scale  $\mu_R = \mu_F = m_A$ .

We also provide Tables VII and VIII with the numerical values of the SV and SV + NSV resummed rapidity distributions at the central scale for benchmark rapidity values for  $m_A = 125, 700$  GeV, respectively. These tables also contain the corresponding maximum increments and decrements in the rapidity distribution from the central scale values. From Fig. 4, we observe that the inclusion of resummed NSV logarithms to the SV resummed predictions increases the 7-point scale uncertainty tremendously at  $m_A = 125$  GeV for each perturbative order till  $\text{NNLO}_A$ . Quantitatively, the uncertainty lies between (+24.66%, -18.15%) and (+10.54%, -10.2%) for  $\text{NLO} + \text{NLL}$  and

$\text{NNLO}_A + \text{NNLL}$ , respectively around  $y = 0$ . When we include the resummed NSV logarithms to these predictions, the uncertainty increases to (+36.53%, -23.92%) and (+21.28%, -15.72%) at  $\text{NLO} + \overline{\text{NLL}}$  and  $\text{NNLO}_A + \overline{\text{NNLL}}$ , respectively. However, for  $m_A = 700$  GeV, the increase in the 7-point uncertainty due to the addition of resummed NSV logarithms is not very large. For instance, the uncertainty varies between (+14.67%, -11.74%) and (+9.11%, -7.74%) for  $\text{NLO} + \overline{\text{NLL}}$  and  $\text{NNLO}_A + \overline{\text{NNLL}}$ , respectively, which is not significantly higher than (+13.40%, -11.68%) and (+4.42%, -6.06%) at  $\text{NLO} + \text{NLL}$  and  $\text{NNLO} + \text{NNLL}$ , respectively, around central rapidity region. We also observe that the bands of SV + NSV resummed results at  $\text{NNLO}_A + \overline{\text{NNLL}}$  are completely within the bands of  $\text{NLO} + \overline{\text{NLL}}$  results for both the values of  $m_A$ . On the other hand, this is not the case with SV resummed results at  $m_A = 125$  GeV. This suggests that the inclusion of resummed NSV logarithms improves the convergence of the perturbative result especially for  $m_A = 125$  GeV.

Before moving forward to the comparison of SV and SV + NSV resummed predictions under the variation of  $\mu_R$  and  $\mu_F$  scales individually, we make few comments which would help in the better understanding of our results. The resummed predictions that we compute numerically for the phenomenological analysis, when truncated to a particular logarithmic accuracy, contain not only the distributions and logarithms that we are resumming using the all-order structure but also certain spurious terms. These spurious terms arise from the “inexact” Mellin inversion of the  $N$ -space resummed result and are beyond the precision of the resummed quantity. For instance, the spurious terms developed in the SV resummation are at the NSV and

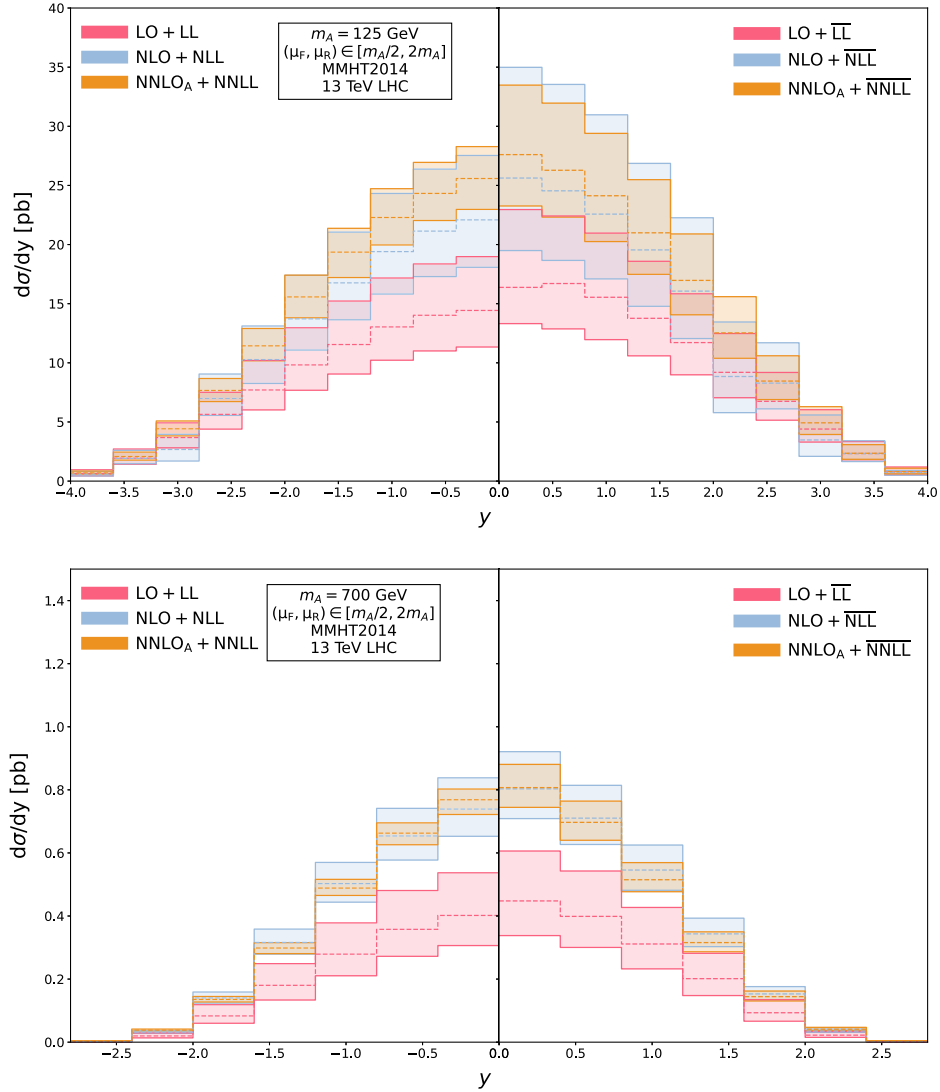


FIG. 4. Comparison of 7-point scale variation between SV and SV + NSV resummed results for  $m_A = 125$  (top) and 700 (bottom) GeV. The dashed lines refer to the corresponding central scale values at each order.

beyond NSV accuracy, and those developed through NSV resummation are beyond NSV accuracy in perturbative QCD. We have discussed the effect of these spurious terms in our numerical results in great detail for the case of inclusive cross-section and the rapidity distribution of the

Higgs Boson production through gluon fusion in Refs. [81,84]. The same behavior is expected to be followed by the SV and SV + NSV resummed results of rapidity distribution of the pseudoscalar Higgs Boson as well.

TABLE VII. Values of SV + NSV resummed rapidity distribution at various orders in comparison to the SV resummed results in pb at the central scale  $\mu_R = \mu_F = m_A = 125$  GeV for 13 TeV LHC.

$y$	LO + LL	LO + $\overline{LL}$	NLO + NLL	NLO + $\overline{NLL}$	NNLO <sub>A</sub> + NNLL	NNLO <sub>A</sub> + $\overline{NNLL}$
0–0.4	14.430 <sup>+4.547</sup> <sub>-3.090</sub>	16.379 <sup>+6.580</sup> <sub>-3.064</sub>	22.086 <sup>+5.446</sup> <sub>-4.008</sub>	25.623 <sup>+9.360</sup> <sub>-6.130</sub>	25.583 <sup>+2.696</sup> <sub>-2.609</sub>	27.605 <sup>+5.873</sup> <sub>-4.340</sub>
0.4–0.8	14.022 <sup>+4.339</sup> <sub>-3.015</sub>	16.704 <sup>+5.712</sup> <sub>-3.833</sub>	21.137 <sup>+5.237</sup> <sub>-3.846</sub>	24.543 <sup>+8.994</sup> <sub>-5.883</sub>	24.326 <sup>+2.621</sup> <sub>-2.292</sub>	26.281 <sup>+5.675</sup> <sub>-3.959</sub>
0.8–1.2	13.035 <sup>+4.135</sup> <sub>-2.814</sub>	15.54 <sup>+5.424</sup> <sub>-3.581</sub>	19.402 <sup>+4.919</sup> <sub>-3.587</sub>	22.572 <sup>+8.396</sup> <sub>-5.474</sub>	22.287 <sup>+2.434</sup> <sub>-2.322</sub>	24.126 <sup>+5.273</sup> <sub>-3.873</sub>
1.2–1.6	11.546 <sup>+3.677</sup> <sub>-2.491</sub>	13.763 <sup>+4.820</sup> <sub>-3.171</sub>	16.759 <sup>+4.291</sup> <sub>-3.120</sub>	19.546 <sup>+7.315</sup> <sub>-4.765</sub>	19.3604 <sup>+2.012</sup> <sub>-2.148</sub>	20.992 <sup>+4.491</sup> <sub>-3.508</sub>
1.6–2.0	9.823 <sup>+3.140</sup> <sub>-2.140</sub>	11.711 <sup>+4.123</sup> <sub>-2.723</sub>	13.715 <sup>+3.681</sup> <sub>-2.636</sub>	16.061 <sup>+6.203</sup> <sub>-4.008</sub>	15.571 <sup>+1.843</sup> <sub>-1.764</sub>	16.968 <sup>+3.926</sup> <sub>-2.906</sub>

TABLE VIII. Values of SV + NSV resummed rapidity distribution at various orders in comparison to the SV resummed results in pb at the central scale  $\mu_R = \mu_F = m_A = 700$  GeV for 13 TeV LHC.

$y$	LO + LL	LO + $\overline{\text{LL}}$	NLO + NLL	NLO + $\overline{\text{NLL}}$	NNLO <sub>A</sub> + NNLL	NNLO <sub>A</sub> + $\overline{\text{NNLL}}$
0–0.4	0.4018 <sup>+0.135</sup> <sub>-0.094</sub>	0.123 <sup>+0.158</sup> <sub>-0.1098</sub>	0.7391 <sup>+0.0990</sup> <sub>-0.0863</sub>	0.803 <sup>+0.1178</sup> <sub>-0.0943</sub>	0.7685 <sup>+0.0340</sup> <sub>-0.0466</sub>	0.807 <sup>+0.0735</sup> <sub>-0.0625</sub>
0.4–0.8	0.3577 <sup>+0.123</sup> <sub>-0.0855</sub>	0.399 <sup>+0.14379</sup> <sub>-0.09845</sub>	0.6538 <sup>+0.0875</sup> <sub>-0.0763</sub>	0.710 <sup>+0.1040</sup> <sub>-0.0834</sub>	0.6628 <sup>+0.0325</sup> <sub>-0.0368</sub>	0.697 <sup>+0.06733</sup> <sub>-0.0566</sub>
0.8–1.2	0.2791 <sup>+0.099</sup> <sub>-0.0685</sub>	0.311 <sup>+0.1158</sup> <sub>-0.0788</sub>	0.5026 <sup>+0.0672</sup> <sub>-0.0586</sub>	0.546 <sup>+0.07919</sup> <sub>-0.0641</sub>	0.4886 <sup>+0.0276</sup> <sub>-0.0233</sub>	0.515 <sup>+0.0543</sup> <sub>-0.0379</sub>
1.2–1.6	0.1803 <sup>+0.0686</sup> <sub>-0.0465</sub>	0.201 <sup>+0.0803</sup> <sub>-0.0535</sub>	0.3162 <sup>+0.0423</sup> <sub>-0.0369</sub>	0.343 <sup>+0.0497</sup> <sub>-0.0405</sub>	0.2985 <sup>+0.0167</sup> <sub>-0.0178</sub>	0.316 <sup>+0.03399</sup> <sub>-0.0291</sub>
1.6–2.0	0.0831 <sup>+0.0355</sup> <sub>-0.0231</sub>	0.093 <sup>+0.0416</sup> <sub>-0.0267</sub>	0.1403 <sup>+0.0186</sup> <sub>-0.0164</sub>	0.153 <sup>+0.0232</sup> <sub>-0.0181</sub>	0.1355 <sup>+0.009</sup> <sub>-0.008</sub>	0.144 <sup>+0.0177</sup> <sub>-0.01365</sub>

Now, let us do the comparison of SV and SV + NSV resummed predictions by varying the factorization scale  $\mu_F$  keeping  $\mu_R$  fixed. In Fig. 5, we provide plots for bin-integrated rapidity distributions for the resummed SV (left

panel) and resummed SV + NSV (right panel) corrections for  $m_A = 125, 700$  GeV keeping  $\mu_R = m_A$  in the top and bottom panels, respectively. The uncertainty bands are obtained by varying the factorization scale in the range

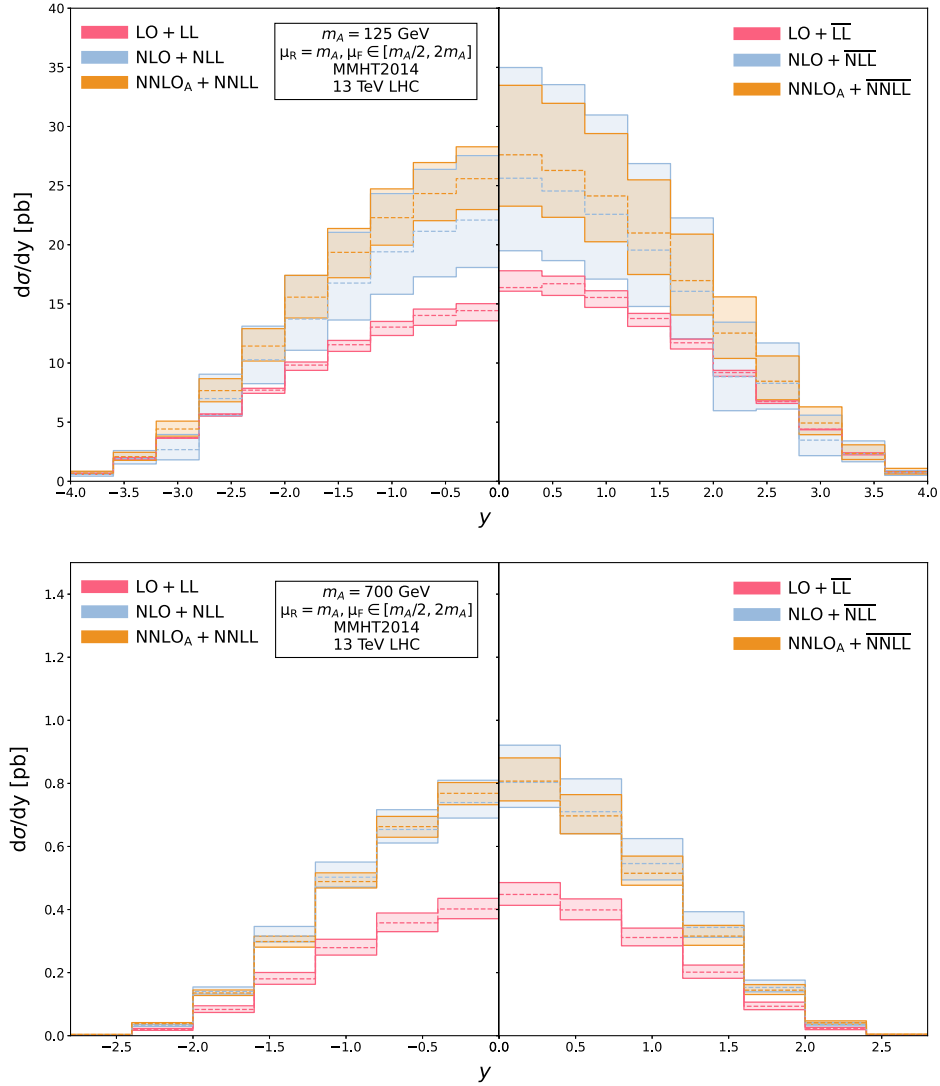


FIG. 5. Comparison of  $\mu_F$  scale variation between SV and SV + NSV resummed results with the scale  $\mu_R = m_A$ . The dashed lines refer to the corresponding central scale values at each order.

$\{1/2, 1\}m_A$  around the central scale  $\mu_F = \mu_R = m_A$ . The plots given in Fig. 5 show that the inclusion of resummed NSV corrections to the SV resummed results worsens the variation of the result with respect to the  $\mu_F$  scale for both  $m_A = 125, 700$  GeV. This can be seen directly from the numerical value of the uncertainty which lies between  $(+36.53\%, -23.92\%)$  and  $(+21.27\%, -15.72\%)$  at  $\text{NLO} + \overline{\text{NLL}}$  and  $\text{NNLO}_A + \overline{\text{NNLL}}$ , respectively, around central rapidity region for  $m_A = 125$  GeV. These values are significantly larger than the corresponding SV resummed uncertainties of  $(+24.66\%, -18.15\%)$  and  $(+10.54\%, -10.19\%)$  at  $\text{NLO} + \text{NLL}$  and  $\text{NNLO}_A + \text{NNLL}$ , respectively. Likewise, for  $m_A = 700$  GeV, the uncertainty lies between  $(+14.66\%, -9.88\%)$  and  $(+9.11\%, -7.75\%)$  for SV + NSV resummed results at  $\text{NLO} + \overline{\text{NLL}}$  and  $\text{NNLO}_A + \overline{\text{NNLL}}$ , respectively, whereas it varies between  $(+9.58\%, -6.63\%)$  and  $(+4.43\%, -4.71\%)$  for SV resummed results at  $\text{NLO} + \text{NLL}$  and  $\text{NNLO}_A + \text{NNLL}$ , respectively, around  $y = 0$ . These values also suggest that the variation with respect to the factorization scale decreases when we go from  $m_A = 125$  GeV to  $m_A = 700$  GeV for both SV and SV + NSV resummed predictions. We need to understand the reason behind this considerable  $\mu_F$  scale variation of the resummed predictions. We stated in the paragraph above that our resummed results contain the spurious terms existing due to the ‘‘inexact’’ Mellin inversion. The detailed analysis done in the Refs. [81] and [84] showed us that these spurious terms play an important role in the  $\mu_F$  scale variation in our results. The study demonstrated that the  $\mu_F$  scale uncertainty arising due to the NSV logarithms gets compensated by the variation coming from the beyond NSV logarithms, and this compensation increases with the increase in the order of perturbation theory.

First, we try to understand the behavior of SV resummed results under  $\mu_F$  variation. The  $\mu_F$  scale variation seen in the SV resummed results comes mainly from the spurious beyond SV terms arising from the inexact Mellin inversion of the  $N$ -space SV resummed results. The plots in Fig. 5 also show us that the uncertainty decreases when we go from  $\text{NLO} + \text{NLL}$  to  $\text{NNLO}_A + \text{NNLL}$ . This confirms our analysis mentioned above that the compensation between  $\mu_F$  uncertainty coming from spurious NSV and beyond NSV terms increases at higher orders thereby decreasing the overall scale dependency for the SV resummed result. Now, let us explore the reason for the huge dependency of SV + NSV resummed results on the factorization scale. For the case of SV resummed results, the spurious terms were the main source of  $\mu_F$  uncertainty; however, for the SV + NSV resummed results, the NSV logarithms contribute significantly toward  $\mu_F$  variation as well. This uncertainty due to the resummed NSV terms can be compensated by adding the resummed beyond NSV terms which is missing

in our calculation. In this case, as well, we have the spurious beyond NSV terms, although now it acts as a compensating factor and cancels the uncertainty due to the resummed NSV logarithms. As a result, we observe that the  $\mu_F$  variation decreases when we go from  $\text{NLO} + \overline{\text{NLL}}$  to  $\text{NNLO}_A + \overline{\text{NNLL}}$  accuracy. However, it can not compensate much, and we need to resum the beyond NSV logarithms in order to completely cancel the uncertainty arising from the resummed NSV logarithms.

We next move on to compare the  $\mu_R$  scale uncertainties of SV and SV + NSV resummed predictions. The plots given in Fig. 6 illustrate the variation of  $\mu_R$  scale in the range  $\{1/2, 1\}m_A$  around the central scale  $\mu_F = \mu_R = m_A$  for the bin-integrated rapidity distributions of the resummed SV (left panel) and resummed SV + NSV (right panel) predictions keeping  $\mu_F = m_A$  for  $m_A = 125, 700$  GeV. The plots show that the inclusion of resummed NSV logarithms reduces the uncertainty due to the  $\mu_R$  scale. The uncertainty varies between  $(+18.22\%, -14.87\%)$  and  $(+7.22\%, -8.21\%)$  for the SV resummed predictions at  $\text{NLO} + \text{NLL}$  and  $\text{NNLO}_A + \text{NNLL}$  around the central rapidity region for  $m_A = 125$  GeV. The corresponding uncertainty bands for the SV + NSV resummed results lie in the range  $(+18.45\%, -15.24\%)$  and  $(+4.16\%, -6.69\%)$  for  $\text{NLO} + \overline{\text{NLL}}$  and  $\text{NNLO}_A + \overline{\text{NNLL}}$ , respectively. Similar trends are observed for the case of  $m_A = 700$  GeV where the  $\mu_R$  scale variation lies in the range  $(+13.40\%, -11.67\%)$  and  $(+4.01\%, -6.06\%)$  for the SV resummed results at  $\text{NLO} + \text{NLL}$  and  $\text{NNLO}_A + \text{NNLL}$ , respectively, whereas for the SV + NSV resummed results, it lies between  $(+13.33\%, -11.74\%)$  and  $(+2.62\%, -5.19\%)$  at  $\text{NLO} + \overline{\text{NLL}}$  and  $\text{NNLO}_A + \overline{\text{NNLL}}$  level, respectively around the central rapidity region. We see from these numerical values that the uncertainty remains almost the same at the next-to-leading level for both SV and SV + NSV resummed results, but at the next-to-next-to-leading order, the  $\mu_R$  scale uncertainty decreases by the addition of the resummed NSV logarithms to the SV resummed results. We know that the inclusion of higher order logarithmic corrections within a particular channel leads to a decrease in the sensitivity of the rapidity distribution with respect to the renormalization scale. This suggests that the percentage contribution of the resummed NSV logarithms is higher at the  $\text{NNLO}_A + \overline{\text{NNLL}}$  as compared to the  $\text{NLO} + \overline{\text{NLL}}$  which results in the significant reduction in the  $\mu_R$  uncertainty at this order.

To summarize the findings of this section, we observed that the resummed SV + NSV results are significantly dependent on the factorization scale and have large uncertainties related to this scale. In order to understand this, we compared our results with the fixed order as well as the SV resummed predictions. We found that the fixed order corrections have negligible dependence on  $\mu_F$  scale,

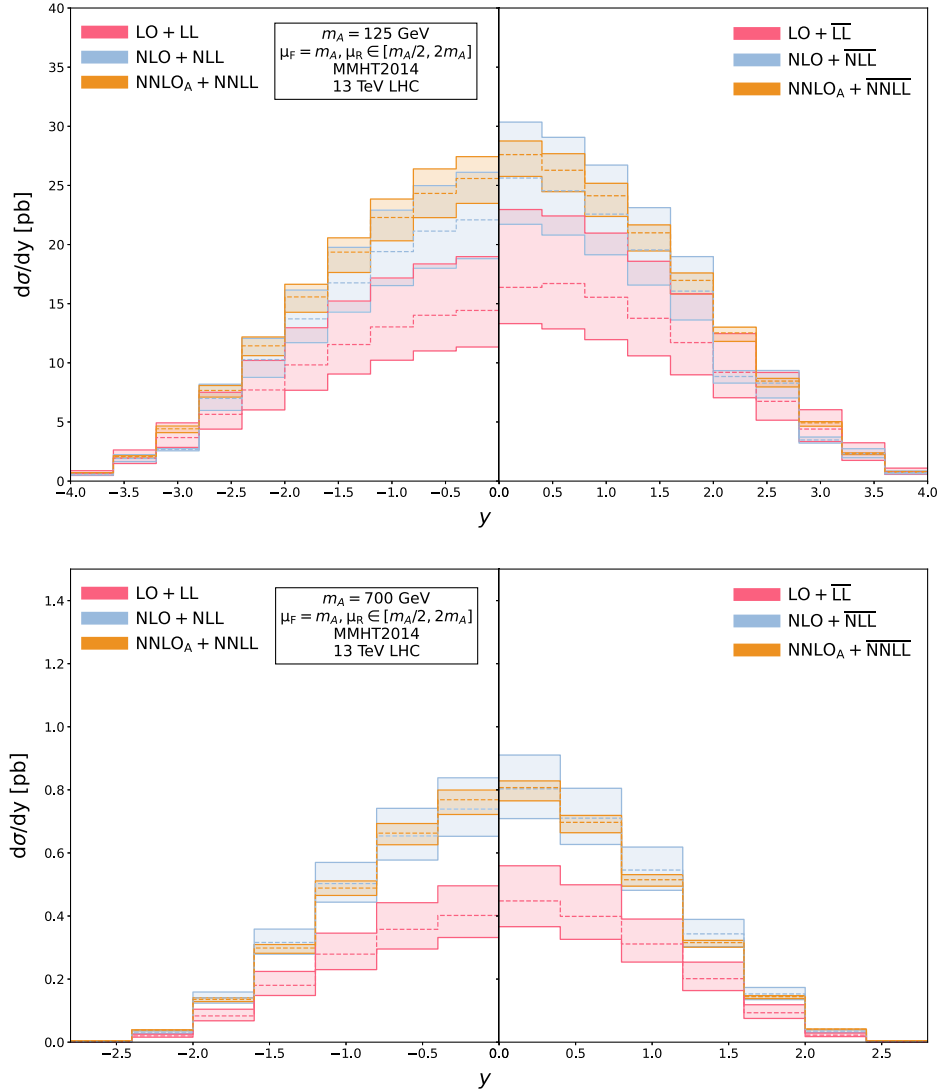


FIG. 6. Comparison of  $\mu_R$  scale variation between SV and SV + NSV resummed results with the scale  $\mu_F = m_A$ . The dashed lines refer to the corresponding central scale values at each order.

whereas for the case of SV resummed results, the main source of  $\mu_F$  variation is the spurious beyond SV terms arising from the “inexact” Mellin inversion of the  $N$ -space resummed results. When we add the resummed NSV logarithms, the  $\mu_F$  uncertainty increases further. Our analysis showed that the reason for this large dependency of the SV + NSV resummed results is the absence of resummed beyond NSV terms which are supposed to cancel the  $\mu_F$  variation of the NSV logarithms. This suggests that it is important to include resummed beyond NSV terms to get a more accurate and reliable prediction for the rapidity distribution of pseudo-scalar Higgs boson in gluon fusion process. We would also like to mention that we have used the same PDF set for both fixed order and resummed predictions. In order to understand the  $\mu_F$  variation in a better way, resummed PDFs should be used if they are available. For the renormalization scale, we

found that the SV + NSV resummed predictions are the least sensitive when we vary  $\mu_R$  around the central scale value keeping  $\mu_F$  fixed. Also, the  $\mu_R$  scale uncertainty decreases when we go to higher orders in perturbation theory. Thus, as expected the  $\mu_R$  scale variation decreases by the addition of higher order logarithmic contributions.

## X. DISCUSSIONS AND CONCLUSIONS

We present the resummed rapidity distribution of pseudo-scalar Higgs Boson production via gluon fusion at LHC up to next-to-next-to-leading-logarithmic (NNLL) accuracy containing both resummed threshold SV contributions as well as next-to-SV ones. It has been matched to the fixed order predictions up to next-to-next-to-leading-order (NNLO<sub>A</sub>) accuracy. Beyond NLO, the fixed order rapidity distribution of the pseudo-scalar Higgs boson has been computed using the corresponding result for the scalar

Higgs case by appropriately multiplying it with the ratio factor  $R_{AH}$ . This ratio method was first established in Ref. [36] by one of the authors for obtaining the inclusive cross section of pseudoscalar Higgs from that of the scalar Higgs boson. In [36], it was shown that the approximate result for the inclusive cross section obtained in this way has an excellent agreement with the exact result, and the difference is found only in terms of next-to-next-to soft distributions which are eventually suppressed in the threshold limit  $z \rightarrow 1$ . The same trend is expected to follow for the rapidity distribution as well. The resummed corrections have been obtained by using our formalism described in [82] where we restrict ourselves to the diagonal channel for the production of the pseudoscalar Higgs.

We have performed a detailed numerical analysis of our computed results around the central scale values  $\mu_R = \mu_F = m_A$  for benchmark rapidity values for two different cases of pseudoscalar mass  $m_A = 125, 700$  GeV. The K-factor values showed that there is a significant enhancement in the rapidity distribution by the addition of resummed SV + NSV corrections up to next-to-leading order. At NNLO<sub>A</sub>, the inclusion of  $\overline{\text{NNLL}}$  resummed results increases the rapidity distribution; however, the percentage enhancement drops substantially compared to that of lower order results. For instance, there is an enhancement of 53.3% and 24.97% by the inclusion of  $\overline{\text{LL}}$  and  $\overline{\text{NLL}}$  resummed results to LO and NLO, respectively, around the central rapidity region which comes down to an 11.48% increase when we include  $\overline{\text{NNLL}}$  to NNLO<sub>A</sub> accuracy at  $m_A = 700$  GeV. This shows that the addition of resummed corrections improves the perturbative convergence of the result thereby making it more reliable. We further used canonical 7-point variation approach to show that the combined uncertainty due to  $\mu_F$  and  $\mu_R$  scales increases

by the inclusion of SV + NSV resummed corrections to the fixed order results throughout the rapidity spectrum and for both the cases of pseudo-scalar Higgs masses. Although, the increase in the sensitivity to the unphysical scales decreases when we go to higher values of pseudoscalar Higgs mass. For example, for  $m_A = 700$  GeV, the 7-point scale uncertainty of the resummed result at NNLO<sub>A</sub> +  $\overline{\text{NNLL}}$  becomes comparable to that of the fixed order rapidity distribution at NNLO<sub>A</sub>.

We studied the impact of the renormalization and the factorization scales individually on our result for the better understanding of their behavior. We found that at higher orders, the uncertainty of our result is mainly driven by the factorization scale. The inclusion of the resummed NSV logarithms to the well-established threshold SV resummed rapidity distribution increases the sensitivity of our result with respect to the  $\mu_F$  scale. The main reason behind this is the absence of resummed beyond NSV terms which is responsible for the cancellation of the uncertainty arising due to the resummed NSV logarithms. On the other hand, the uncertainty due to the  $\mu_R$  scale decreases by the addition of the resummed NSV logarithms. This is expected because the addition of more corrections within the same partonic channel improves the  $\mu_R$  scale uncertainties.

## ACKNOWLEDGMENTS

We would like to thank the computer administrative unit of IMSc for their help and support. We thank Saurav Goyal for pointing out some typos in the paper. S. T. is funded by the Deutsche Forschungsgemeinschaft (DFG, German Research Foundation) under Grant No. 396021762-TRR 257 ‘‘Particle Physics Phenomenology after the Higgs Discovery’’.

## APPENDIX A: QCD $\beta$ FUNCTIONS

$$\begin{aligned}\beta_0 &= \frac{11}{3}C_A - \frac{2}{3}n_f, \\ \beta_1 &= \frac{34}{3}C_A^2 - 2n_fC_F - \frac{10}{3}n_fC_A, \\ \beta_2 &= \frac{2857}{54}C_A^3 - \frac{1415}{54}C_A^2n_f + \frac{79}{54}C_An_f^2 + \frac{11}{9}C_Fn_f^2 - \frac{205}{18}C_FC_An_f + C_F^2n_f.\end{aligned}\tag{A1}$$

## APPENDIX B: NLO RESULTS

In this section, we present the analytical results of the NLO hadronic rapidity distribution for the production of the pseudo-scalar Higgs boson via gluon fusion as follows:

$$\begin{aligned}
\frac{d\sigma_{gg}^{A,(1)}}{dY} = & C_A \left[ H_{gg}(x_1^0, x_2^0, \mu_F^2) \{ (4 + 6\zeta_2) + (2L_{QF})\mathcal{K}(x_1^0, x_2^0) + \mathcal{K}^2(x_1^0, x_2^0) \} + \int dx_1 \frac{H_{gg,1}(x_1, x_2^0, \mu_F^2)}{(x_1 - x_1^0)} (4\mathcal{K}_b^1) \right. \\
& + \int dx_1 H_{gg}(x_1, x_2^0, \mu_F^2) \left\{ \left( -4 \frac{(x_1^0)^2}{x_1^3} + 4 \frac{x_1^0}{x_1^2} - \frac{8}{x_1} + \frac{4}{x_1^0} \right) \mathcal{K}_a^1 + \frac{4\mathcal{K}_c^1}{(x_1 - x_1^0)} \right\} \\
& + \int dx_1 \int dx_2 \frac{H_{gg,1}(x_1, x_2, \mu_F^2)}{(x_1 - x_1^0)} \left( -4 \frac{(x_1^0)^2}{x_1^3} + 4 \frac{x_1^0}{x_1^2} - \frac{8}{x_1} + \frac{4}{x_1^0} \right) + \int dx_1 \int dx_2 \frac{2H_{gg,12}(x_1, x_2, \mu_F^2)}{(x_1 - x_1^0)(x_2 - x_2^0)} \\
& + \int dx_1 \int dx_2 \frac{H_{gg}(x_1, x_2, \mu_F^2)}{(x_1 + x_1^0)(x_2 + x_2^0)(x_1 x_2^0 + x_2 x_1^0)^4} \left\{ \frac{1}{x_1^3} (4(x_1^0)^7(x_2)^4 + 8(x_1^0)^7(x_2)^3 x_2^0 + 8(x_1^0)^7(x_2)^2(x_2^0)^2 \right. \\
& + 8(x_1^0)^7 x_2(x_2^0)^3) + \frac{1}{x_1^2} (16(x_1^0)^6(x_2)^3 x_2^0 + 32(x_1^0)^6(x_2)^2(x_2^0)^2 + 24(x_1^0)^6 x_2(x_2^0)^3 + 16(x_1^0)^6(x_2^0)^4) \\
& + \frac{1}{x_1} (4(x_1^0)^5(x_2)^4 + 8(x_1^0)^5(x_2)^3 x_2^0 + 32(x_1^0)^5(x_2)^2(x_2^0)^2 + 48(x_1^0)^5 x_2(x_2^0)^3 + 40(x_1^0)^5(x_2^0)^4) \\
& + \frac{1}{x_1 x_2} (12(x_1^0 x_2^0)^5) + \frac{1}{x_1^0} (8x_1^5 x_2(x_2^0)^3 + 4x_1^5(x_2^0)^4) + x_1^4 ((16x_2 x_2^0)^2 + 4x_2(x_2^0)^3 + 4(x_2^0)^4) \\
& + x_1^3 (12x_2^3 x_1^0 x_2^0 + 8x_1^0 x_2(x_2^0)^3 + 28x_1^0(x_2^0)^4) + x_1^2 (20(x_2 x_1^0 x_2^0)^2 + 88(x_1^0)^2(x_2^0)^3 x_2 + 48(x_1^0)^2(x_2^0)^4) \\
& \left. + x_1 (68(x_1^0 x_2^0)^3 x_2^0) + x_1 x_2 (64(x_1^0 x_2^0)^3) + 40(x_1^0 x_2^0)^4 \right\} \Big] + (1 \leftrightarrow 2). \tag{B1}
\end{aligned}$$

For the  $qg$  and  $gq$  channels, we obtain

$$\begin{aligned}
\frac{d\sigma_{qg}^{A,(1)}}{dY} = & C_F \left[ \int dx_1 H_{qg}(x_1, x_2^0, \mu_F^2) \left\{ \left( \frac{2x_1^0}{x_1^2} \right) + \left( -\frac{4}{x_1} + \frac{4}{x_1^0} + \frac{2x_1^0}{x_1^2} \right) K_a^1 \right\} + \int dx_1 \int dx_2 \frac{H_{qg,2}(x_1, x_2, \mu_F^2)}{(x_2 - x_2^0)} \left\{ \frac{2x_1^0}{x_1^2} \right. \right. \\
& - \left. \frac{4}{x_1} + \frac{4}{x_1^0} \right\} + \int dx_1 \int dx_2 \frac{H_{qg}(x_1, x_2, \mu_F^2)}{(x_1 + x_1^0)(x_2 + x_2^0)(x_1 x_2^0 + x_2 x_1^0)^4} \left\{ \frac{1}{x_1^2} (-2(x_1^0)^5 x_2^3 - 4(x_1^0)^5 x_2^2 x_2^0 \right. \\
& - 4(x_1^0)^5 x_2(x_2^0)^2) + \frac{1}{x_1} (2(x_1^0)^4 x_2^3 - 2(x_1^0)^4 x_2^2 x_2^0 - 4(x_1^0)^4 x_2(x_2^0)^2) + \frac{1}{x_1^0} (8x_1^4 x_2(x_2^0)^2 + 4x_1^4(x_2^0)^3) \\
& + (4x_1^3 x_2^2 x_2^0 + 2x_1^3 x_2(x_2^0)^2) + 2x_1^2 x_1^0 x_2^3 - 6x_1^2 x_1^0 x_2(x_2^0)^2 - x_1^2 x_1^0(x_2^0)^3 + 3x_1(x_1^0)^2 x_2(x_2^0)^2 + x_1(x_1^0)^2(x_2^0)^3 \\
& \left. \left. + 5(x_1^0)^3 x_2^2 x_2^0 + 7(x_1^0)^3 x_2(x_2^0)^2 \right\} \right], \tag{B2}
\end{aligned}$$

$$\frac{d\sigma_{qg}^{A,(1)}}{dY} = \frac{d\sigma_{gq}^{A,(1)}}{dY} \Big|_{1 \leftrightarrow 2}. \tag{B3}$$

For the  $q\bar{q}$ -channel, we find

$$\begin{aligned}
\frac{d\sigma_{q\bar{q}}^{A,(1)}}{dY} = & \frac{(N^2 - 1)C_F}{N} \left[ \int dx_1 dx_2 H_{q\bar{q}}(x_1, x_2, \mu_F^2) \left\{ \frac{1}{x_1^2} (4(x_1^0)^3(x_1^0 x_2^0)^3 x_2 + 4(x_1^0 x_2^0)^4(x_1^0)^2) + \frac{1}{x_1} (4(x_1^0)^5(x_2 x_2^0)^2 \right. \right. \\
& + 8(x_1^0)^5 x_2(x_2^0)^3 + 4(x_1^0)^5(x_2^0)^4) + x_1^4 (4(x_2 x_2^0)^4 + 4x_2(x_2^0)^3) + x_1^3 (4x_1^0(x_2 x_2^0)^2 + 8x_1^0 x_2(x_2^0)^3 + x_1^0(x_2^0)^4) \\
& + x_1^2 (-8(x_1^0 x_2^0 x_2^0)^2 + x_2(x_1^0)^2(x_2^0)^3 + (x_1^0 x_2^0)^2(x_2^0)^2) + x_1 x_2 (-16(x_1^0 x_2^0)^3) \\
& \left. \left. + x_1 (-12(x_1^0 x_2^0)^3 x_2^0) - 8(x_1^0 x_2^0)^4 \right\} \right] + (1 \leftrightarrow 2). \tag{B4}
\end{aligned}$$

In the above equations, we have introduced the following abbreviations:

$$\begin{aligned}
H_{ab,12}(x_1, x_2, \mu_F^2) &= H_{ab}(x_1, x_2, \mu_F^2) - H_{ab}(x_1^0, x_2, \mu_F^2) - H_{ab}(x_1, x_2^0, \mu_F^2) + H_{ab}(x_1^0, x_2^0, \mu_F^2), \\
H_{ab,1}(x_1, z, \mu_F^2) &= H_{ab}(x_1, z, \mu_F^2) - H_{ab}(x_1^0, z, \mu_F^2), \\
H_{ab,2}(z, x_2, \mu_F^2) &= H_{ab}(z, x_2, \mu_F^2) - H_{ab}(z, x_2^0, \mu_F^2),
\end{aligned} \tag{B5}$$

where

$$\begin{aligned}
H_{q\bar{q}}(x_1, x_2, \mu_F^2) &= f_q(x_1, \mu_F^2)f_{\bar{q}}(x_2, \mu_F^2) + f_{\bar{q}}(x_1, \mu_F^2)f_q(x_2, \mu_F^2), \\
H_{gq}(x_1, x_2, \mu_F^2) &= f(x_1, \mu_F^2)(f_q(x_2, \mu_F^2) + f_{\bar{q}}(x_2, \mu_F^2)), \\
H_{qg}(x_1, x_2, \mu_F^2) &= H_{gq}(x_2, x_1, \mu_F^2), \\
H_{gg}(x_1, x_2, \mu_F^2) &= f_g(x_1, \mu_F^2)f_g(x_2, \mu_F^2).
\end{aligned} \tag{B6}$$

$$\begin{aligned}
\mathcal{K}_{a_1} &= \ln\left(\frac{2Q^2(1-x_2^0)(x_1-x_1^0)}{\mu_F^2(x_1+x_1^0)x_2^0}\right), & \mathcal{K}_{b_1} &= \ln\left(\frac{Q^2(1-x_2^0)(x_1-x_1^0)}{\mu_F^2x_1^0x_2^0}\right), \\
\mathcal{K}_{c_1} &= \ln\left(\frac{2x_1^0}{x_1+x_1^0}\right), & \mathcal{K}(x_1^0, x_2^0) &= \ln\left(\frac{(1-x_1^0)(1-x_2^0)}{x_1^0x_2^0}\right).
\end{aligned} \tag{B7}$$

The  $\mathcal{K}_{a_2}$ ,  $\mathcal{K}_{b_2}$ , and  $\mathcal{K}_{c_2}$  can be obtained from  $\mathcal{K}_{a_1}$ ,  $\mathcal{K}_{b_1}$ , and  $\mathcal{K}_{c_1}$  by using  $1 \leftrightarrow 2$  symmetry.

### APPENDIX C: ANOMALOUS DIMENSIONS

$$\begin{aligned}
\gamma_{g,1}^A &= \frac{11}{3}C_A - \frac{2}{3}n_f, \\
\gamma_{g,2}^A &= \frac{34}{3}C_A^2 - 2n_fC_F - \frac{10}{3}n_fC_A, \\
\gamma_{g,3}^A &= \frac{2857}{54}C_A^3 - \frac{1415}{54}C_A^2n_f + \frac{79}{54}C_An_f^2 + \frac{11}{9}C_Fn_f^2 - \frac{205}{18}C_FC_An_f + C_F^2n_f.
\end{aligned} \tag{C1}$$

$$\begin{aligned}
A_{g,1}^A &= 4C_A, \\
A_{g,2}^A &= 8C_A^2\left\{\frac{67}{18} - \zeta_2\right\} + 8C_An_f\left\{-\frac{5}{9}\right\}, \\
A_{g,3}^A &= 16C_A^3\left\{\frac{245}{24} - \frac{67}{9}\zeta_2 + \frac{11}{6}\zeta_3 + \frac{11}{5}\zeta_2^2\right\} + 16C_AC_Fn_f\left\{-\frac{55}{24} + 2\zeta_3\right\} \\
&\quad + 16C_A^2n_f\left\{-\frac{209}{108} + \frac{10}{9}\zeta_2 - \frac{7}{3}\zeta_3\right\} + 16C_An_f^2\left\{-\frac{1}{27}\right\}.
\end{aligned} \tag{C2}$$

$$\begin{aligned}
B_{g,1}^A &= n_f\left\{-\frac{2}{3}\right\} + C_A\left\{\frac{11}{3}\right\}, \\
B_{g,2}^A &= C_Fn_f\{-2\} + C_An_f\left\{-\frac{8}{3}\right\} + C_A^2\left\{\frac{32}{3} + 12\zeta_3\right\}, \\
B_{g,3}^A &= C_Fn_f^2\left\{\frac{11}{9}\right\} + C_F^2n_f + C_An_f^2\left\{\frac{29}{18}\right\} + C_AC_Fn_f\left\{-\frac{241}{18}\right\} + C_A^2n_f\left\{-\frac{233}{18}\right. \\
&\quad \left. - \frac{80}{3}\zeta_3 - \frac{8}{3}\zeta_2 - \frac{4}{3}\zeta_2^2\right\} + C_A^3\left\{\frac{79}{2} - 80\zeta_5 + \frac{536}{3}\zeta_3 + \frac{8}{3}\zeta_2 - 16\zeta_2\zeta_3 + \frac{22}{3}\zeta_2^2\right\}.
\end{aligned} \tag{C3}$$

$$\begin{aligned}
f_{g,1}^A &= 0, \\
f_{g,2}^A &= C_A^2 \left\{ -\frac{22}{3} \zeta_2 - 28 \zeta_3 + \frac{808}{27} \right\} + C_A n_f \left\{ \frac{4}{3} \zeta_2 - \frac{112}{27} \right\}, \\
f_{g,3}^A &= C_A^3 \left\{ \frac{352}{5} \zeta_2^2 + \frac{176}{3} \zeta_2 \zeta_3 - \frac{12650}{81} \zeta_2 - \frac{1316}{3} \zeta_3 + 192 \zeta_5 + \frac{136781}{729} \right\} \\
&\quad + C_A^2 n_f \left\{ -\frac{96}{5} \zeta_2^2 + \frac{2828}{81} \zeta_2 + \frac{728}{27} \zeta_3 - \frac{11842}{729} \right\} \\
&\quad + C_A C_F n_f \left\{ \frac{32}{5} \zeta_2^2 + 4 \zeta_2 + \frac{304}{9} \zeta_3 - \frac{1711}{27} \right\} + C_A n_f^2 \left\{ -\frac{40}{27} \zeta_2 + \frac{112}{27} \zeta_3 - \frac{2080}{729} \right\}. \tag{C4}
\end{aligned}$$

$$\begin{aligned}
\mathbf{D}_{d,g,1}^A &= 0, \\
\mathbf{D}_{d,g,2}^A &= C_A n_f \left\{ \frac{112}{27} - \frac{8}{3} \zeta_2 \right\} + C_A^2 \left\{ -\frac{808}{27} + 28 \zeta_3 + \frac{44}{3} \zeta_2 \right\}, \\
\mathbf{D}_{d,g,3}^A &= C_A n_f^2 \left\{ -\frac{1856}{729} - \frac{32}{27} \zeta_3 + \frac{160}{27} \zeta_2 \right\} + C_A C_F n_f \left\{ \frac{1711}{27} - \frac{304}{9} \zeta_3 - 8 \zeta_2 - \frac{32}{5} \zeta_2^2 \right\} \\
&\quad + C_A^2 n_f \left\{ \frac{62626}{729} - \frac{536}{9} \zeta_3 - \frac{7760}{81} \zeta_2 + \frac{208}{15} \zeta_2^2 \right\} + C_A^3 \left\{ -\frac{297029}{729} - 192 \zeta_5 + \frac{14264}{27} \zeta_3 \right. \\
&\quad \left. + \frac{27752}{81} \zeta_2 - \frac{176}{3} \zeta_2 \zeta_3 - \frac{616}{15} \zeta_2^2 \right\}. \tag{C5}
\end{aligned}$$

#### APPENDIX D: RESULTS OF SV RAPIDITY DISTRIBUTION TO THIRD ORDER

$$\Delta_{d,g,1}^{A,SV} = \delta \bar{\delta} \{ C_A (4 + 6 \zeta_2) \} + \bar{\mathcal{D}}_0 \mathcal{D}_0 \{ C_A (2) \} + \delta \bar{\mathcal{D}}_1 \{ C_A (4) \} + (z_1 \leftrightarrow z_2), \tag{D1}$$

$$\begin{aligned}
\Delta_{d,g,2}^{A,SV} &= \delta \bar{\delta} \left[ \left\{ C_F n_f \left( -\frac{80}{3} + 6 \ln \left( \frac{\mu_R^2}{m_t^2} \right) + 8 \zeta_3 \right) \right\} + \left\{ C_A n_f \left( -\frac{41}{3} - 4 \zeta_3 - \frac{20}{3} \zeta_2 \right) \right\} \right. \\
&\quad + \left. \left\{ C_A^2 \left( \frac{247}{3} - 22 \zeta_3 + \frac{278}{3} \zeta_2 + \frac{126}{5} \zeta_2^2 \right) \right\} \right] + \bar{\mathcal{D}}_0 \mathcal{D}_0 \left[ \left\{ C_A n_f \left( -\frac{20}{9} \right) \right\} \right. \\
&\quad + \left. \left\{ C_A^2 \left( \frac{278}{9} + 4 \zeta_2 \right) \right\} \right] + \bar{\mathcal{D}}_1 \mathcal{D}_0 \left[ \left\{ C_A n_f \left( \frac{8}{3} \right) \right\} + \left\{ C_A^2 \left( -\frac{44}{3} \right) \right\} \right] \\
&\quad + \mathcal{D}_0 \bar{\mathcal{D}}_2 \{ C_A^2 (24) \} + \bar{\mathcal{D}}_1 \mathcal{D}_1 \{ C_A^2 (24) \} + \delta \bar{\mathcal{D}}_0 \left[ \left\{ C_A n_f \left( +\frac{112}{27} - \frac{8}{3} \zeta_2 \right) \right\} \right. \\
&\quad + \left. \left\{ C_A^2 \left( -\frac{808}{27} + 60 \zeta_3 + \frac{44}{3} \zeta_2 \right) \right\} \right] + \delta \bar{\mathcal{D}}_1 \left[ \left\{ C_A n_f \left( -\frac{40}{9} \right) \right\} + \left\{ C_A^2 \left( \frac{556}{9} + 8 \zeta_2 \right) \right\} \right] \\
&\quad + \delta \bar{\mathcal{D}}_2 \left[ \left\{ C_A n_f \left( \frac{4}{3} \right) \right\} + \left\{ C_A^2 \left( -\frac{22}{3} \right) \right\} \right] + \delta \bar{\mathcal{D}}_3 \{ C_A^2 (8) \} + (z_1 \leftrightarrow z_2), \tag{D2}
\end{aligned}$$

$$\begin{aligned}
\Delta_{d,g,3}^{A,SV} = & \delta\bar{\delta} \left[ \left\{ n_f(-2C_f^{(2)}) \right\} + \left\{ C_F n_f^2 \left( \frac{749}{9} - \frac{8}{9}\zeta_4 - \frac{112}{3}\zeta_3 - \frac{20}{9}\zeta_2 \right) \right\} \right. \\
& + \left\{ C_F^2 n_f \left( \frac{457}{6} - 160\zeta_5 + 104\zeta_3 \right) \right\} + \left\{ C_A n_f^2 \left( \frac{3457}{81} - \frac{152}{9}\zeta_4 + \frac{56}{3}\zeta_3 - 8\zeta_2 \right. \right. \\
& \left. \left. - \frac{8}{45}\zeta_2^2 \right) \right\} + \left\{ C_A C_F n_f \left( -\frac{1797}{2} + 48 \ln \left( \frac{\mu_R^2}{m_f^2} \right) + 80\zeta_5 + \frac{44}{9}\zeta_4 + \frac{904}{3}\zeta_3 - \frac{3205}{9}\zeta_2 \right. \right. \\
& \left. \left. + 72\zeta_2 \ln \left( \frac{\mu_R^2}{m_f^2} \right) + 144\zeta_2\zeta_3 \right) \right\} + \left\{ C_A^2 n_f \left( -\frac{56683}{81} + \frac{596}{9}\zeta_5 + \frac{5258}{27}\zeta_4 + \frac{188}{27}\zeta_3 \right. \right. \\
& \left. \left. - \frac{5138}{27}\zeta_2 - 136\zeta_2\zeta_3 - \frac{824}{15}\zeta_2^2 \right) \right\} + \left\{ C_A^3 \left( \frac{57284}{27} - \frac{4006}{3}\zeta_6 + \frac{682}{9}\zeta_5 - \frac{15257}{27}\zeta_4 \right. \right. \\
& \left. \left. - \frac{33098}{27}\zeta_3 + \frac{800}{3}\zeta_3^2 + \frac{40235}{27}\zeta_2 - 44\zeta_2\zeta_3 + \frac{25982}{45}\zeta_2^2 + \frac{12688}{35}\zeta_2^3 \right) \right\} \Big] \\
& + \delta\bar{D}_0 \left\{ C_A n_f^2 \left( -\frac{1856}{729} - \frac{32}{27}\zeta_3 + \frac{160}{27}\zeta_2 \right) \right\} + \delta\bar{D}_0 \left\{ C_A C_F n_f \left( \frac{1711}{27} - \frac{304}{9}\zeta_3 - 8\zeta_2 \right. \right. \\
& \left. \left. - \frac{32}{5}\zeta_2^2 \right) \right\} + \delta\bar{D}_0 \left\{ C_A^2 n_f \left( \frac{86818}{729} - \frac{392}{3}\zeta_3 - \frac{8144}{81}\zeta_2 + \frac{16}{5}\zeta_2^2 \right) \right\} + \delta\bar{D}_0 \left\{ C_A^3 \left( -\frac{471557}{729} \right. \right. \\
& \left. \left. + 192\zeta_5 + \frac{40088}{27}\zeta_3 + \frac{27560}{81}\zeta_2 - \frac{608}{3}\zeta_2\zeta_3 + \frac{88}{5}\zeta_2^2 \right) \right\} + \delta\bar{D}_1 \left\{ C_A n_f^2 \left( \frac{400}{81} - \frac{32}{9}\zeta_2 \right) \right\} \\
& + \delta\bar{D}_1 \left\{ C_A C_F n_f \left( -250 + 48 \ln \left( \frac{\mu_R^2}{m_f^2} \right) + 96\zeta_3 \right) \right\} + \delta\bar{D}_1 \left\{ C_A^2 n_f \left( -\frac{19940}{81} + 32\zeta_3 \right. \right. \\
& \left. \left. + \frac{64}{3}\zeta_2 \right) \right\} + \delta\bar{D}_1 \left\{ C_A^3 \left( \frac{103654}{81} - 704\zeta_3 + \frac{680}{9}\zeta_2 - \frac{64}{5}\zeta_2^2 \right) \right\} + \delta\bar{D}_2 \left\{ C_A n_f^2 \left( -\frac{80}{27} \right) \right\} \\
& + \delta\bar{D}_2 \{ C_A C_F n_f(4) \} + \delta\bar{D}_2 \left\{ C_A^2 n_f \left( \frac{2116}{27} - \frac{112}{3}\zeta_2 \right) \right\} + \delta\bar{D}_2 \left\{ C_A^3 \left( -\frac{9992}{27} + 488\zeta_3 \right. \right. \\
& \left. \left. + \frac{616}{3}\zeta_2 \right) \right\} + \delta\bar{D}_3 \left\{ C_A n_f^2 \left( \frac{16}{27} \right) \right\} + \delta\bar{D}_3 \left\{ C_A^2 n_f \left( -\frac{656}{27} \right) \right\} + \delta\bar{D}_3 \left\{ C_A^3 \left( \frac{5428}{27} - 64\zeta_2 \right) \right\} \\
& + \delta\bar{D}_4 \left\{ C_A^2 n_f \left( \frac{40}{9} \right) \right\} + \delta\bar{D}_4 \left\{ C_A^3 \left( -\frac{220}{9} \right) \right\} + \delta\bar{D}_5 \{ C_A^3(8) \} + \bar{D}_0 \bar{D}_0 \left\{ C_A n_f^2 \left( \frac{200}{81} - \frac{16}{9}\zeta_2 \right) \right\} \\
& + \bar{D}_0 \bar{D}_0 \left\{ C_A C_F n_f \left( -125 + 24 \ln \left( \frac{\mu_R^2}{m_f^2} \right) + 48\zeta_3 \right) \right\} + \bar{D}_0 \bar{D}_0 \left\{ C_A^2 n_f \left( -\frac{9970}{81} + 16\zeta_3 \right. \right. \\
& \left. \left. + \frac{32}{3}\zeta_2 \right) \right\} + \bar{D}_0 \bar{D}_0 \left\{ C_A^3 \left( \frac{51827}{81} - 352\zeta_3 + \frac{340}{9}\zeta_2 - \frac{32}{5}\zeta_2^2 \right) \right\} + \bar{D}_1 \bar{D}_0 \left\{ C_A n_f^2 \left( -\frac{160}{27} \right) \right\} \\
& + \bar{D}_1 \bar{D}_0 \{ C_A C_F n_f(8) \} + \bar{D}_1 \bar{D}_0 \left\{ C_A^2 n_f \left( \frac{4232}{27} - \frac{224}{3}\zeta_2 \right) \right\} + \bar{D}_1 \bar{D}_0 \left\{ C_A^3 \left( -\frac{19984}{27} + 976\zeta_3 \right. \right. \\
& \left. \left. + \frac{1232}{3}\zeta_2 \right) \right\} + \bar{D}_0 \bar{D}_2 \left\{ C_A n_f^2 \left( \frac{16}{9} \right) \right\} + \bar{D}_0 \bar{D}_2 \left\{ C_A^2 n_f \left( -\frac{656}{9} \right) \right\} + \bar{D}_0 \bar{D}_2 \left\{ C_A^3 \left( \frac{5428}{9} - 192\zeta_2 \right) \right\} \\
& + \bar{D}_0 \bar{D}_3 \left\{ C_A^2 n_f \left( \frac{160}{9} \right) \right\} + \bar{D}_0 \bar{D}_3 \left\{ C_A^3 \left( -\frac{880}{9} \right) \right\} + \bar{D}_0 \bar{D}_4 \{ C_A^3(40) \} + \bar{D}_1 \bar{D}_1 \left\{ C_A n_f^2 \left( \frac{16}{9} \right) \right\} \\
& + \bar{D}_1 \bar{D}_1 \left\{ C_A^2 n_f \left( -\frac{656}{9} \right) \right\} + \bar{D}_1 \bar{D}_1 \left\{ C_A^3 \left( \frac{5428}{9} - 192\zeta_2 \right) \right\} + \bar{D}_1 \bar{D}_2 \left\{ C_A^2 n_f \left( \frac{160}{3} \right) \right\} \\
& + \bar{D}_1 \bar{D}_2 \left\{ C_A^3 \left( -\frac{880}{3} \right) \right\} + \bar{D}_1 \bar{D}_3 \{ C_A^3(160) \} + \bar{D}_2 \bar{D}_2 \{ C_A^3(120) \} + (z_1 \leftrightarrow z_2). \tag{D3}
\end{aligned}$$

Here,  $\mathcal{D}_j = \left[ \frac{\ln^j(1-z_1)}{(1-z_1)} \right]_+$ ,  $\bar{\mathcal{D}}_j = \left[ \frac{\ln^j(1-z_2)}{(1-z_2)} \right]_+$ ,  $\delta = \delta(1-z_1)$  and  $\bar{\delta} = \delta(1-z_2)$ .

APPENDIX E: THE RESUMMATION CONSTANT  $\tilde{g}_{d,g,0}^A$ 

$$\tilde{g}_{d,g,0}^A(a_s(\mu_R^2)) = \sum_{i=0}^{\infty} a_s^i(\mu_R^2) \tilde{g}_{d,g,0,i}^A \quad (\text{E1})$$

$$\tilde{g}_{d,g,0,0}^A = 1, \quad (\text{E2})$$

$$\tilde{g}_{d,g,0,1}^A = n_f \left\{ \frac{4}{3} L_{fr} \right\} + C_A \left\{ 8 + 16\zeta_2 - \frac{22}{3} L_{fr} \right\} + \gamma_E C_A \{-8L_{qr} + 8L_{fr}\} + \gamma_E^2 C_A \{8\}, \quad (\text{E3})$$

$$\begin{aligned} \tilde{g}_{d,g,0,2}^A = & n_f C_F \left\{ -\frac{160}{3} + 12L_{rmt} + 16\zeta_3 + 4L_{fr} \right\} + n_f^2 \left\{ \frac{4}{3} L_{fr}^2 \right\} + C_A n_f \left\{ -\frac{82}{3} - \frac{88}{9} \zeta_3 - \frac{160}{9} \zeta_2 + \frac{20}{3} L_{qr} \right. \\ & + \frac{32}{3} L_{qr} \zeta_2 + 16L_{fr} + \frac{64}{3} L_{fr} \zeta_2 - \frac{44}{3} L_{fr}^2 \left. \right\} + C_A^2 \left\{ \frac{494}{3} - \frac{308}{9} \zeta_3 + \frac{2224}{9} \zeta_2 + 92\zeta_2^2 - \frac{92}{3} L_{qr} + 24L_{qr} \zeta_3 \right. \\ & - \frac{176}{3} L_{qr} \zeta_2 - 80L_{fr} - 24L_{fr} \zeta_3 - \frac{352}{3} L_{fr} \zeta_2 + \frac{121}{3} L_{fr}^2 \left. \right\} + \gamma_E C_A n_f \left\{ -\frac{224}{27} + \frac{80}{9} L_{qr} - \frac{8}{3} L_{qr}^2 - \frac{80}{9} L_{fr} \right. \\ & - \frac{32}{3} L_{fr} L_{qr} + \frac{40}{3} L_{fr}^2 \left. \right\} + \gamma_E C_A^2 \left\{ \frac{1616}{27} - 56\zeta_3 - \frac{1112}{9} L_{qr} - 112L_{qr} \zeta_2 + \frac{44}{3} L_{qr}^2 + \frac{1112}{9} L_{fr} + 112L_{fr} \zeta_2 \right. \\ & + \frac{176}{3} L_{fr} L_{qr} - \frac{220}{3} L_{fr}^2 \left. \right\} + \gamma_E^2 C_A n_f \left\{ -\frac{80}{9} + \frac{16}{3} L_{qr} + \frac{32}{3} L_{fr} \right\} + \gamma_E^2 C_A^2 \left\{ \frac{1112}{9} + 112\zeta_2 - \frac{88}{3} L_{qr} + 32L_{qr}^2 \right. \\ & - \frac{176}{3} L_{fr} - 64L_{fr} L_{qr} + 32L_{fr}^2 \left. \right\} + \gamma_E^3 C_A n_f \left\{ -\frac{32}{9} \right\} + \gamma_E^3 C_A^2 \left\{ \frac{176}{9} - 64L_{qr} + 64L_{fr} \right\} + \gamma_E^4 C_A^2 \{32\}, \quad (\text{E4}) \end{aligned}$$

$$\begin{aligned} \tilde{g}_{d,g,0,3}^A = & n_f \{-4C_F^{(2)}\} + n_f C_F^2 \left\{ \frac{457}{3} - 320\zeta_5 + 208\zeta_3 - 2L_{fr} \right\} + n_f^2 C_F \left\{ \frac{1498}{9} - \frac{16}{9} \zeta_4 - \frac{224}{3} \zeta_3 - \frac{40}{9} \zeta_2 - \frac{640}{9} L_{qr} \right. \\ & + 16L_{qr} L_{rmt} + \frac{64}{3} L_{qr} \zeta_3 - \frac{662}{9} L_{fr} + 16L_{fr} L_{rmt} + \frac{64}{3} L_{fr} \zeta_3 + \frac{28}{3} L_{fr}^2 \left. \right\} + n_f^3 \left\{ \frac{32}{27} L_{fr}^3 \right\} + C_A n_f C_F \left\{ -1797 \right. \\ & + 96L_{rmt} + \frac{88}{9} \zeta_4 + 160\zeta_5 + \frac{1792}{3} \zeta_3 - \frac{8660}{9} \zeta_2 + 192\zeta_2 L_{rmt} + 384\zeta_2 \zeta_3 + \frac{3628}{9} L_{qr} - 88L_{qr} L_{rmt} - \frac{352}{3} L_{qr} \zeta_3 \\ & + 32L_{qr} \zeta_2 + \frac{4049}{9} L_{fr} - 88L_{fr} L_{rmt} - \frac{352}{3} L_{fr} \zeta_3 + 64L_{fr} \zeta_2 - \frac{154}{3} L_{fr}^2 \left. \right\} + C_A n_f^2 \left\{ \frac{6914}{81} - \frac{304}{9} \zeta_4 + \frac{3344}{81} \zeta_3 \right. \\ & - \frac{896}{81} \zeta_2 - \frac{64}{45} \zeta_2^2 - \frac{976}{27} L_{qr} - \frac{352}{27} L_{qr} \zeta_3 - \frac{640}{27} L_{qr} \zeta_2 + \frac{40}{9} L_{qr}^2 + \frac{64}{9} L_{qr}^2 \zeta_2 - \frac{119}{3} L_{fr} - \frac{352}{27} L_{fr} \zeta_3 - \frac{640}{27} L_{fr} \zeta_2 \\ & + \frac{80}{9} L_{fr} L_{qr} + \frac{128}{9} L_{fr} L_{qr} \zeta_2 + \frac{212}{9} L_{fr}^2 + \frac{64}{3} L_{fr}^2 \zeta_2 - \frac{176}{9} L_{fr}^3 \left. \right\} + C_A^2 n_f \left\{ -\frac{113366}{81} + \frac{10516}{27} \zeta_4 + \frac{808}{9} \zeta_5 \right. \\ & - \frac{7336}{81} \zeta_3 - \frac{50768}{81} \zeta_2 - \frac{784}{3} \zeta_2 \zeta_3 - \frac{8576}{45} \zeta_2^2 + \frac{13064}{27} L_{qr} - \frac{736}{27} L_{qr} \zeta_3 + \frac{14288}{27} L_{qr} \zeta_2 + 120L_{qr} \zeta_2^2 - \frac{404}{9} L_{qr}^2 \\ & + 16L_{qr}^2 \zeta_3 - \frac{704}{9} L_{qr}^2 \zeta_2 + \frac{4397}{9} L_{fr} + \frac{2144}{27} L_{fr} \zeta_3 + \frac{14864}{27} L_{fr} \zeta_2 + \frac{376}{3} L_{fr} \zeta_2^2 - \frac{808}{9} L_{fr} L_{qr} + 32L_{fr} L_{qr} \zeta_3 \\ & - \frac{1408}{9} L_{fr} L_{qr} \zeta_2 - \frac{2146}{9} L_{fr}^2 - 48L_{fr}^2 \zeta_3 - \frac{704}{3} L_{fr}^2 \zeta_2 + \frac{968}{9} L_{fr}^3 \left. \right\} + C_A^3 \left\{ \frac{114568}{27} - \frac{8012}{3} \zeta_6 - \frac{30514}{27} \zeta_4 \right. \end{aligned}$$

$$\begin{aligned}
& + \frac{3476}{9} \zeta_5 - \frac{158620}{81} \zeta_3 + 96 \zeta_3^2 + \frac{345064}{81} \zeta_2 - \frac{2024}{3} \zeta_2 \zeta_3 + \frac{6224}{3} \zeta_2^2 + \frac{6080}{7} \zeta_2^3 - \frac{36064}{27} L_{qr} - 160 L_{qr} \zeta_5 \\
& + \frac{21608}{27} L_{qr} \zeta_3 - \frac{54256}{27} L_{qr} \zeta_2 + 352 L_{qr} \zeta_2 \zeta_3 - 660 L_{qr} \zeta_2^2 + \frac{1012}{9} L_{qr}^2 - 88 L_{qr}^2 \zeta_3 + \frac{1936}{9} L_{qr}^2 \zeta_2 - \frac{13115}{9} L_{fr} \\
& + 160 L_{fr} \zeta_5 - \frac{8056}{27} L_{fr} \zeta_3 - \frac{58288}{27} L_{fr} \zeta_2 - 352 L_{fr} \zeta_2 \zeta_3 - \frac{2068}{3} L_{fr} \zeta_2^2 + \frac{2024}{9} L_{fr} L_{qr} - 176 L_{fr} L_{qr} \zeta_3 \\
& + \frac{3872}{9} L_{fr} L_{qr} \zeta_2 + \frac{5390}{9} L_{fr}^2 + 264 L_{fr}^2 \zeta_3 + \frac{1936}{3} L_{fr}^2 \zeta_2 - \frac{5324}{27} L_{fr}^3 \left. \right\} + \gamma_E C_A n_f C_F \left\{ -\frac{3422}{27} + \frac{608}{9} \zeta_3 \right. \\
& + \left. \frac{64}{5} \zeta_2^2 + 500 L_{qr} - 96 L_{qr} L_{rmt} - 192 L_{qr} \zeta_3 - 8 L_{qr}^2 - 500 L_{fr} + 96 L_{fr} L_{rmt} + 192 L_{fr} \zeta_3 - 32 L_{fr} L_{qr} + 40 L_{fr}^2 \right\} \\
& + \gamma_E C_A n_f^2 \left\{ \frac{3712}{729} + \frac{64}{9} \zeta_3 - \frac{800}{81} L_{qr} + \frac{160}{27} L_{qr}^2 - \frac{32}{27} L_{qr}^3 - \frac{992}{81} L_{fr} + \frac{320}{27} L_{fr} L_{qr} - \frac{32}{9} L_{fr} L_{qr}^2 - \frac{160}{9} L_{fr}^2 \right. \\
& - \left. \frac{32}{3} L_{fr}^2 L_{qr} + \frac{416}{27} L_{fr}^3 \right\} + \gamma_E C_A^2 n_f \left\{ -\frac{173636}{729} + \frac{1808}{27} \zeta_3 - \frac{9104}{81} \zeta_2 - \frac{32}{5} \zeta_2^2 + \frac{39880}{81} L_{qr} + \frac{704}{9} L_{qr} \zeta_3 \right. \\
& + \frac{2240}{9} L_{qr} \zeta_2 - \frac{4328}{27} L_{qr}^2 - \frac{352}{3} L_{qr}^2 \zeta_2 + \frac{352}{27} L_{qr}^3 - \frac{17096}{81} L_{fr} - \frac{2048}{9} L_{fr} \zeta_3 - \frac{2240}{9} L_{fr} \zeta_2 - \frac{5920}{27} L_{fr} L_{qr} \\
& - 64 L_{fr} L_{qr} \zeta_2 + \frac{352}{9} L_{fr} L_{qr}^2 + \frac{3416}{9} L_{fr}^2 + \frac{544}{3} L_{fr}^2 \zeta_2 + \frac{352}{3} L_{fr}^2 L_{qr} - \frac{4576}{27} L_{fr}^3 \left. \right\} + \gamma_E C_A^3 \left\{ \frac{943114}{729} + 384 \zeta_5 \right. \\
& - \frac{36752}{27} \zeta_3 + \frac{64784}{81} \zeta_2 - \frac{2336}{3} \zeta_2 \zeta_3 - \frac{176}{5} \zeta_2^2 - \frac{207308}{81} L_{qr} + \frac{5632}{9} L_{qr} \zeta_3 - \frac{23072}{9} L_{qr} \zeta_2 - \frac{2752}{5} L_{qr} \zeta_2^2 \\
& + \frac{16912}{27} L_{qr}^2 - 192 L_{qr}^2 \zeta_3 + \frac{1936}{3} L_{qr}^2 \zeta_2 - \frac{968}{27} L_{qr}^3 + \frac{136204}{81} L_{fr} + \frac{1760}{9} L_{fr} \zeta_3 + \frac{23072}{9} L_{fr} \zeta_2 + \frac{2752}{5} L_{fr} \zeta_2^2 \\
& + \frac{22448}{27} L_{fr} L_{qr} + 384 L_{fr} L_{qr} \zeta_3 + 352 L_{fr} L_{qr} \zeta_2 - \frac{968}{9} L_{fr} L_{qr}^2 - \frac{13120}{9} L_{fr}^2 - 192 L_{fr}^2 \zeta_3 - \frac{2992}{3} L_{fr}^2 \zeta_2 \\
& - \frac{968}{3} L_{fr}^2 L_{qr} + \frac{12584}{27} L_{fr}^3 \left. \right\} + \gamma_E^2 C_A n_f C_F \left\{ -500 + 96 L_{rmt} + 192 \zeta_3 + 16 L_{qr} + 32 L_{fr} \right\} + \gamma_E^2 C_A n_f^2 \left\{ \frac{800}{81} \right. \\
& - \frac{320}{27} L_{qr} + \frac{32}{9} L_{qr}^2 - \frac{320}{27} L_{fr} + \frac{64}{9} L_{fr} L_{qr} + \frac{32}{3} L_{fr}^2 \left. \right\} + \gamma_E^2 C_A^2 n_f \left\{ -\frac{39880}{81} - \frac{704}{9} \zeta_3 - \frac{2240}{9} \zeta_2 + \frac{9008}{27} L_{qr} \right. \\
& + \frac{448}{3} L_{qr} \zeta_2 - \frac{992}{9} L_{qr}^2 + \frac{64}{3} L_{qr}^3 + \frac{1856}{9} L_{fr} + \frac{448}{3} L_{fr} \zeta_2 + 64 L_{fr} L_{qr} + \frac{64}{3} L_{fr} L_{qr}^2 - \frac{1696}{9} L_{fr}^2 - \frac{320}{3} L_{fr}^2 L_{qr} \\
& + 64 L_{fr}^3 \left. \right\} + \gamma_E^2 C_A^3 \left\{ \frac{207308}{81} - \frac{5632}{9} \zeta_3 + \frac{23072}{9} \zeta_2 + \frac{2752}{5} \zeta_2^2 - \frac{13376}{9} L_{qr} + 640 L_{qr} \zeta_3 - \frac{2464}{3} L_{qr} \zeta_2 + 840 L_{qr}^2 \right. \\
& + 384 L_{qr}^2 \zeta_2 - \frac{352}{3} L_{qr}^3 - \frac{16144}{27} L_{fr} - 640 L_{fr} \zeta_3 - \frac{2464}{3} L_{fr} \zeta_2 - \frac{11248}{9} L_{fr} L_{qr} - 768 L_{fr} L_{qr} \zeta_2 - \frac{352}{3} L_{fr} L_{qr}^2 \\
& + \frac{9496}{9} L_{fr}^2 + 384 L_{fr}^2 \zeta_2 + \frac{1760}{3} L_{fr}^2 L_{qr} - 352 L_{fr}^3 \left. \right\} + \gamma_E^3 C_A n_f C_F \left\{ -\frac{32}{3} \right\} + \gamma_E^3 C_A n_f^2 \left\{ \frac{640}{81} - \frac{128}{27} L_{qr} \right. \\
& - \left. \frac{128}{27} L_{fr} \right\} + \gamma_E^3 C_A^2 n_f \left\{ -\frac{16928}{81} - \frac{128}{3} \zeta_2 + \frac{5248}{27} L_{qr} - 64 L_{qr}^2 - \frac{2432}{27} L_{fr} - \frac{128}{3} L_{fr} L_{qr} + \frac{320}{3} L_{fr}^2 \right\} \\
& + \gamma_E^3 C_A^3 \left\{ \frac{79936}{81} - 448 \zeta_3 + \frac{704}{3} \zeta_2 - \frac{43424}{27} L_{qr} - 768 L_{qr} \zeta_2 + 352 L_{qr}^2 - \frac{256}{3} L_{qr}^3 + \frac{35680}{27} L_{fr} + 768 L_{fr} \zeta_2 \right. \\
& + \left. \frac{704}{3} L_{fr} L_{qr} + 256 L_{fr} L_{qr}^2 - \frac{1760}{3} L_{fr}^2 - 256 L_{fr}^2 L_{qr} + \frac{256}{3} L_{fr}^3 \right\} + \gamma_E^4 C_A n_f^2 \left\{ \frac{64}{27} \right\} + \gamma_E^4 C_A^2 n_f \left\{ -\frac{2624}{27} \right.
\end{aligned}$$

$$\begin{aligned}
& + \frac{640}{9}L_{qr} + \frac{128}{9}L_{fr} \left. \right\} + \gamma_E^4 C_A^3 \left\{ \frac{21712}{27} + 384\zeta_2 - \frac{3520}{9}L_{qr} + 256L_{qr}^2 - \frac{704}{9}L_{fr} - 512L_{fr}L_{qr} + 256L_{fr}^2 \right\} \\
& + \gamma_E^5 C_A^2 n_f \left\{ -\frac{256}{9} \right\} + \gamma_E^5 C_A^3 \left\{ \frac{1408}{9} - 256L_{qr} + 256L_{fr} \right\} + \gamma_E^6 C_A^3 \left\{ +\frac{256}{3} \right\}. \tag{E5}
\end{aligned}$$

### APPENDIX F: NSV RESUMMATION EXPONENTS $\bar{g}_{d,g,i}^A(\omega)$

$$\bar{g}_{d,g,1}^A(\omega) = 0, \quad \bar{g}_{d,g,2}^A(\omega) = \frac{1}{\beta_0} C_A \{2L_\omega\}, \tag{F1}$$

$$\bar{g}_{d,g,3}^A(\omega) = \frac{\beta_1}{\beta_0^2} C_A \{2\omega + 2L_\omega\} + \frac{1}{\beta_0} C_A n_f \left\{ \frac{20}{9}\omega \right\} + \frac{1}{\beta_0} C_A^2 \left\{ -\frac{134}{9}\omega + 4\omega\zeta_2 \right\} + C_A \{-2 + 2L_{qr} - 2L_{fr} + 2L_{fr}\omega - 4\gamma_E\}, \tag{F2}$$

$$\begin{aligned}
\bar{g}_{d,g,4}^A(\omega) = & \frac{\beta_1^2}{\beta_0^3} C_A \{\omega^2 - L_\omega^2\} + \frac{\beta_2}{\beta_0^2} C_A \{-\omega^2\} + \frac{\beta_1}{\beta_0^2} C_A n_f \left\{ -\frac{20}{9}\omega + \frac{10}{9}\omega^2 - \frac{20}{9}L_\omega \right\} + \frac{\beta_1}{\beta_0^2} C_A^2 \left\{ \frac{134}{9}\omega - 4\omega\zeta_2 \right. \\
& - \frac{67}{9}\omega^2 + 2\omega^2\zeta_2 + \frac{134}{9}L_\omega - 4L_\omega\zeta_2 \left. \right\} + \frac{1}{\beta_0} C_A n_f^2 \left\{ \frac{8}{27}\omega - \frac{4}{27}\omega^2 \right\} + \frac{1}{\beta_0} C_A C_F n_f \left\{ \frac{55}{3}\omega - 16\omega\zeta_3 - \frac{55}{6}\omega^2 \right. \\
& + 8\omega^2\zeta_3 \left. \right\} + \frac{1}{\beta_0} C_A^2 n_f \left\{ \frac{418}{27}\omega + \frac{56}{3}\omega\zeta_3 - \frac{80}{9}\omega\zeta_2 - \frac{209}{27}\omega^2 - \frac{28}{3}\omega^2\zeta_3 + \frac{40}{9}\omega^2\zeta_2 \right\} + \frac{1}{\beta_0} C_A^3 \left\{ -\frac{245}{3}\omega \right. \\
& - \frac{44}{3}\omega\zeta_3 + \frac{536}{9}\omega\zeta_2 - \frac{88}{5}\omega\zeta_2^2 + \frac{245}{6}\omega^2 + \frac{22}{3}\omega^2\zeta_3 - \frac{268}{9}\omega^2\zeta_2 + \frac{44}{5}\omega^2\zeta_2^2 \left. \right\} + \frac{\beta_1}{\beta_0} C_A \{2L_\omega - 2L_\omega L_{qr} \\
& + 4L_\omega\gamma_E\} + C_A n_f \left\{ \frac{116}{27} - \frac{2}{3}\zeta_2 - \frac{20}{9}L_{qr} + \frac{20}{9}L_{fr} - \frac{40}{9}L_{fr}\omega + \frac{20}{9}L_{fr}\omega^2 + \frac{40}{9}\gamma_E \right\} + C_A^2 \left\{ -\frac{806}{27} \right. \\
& + 14\zeta_3 + \frac{23}{3}\zeta_2 + \frac{134}{9}L_{qr} - 4L_{qr}\zeta_2 - \frac{134}{9}L_{fr} + 4L_{fr}\zeta_2 + \frac{268}{9}L_{fr}\omega - 8L_{fr}\omega\zeta_2 - \frac{134}{9}L_{fr}\omega^2 + 4L_{fr}\omega^2\zeta_2 \\
& \left. - \frac{268}{9}\gamma_E + 8\gamma_E\zeta_2 \right\} + \beta_0 C_A \{-\zeta_2 + 2L_{qr} - L_{qr}^2 + L_{fr}^2 - 2L_{fr}^2\omega + L_{fr}^2\omega^2 - 4\gamma_E + 4\gamma_E L_{qr} - 4\gamma_E^2\}, \tag{F3}
\end{aligned}$$

### APPENDIX G: NSV RESUMMATION EXPONENTS $h_{d,g,ij}^A(\omega)$ AND $\tilde{h}_{d,g,ij}^A(\omega, \omega_l)$

$$h_{d,g,00}^A(\omega) = \frac{1}{\beta_0} C_A \{-4L_\omega\} \quad h_{d,g,01}^A(\omega) = 0, \tag{G1}$$

$$\begin{aligned}
h_{d,g,10}^A(\omega) = & \frac{1}{2\beta_0^2(\omega-1)} \left[ \beta_1 C_A \{8\omega + 8L_\omega\} + \beta_0 C_A n_f \left\{ \frac{80}{9}\omega \right\} + \beta_0 C_A^2 \left\{ -\frac{536}{9}\omega + 16\omega\zeta_2 - 32\gamma_E\omega \right\} \right. \\
& \left. + \beta_0^2 C_A \{-4 - 8L_{fr} + 8L_{fr}\omega + 8L_{qr} - 16\gamma_E\} \right], \tag{G2}
\end{aligned}$$

$$\tilde{h}_{d,g,11}^A(\omega, \omega_l) = \frac{C_A^2}{\beta_0} \left\{ -\frac{4\omega_l}{(\omega-1)^2} - \frac{16\omega}{(\omega-1)} \right\}, \tag{G3}$$

$$\begin{aligned}
h_{d,g,20}^A(\omega) = & \frac{1}{2\beta_0^3(\omega-1)^2} \left[ \beta_1^2 C_A \{-4\omega^2 + 4L_\omega^2\} + \beta_0\beta_2 C_A \{4\omega^2\} + \beta_0\beta_1 C_{An_f} \left\{ \frac{80}{9}\omega - \frac{40}{9}\omega^2 + \frac{80}{9}L_\omega \right\} \right. \\
& + \beta_0\beta_1 C_A^2 \left\{ -\frac{536}{9}\omega + 16\omega\zeta_2 + \frac{268}{9}\omega^2 - 8\omega^2\zeta_2 - 32\gamma_E\omega + 16\gamma_E\omega^2 - \frac{536}{9}L_\omega + 16L_\omega\zeta_2 - 32L_\omega\gamma_E \right\} \\
& + \beta_0^2 C_{An_f}^2 \left\{ -\frac{32}{27}\omega + \frac{16}{27}\omega^2 \right\} + \beta_0^2 C_A C_{Fn_f} \left\{ -\frac{172}{3}\omega + 64\omega\zeta_3 + \frac{86}{3}\omega^2 - 32\omega^2\zeta_3 \right\} \\
& + \beta_0^2 C_{An_f}^2 \left\{ -\frac{1096}{27}\omega - \frac{224}{3}\omega\zeta_3 + \frac{320}{9}\omega\zeta_2 + \frac{548}{27}\omega^2 + \frac{112}{3}\omega^2\zeta_3 - \frac{160}{9}\omega^2\zeta_2 - \frac{640}{9}\gamma_E\omega + \frac{320}{9}\gamma_E\omega^2 \right\} \\
& + \beta_0^2 C_A^3 \left\{ \frac{724}{3}\omega - \frac{112}{3}\omega\zeta_3 - \frac{2144}{9}\omega\zeta_2 + \frac{352}{5}\omega\zeta_2^2 - \frac{362}{3}\omega^2 + \frac{56}{3}\omega^2\zeta_3 + \frac{1072}{9}\omega^2\zeta_2 - \frac{176}{5}\omega^2\zeta_2^2 + \frac{4288}{9}\gamma_E\omega \right. \\
& - 128\gamma_E\omega\zeta_2 - \frac{2144}{9}\gamma_E\omega^2 + 64\gamma_E\omega^2\zeta_2 \left. \right\} + \beta_0^2\beta_1 C_A \{8\omega - 4\omega^2 - 4L_\omega + 8L_\omega L_{qr} - 16L_\omega\gamma_E\} \\
& + \beta_0^3 C_{An_f} \left\{ -\frac{272}{27} + \frac{32}{3}\zeta_2 - \frac{80}{9}L_{fr} + \frac{160}{9}L_{fr}\omega - \frac{80}{9}L_{fr}\omega^2 + \frac{80}{9}L_{qr} - \frac{148}{9}\gamma_E \right\} + \beta_0^3 C_A^2 \left\{ \frac{1808}{27} \right. \\
& - 56\zeta_3 - \frac{224}{3}\zeta_2 + \frac{536}{9}L_{fr} - 16L_{fr}\zeta_2 - \frac{1072}{9}L_{fr}\omega + 32L_{fr}\omega\zeta_2 + \frac{536}{9}L_{fr}\omega^2 - 16L_{fr}\omega^2\zeta_2 - \frac{536}{9}L_{qr} \\
& + 16L_{qr}\zeta_2 + \frac{1060}{9}\gamma_E - 32\gamma_E\zeta_2 + 32\gamma_EL_{fr} - 64\gamma_EL_{fr}\omega + 32\gamma_EL_{fr}\omega^2 - 32\gamma_EL_{qr} + 56\gamma_E^2 \left. \right\} \\
& \left. + \beta_0^4 C_A \{16\zeta_2 - 4L_{fr}^2 + 8L_{fr}^2\omega - 4L_{fr}^2\omega^2 - 4L_{qr} + 4L_{qr}^2 + 8\gamma_E - 16\gamma_EL_{qr} + 16\gamma_E^2\} \right], \tag{G4}
\end{aligned}$$

$$\begin{aligned}
h_{d,g,21}^A(\omega) = & \frac{1}{2\beta_0^2(\omega-1)^2} \left[ \beta_1 C_A^2 \{-32\omega + 16\omega^2 - 32L_\omega\} + \beta_0 C_{An_f}^2 \left\{ -\frac{640}{9}\omega + \frac{320}{9}\omega^2 \right\} + \beta_0 C_A^3 \left\{ \frac{4288}{9}\omega \right. \right. \\
& - 128\omega\zeta_2 - \frac{2144}{9}\omega^2 + 64\omega^2\zeta_2 \left. \right\} + \beta_0^2 C_{An_f} \left\{ \frac{4}{3} \right\} + \beta_0^2 C_A^2 \left\{ -\frac{4}{3} + 32L_{fr} - 64L_{fr}\omega + 32L_{fr}\omega^2 \right. \\
& \left. - 32L_{qr} + 48\gamma_E \right\} \left. \right], \tag{G5}
\end{aligned}$$

$$\tilde{h}_{d,22}^g(\omega, \omega_l) = \frac{\omega_l}{\beta_0(\omega-1)^3} \left[ C_{An_f}^2 \left\{ \frac{32}{27} \right\} + C_A^3 \left\{ -\frac{176}{27} \right\} \right], \tag{G6}$$

where  $\gamma_E$  is the Euler-Mascheroni constant. Here,  $L_\omega = \ln(1-\omega)$  with  $\omega = \beta_0 a_s(\mu_R^2) \ln N_1 N_2$ ,  $\omega_l = \beta_0 a_s(\mu_R^2) \ln N_l$  with  $l = 1, 2$ ,  $L_{qr} = \ln\left(\frac{q^2}{\mu_R^2}\right)$  and  $L_{fr} = \ln\left(\frac{f^2}{\mu_R^2}\right)$ .

- 
- [1] G. Aad *et al.* (ATLAS Collaboration), *Phys. Lett. B* **716**, 1 (2012).  
[2] S. Chatrchyan *et al.* (CMS Collaboration), *Phys. Lett. B* **716**, 30 (2012).  
[3] P. W. Higgs, *Phys. Lett.* **12**, 132 (1964).  
[4] P. W. Higgs, *Phys. Rev. Lett.* **13**, 508 (1964).  
[5] P. W. Higgs, *Phys. Rev.* **145**, 1156 (1966).  
[6] F. Englert and R. Brout, *Phys. Rev. Lett.* **13**, 321 (1964).  
[7] G. S. Guralnik, C. R. Hagen, and T. W. B. Kibble, *Phys. Rev. Lett.* **13**, 585 (1964).  
[8] P. Fayet, *Nucl. Phys.* **B90**, 104 (1975).  
[9] P. Fayet, *Phys. Lett. B* **64**, 159 (1976).  
[10] P. Fayet, *Phys. Lett.* **69B**, 489 (1977).  
[11] S. Dimopoulos and H. Georgi, *Nucl. Phys.* **B193**, 150 (1981).  
[12] N. Sakai, *Z. Phys. C* **11**, 153 (1981).  
[13] K. Inoue, A. Kakuto, H. Komatsu, and S. Takeshita, *Prog. Theor. Phys.* **68**, 927 (1982); **70**, 330(E) (1983).  
[14] K. Inoue, A. Kakuto, H. Komatsu, and S. Takeshita, *Prog. Theor. Phys.* **71**, 413 (1984).  
[15] K. Inoue, A. Kakuto, H. Komatsu, and S. Takeshita, *Prog. Theor. Phys.* **67**, 1889 (1982).

- [16] S. Chatrchyan *et al.* (CMS Collaboration), *Phys. Lett. B* **716**, 30 (2012).
- [17] C. Anastasiou and K. Melnikov, *Nucl. Phys.* **B646**, 220 (2002).
- [18] R. V. Harlander and W. B. Kilgore, *Phys. Rev. Lett.* **88**, 201801 (2002).
- [19] V. Ravindran, J. Smith, and W. L. van Neerven, *Nucl. Phys.* **B665**, 325 (2003).
- [20] C. Anastasiou, C. Duhr, F. Dulat, F. Herzog, and B. Mistlberger, *Phys. Rev. Lett.* **114**, 212001 (2015).
- [21] J. R. Ellis, M. K. Gaillard, and D. V. Nanopoulos, *Nucl. Phys.* **B106**, 292 (1976).
- [22] M. A. Shifman, A. I. Vainshtein, M. B. Voloshin, and V. I. Zakharov, *Sov. J. Nucl. Phys.* **30**, 711 (1979), <https://inspirehep.net/literature/141287>.
- [23] B. A. Kniehl and M. Spira, *Z. Phys. C* **69**, 77 (1995).
- [24] R. P. Kauffman and W. Schaffer, *Phys. Rev. D* **49**, 551 (1994).
- [25] A. Djouadi, M. Spira, and P. M. Zerwas, *Phys. Lett. B* **311**, 255 (1993).
- [26] R. V. Harlander and W. B. Kilgore, *J. High Energy Phys.* **10** (2002) 017.
- [27] C. Anastasiou and K. Melnikov, *Phys. Rev. D* **67**, 037501 (2003).
- [28] K. G. Chetyrkin, B. A. Kniehl, M. Steinhauser, and W. A. Bardeen, *Nucl. Phys.* **B535**, 3 (1998).
- [29] M. Spira, A. Djouadi, D. Graudenz, and P. M. Zerwas, *Phys. Lett. B* **318**, 347 (1993).
- [30] M. Spira, A. Djouadi, D. Graudenz, and P. Zerwas, *Nucl. Phys.* **B453**, 17 (1995).
- [31] T. Ahmed, T. Gehrmann, P. Mathews, N. Rana, and V. Ravindran, *J. High Energy Phys.* **11** (2015) 169.
- [32] V. Ravindran, *Nucl. Phys.* **B746**, 58 (2006).
- [33] V. Ravindran, *Nucl. Phys.* **B752**, 173 (2006).
- [34] T. Ahmed, M. Mahakhud, N. Rana, and V. Ravindran, *Phys. Rev. Lett.* **113**, 112002 (2014).
- [35] T. Ahmed, M. C. Kumar, P. Mathews, N. Rana, and V. Ravindran, *Eur. Phys. J. C* **76**, 355 (2016).
- [36] T. Ahmed, M. Bonvini, M. C. Kumar, P. Mathews, N. Rana, V. Ravindran, and L. Rottoli, *Eur. Phys. J. C* **76**, 663 (2016).
- [37] C. Anastasiou, C. Duhr, F. Dulat, E. Furlan, T. Gehrmann, F. Herzog, A. Lazopoulos, and B. Mistlberger, *J. High Energy Phys.* **05** (2016) 058.
- [38] V. Ravindran, J. Smith, and W. L. van Neerven, *Nucl. Phys.* **B704**, 332 (2005).
- [39] D. de Florian, M. Grazzini, and Z. Kunszt, *Phys. Rev. Lett.* **82**, 5209 (1999).
- [40] B. Field, J. Smith, M. E. Tejeda-Yeomans, and W. L. van Neerven, *Phys. Lett. B* **551**, 137 (2003).
- [41] G. F. Sterman, *Nucl. Phys.* **B281**, 310 (1987).
- [42] S. Catani and L. Trentadue, *Nucl. Phys.* **B327**, 323 (1989).
- [43] S. Catani, D. de Florian, M. Grazzini, and P. Nason, *J. High Energy Phys.* **07** (2003) 028.
- [44] S. Moch and A. Vogt, *Phys. Lett. B* **631**, 48 (2005).
- [45] A. Idilbi, X.-d. Ji, J.-P. Ma, and F. Yuan, *Phys. Rev. D* **73**, 077501 (2006).
- [46] V. Ahrens, T. Becher, M. Neubert, and L. L. Yang, *Eur. Phys. J. C* **62**, 333 (2009).
- [47] D. de Florian and M. Grazzini, *Phys. Lett. B* **674**, 291 (2009).
- [48] M. Bonvini and S. Marzani, *J. High Energy Phys.* **09** (2014) 007.
- [49] S. Catani, L. Cieri, D. de Florian, G. Ferrera, and M. Grazzini, *Nucl. Phys.* **B888**, 75 (2014).
- [50] D. de Florian and J. Zurita, *Phys. Lett. B* **659**, 813 (2008).
- [51] N. Agarwal, P. Banerjee, G. Das, P. K. Dhani, A. Mukhopadhyay, V. Ravindran, and A. Tripathi, *J. High Energy Phys.* **12** (2018) 105.
- [52] V. Ravindran, J. Smith, and W. L. van Neerven, *Nucl. Phys.* **B767**, 100 (2007).
- [53] P. Banerjee, G. Das, P. K. Dhani, and V. Ravindran, *Phys. Rev. D* **97**, 054024 (2018).
- [54] P. Banerjee, G. Das, P. K. Dhani, and V. Ravindran, *Phys. Rev. D* **98**, 054018 (2018).
- [55] E. Laenen and G. F. Sterman, in *Proceedings of the 7th Meeting of the APS Division of Particles Fields* (World Scientific, Singapore, 1992), pp. 987–989.
- [56] G. F. Sterman and W. Vogelsang, *J. High Energy Phys.* **02** (2001) 016.
- [57] A. Mukherjee and W. Vogelsang, *Phys. Rev. D* **73**, 074005 (2006).
- [58] P. Bolzoni, *Phys. Lett. B* **643**, 325 (2006).
- [59] T. Becher and M. Neubert, *Phys. Rev. Lett.* **97**, 082001 (2006).
- [60] T. Becher, M. Neubert, and G. Xu, *J. High Energy Phys.* **07** (2008) 030.
- [61] M. Bonvini, S. Forte, G. Ridolfi, and L. Rottoli, *J. High Energy Phys.* **01** (2015) 046.
- [62] M. A. Ebert, J. K. L. Michel, and F. J. Tackmann, *J. High Energy Phys.* **05** (2017) 088.
- [63] M. Cacciari and S. Catani, *Nucl. Phys.* **B617**, 253 (2001).
- [64] E. Laenen, L. Magnea, and G. Stavenga, *Phys. Lett. B* **669**, 173 (2008).
- [65] E. Laenen, L. Magnea, G. Stavenga, and C. D. White, *J. High Energy Phys.* **01** (2011) 141.
- [66] D. Bonocore, E. Laenen, L. Magnea, L. Vernazza, and C. D. White, *Phys. Lett. B* **742**, 375 (2015).
- [67] D. Bonocore, E. Laenen, L. Magnea, S. Melville, L. Vernazza, and C. White, *J. High Energy Phys.* **06** (2015) 008.
- [68] D. Bonocore, E. Laenen, L. Magnea, L. Vernazza, and C. White, *J. High Energy Phys.* **12** (2016) 121.
- [69] V. Del Duca, E. Laenen, L. Magnea, L. Vernazza, and C. White, *J. High Energy Phys.* **11** (2017) 057.
- [70] N. Bahjat-Abbas, D. Bonocore, J. Sinninghe Damsté, E. Laenen, L. Magnea, L. Vernazza, and C. White, *J. High Energy Phys.* **11** (2019) 002.
- [71] G. Soar, S. Moch, J. Vermaseren, and A. Vogt, *Nucl. Phys.* **B832**, 152 (2010).
- [72] S. Moch and A. Vogt, *J. High Energy Phys.* **11** (2009) 099.
- [73] D. de Florian, J. Mazzitelli, S. Moch, and A. Vogt, *J. High Energy Phys.* **10** (2014) 176.
- [74] M. Beneke, A. Broggio, M. Garny, S. Jaskiewicz, R. Szafron, L. Vernazza, and J. Wang, *J. High Energy Phys.* **03** (2019) 043.
- [75] M. Beneke, M. Garny, S. Jaskiewicz, R. Szafron, L. Vernazza, and J. Wang, *J. High Energy Phys.* **01** (2020) 094.

- [76] M. Beneke, A. Broggio, S. Jaskiewicz, and L. Vernazza, *J. High Energy Phys.* **07** (2020) 078.
- [77] A. H. Ajjath, P. Mukherjee, and V. Ravindran, *Phys. Rev. D* **105**, L091503 (2022).
- [78] A. H. Ajjath, P. Mukherjee, and V. Ravindran, *Phys. Rev. D* **105**, 094035 (2022).
- [79] A. H. Ajjath, P. Mukherjee, V. Ravindran, A. Sankar, and S. Tiwari, *J. High Energy Phys.* **04** (2021) 131.
- [80] A. H. Ajjath, P. Mukherjee, V. Ravindran, A. Sankar, and S. Tiwari, *Eur. Phys. J. C* **82**, 234 (2022).
- [81] A. H. Ajjath, P. Mukherjee, V. Ravindran, A. Sankar, and S. Tiwari, *Eur. Phys. J. C* **82**, 774 (2022).
- [82] A. H. Ajjath, P. Mukherjee, V. Ravindran, A. Sankar, and S. Tiwari, *Phys. Rev. D* **103**, L111502 (2021).
- [83] A. H. Ajjath, P. Mukherjee, V. Ravindran, A. Sankar, and S. Tiwari, *Phys. Rev. D* **106**, 034005 (2022).
- [84] V. Ravindran, A. Sankar, and S. Tiwari, *Phys. Rev. D* **108**, 014012 (2023).
- [85] A. Bhattacharya, M. C. Kumar, P. Mathews, and V. Ravindran, *Phys. Rev. D* **105**, 116015 (2022).
- [86] S. L. Adler, *Phys. Rev.* **177**, 2426 (1969).
- [87] O. Tarasov, A. Vladimirov, and A. Zharkov, *Phys. Lett.* **93B**, 429 (1980).
- [88] T. Kinoshita, *J. Math. Phys. (N.Y.)* **3**, 650 (1962).
- [89] T. Lee and M. Nauenberg, *Phys. Rev.* **133**, B1549 (1964).
- [90] G. Altarelli and G. Parisi, *Nucl. Phys.* **B126**, 298 (1977).
- [91] C. Anastasiou, L. J. Dixon, and K. Melnikov, *Nucl. Phys. B, Proc. Suppl.* **116**, 193 (2003).
- [92] K. G. Chetyrkin, B. A. Kniehl, and M. Steinhauser, *Phys. Rev. Lett.* **79**, 353 (1997).
- [93] C. Anastasiou, C. Duhr, F. Dulat, F. Herzog, and B. Mistlberger, *Phys. Rev. Lett.* **114**, 212001 (2015).
- [94] C. Anastasiou, K. Melnikov, and F. Petriello, *Nucl. Phys.* **B724**, 197 (2005).
- [95] F. Dulat, B. Mistlberger, and A. Pelloni, *Phys. Rev. D* **99**, 034004 (2019).
- [96] V. Sudakov, *Sov. Phys. JETP* **3**, 65 (1956), <https://inspirehep.net/literature/9137>.
- [97] A. H. Mueller, *Phys. Rev. D* **20**, 2037 (1979).
- [98] J. C. Collins, *Phys. Rev. D* **22**, 1478 (1980).
- [99] A. Sen, *Phys. Rev. D* **24**, 3281 (1981).
- [100] S. Moch, J. A. M. Vermaseren, and A. Vogt, *Nucl. Phys.* **B688**, 101 (2004).
- [101] A. Vogt, S. Moch, and J. A. M. Vermaseren, *Nucl. Phys.* **B691**, 129 (2004).
- [102] S. Catani and L. Trentadue, *Nucl. Phys.* **B353**, 183 (1991).
- [103] A. Vogt, *Phys. Lett. B* **497**, 228 (2001).
- [104] T. Becher and M. Neubert, *Phys. Rev. Lett.* **102**, 162001 (2009); **111**, 199905(E) (2013).
- [105] E. Gardi and L. Magnea, *J. High Energy Phys.* **03** (2009) 079.
- [106] A. Gonzalez-Arroyo, C. Lopez, and F. Yndurain, *Nucl. Phys.* **B153**, 161 (1979).
- [107] G. Curci, W. Furmanski, and R. Petronzio, *Nucl. Phys.* **B175**, 27 (1980).
- [108] W. Furmanski and R. Petronzio, *Phys. Lett.* **97B**, 437 (1980).
- [109] R. Hamberg and W. van Neerven, *Nucl. Phys.* **B379**, 143 (1992).
- [110] R. Ellis and W. Vogelsang, [arXiv:hep-ph/9602356](https://arxiv.org/abs/hep-ph/9602356).
- [111] J. Ablinger, A. Behring, J. Blümlein, A. De Freitas, A. von Manteuffel, and C. Schneider, *Nucl. Phys.* **B922**, 1 (2017).
- [112] S. Moch, B. Ruijl, T. Ueda, J. A. M. Vermaseren, and A. Vogt, *J. High Energy Phys.* **10** (2017) 041.
- [113] P. Banerjee, P. K. Dhani, M. C. Kumar, P. Mathews, and V. Ravindran, *Phys. Rev. D* **97**, 094028 (2018).
- [114] T. Ahmed, A. A. H., P. Mukherjee, V. Ravindran, and A. Sankar, *Eur. Phys. J. C* **81**, 943 (2021).
- [115] L. A. Harland-Lang, A. D. Martin, P. Motylinski, and R. S. Thorne, *Eur. Phys. J. C* **75**, 204 (2015).
- [116] A. Buckley, J. Ferrando, S. Lloyd, K. Nordström, B. Page, M. Rufenacht, M. Schönherr, and G. Watt, *Eur. Phys. J. C* **75**, 132 (2015).
- [117] P. A. Zyla *et al.* (Particle Data Group), *Prog. Theor. Exp. Phys.* **2020**, 083C01 (2020).